CYCLIZATION STRATEGIES TO STABILIZE EPIDERMAL GROWTH FACTOR RECEPTOR DIMERIZATION ARM MIMICS

by

LAURA ELIZABETH HANOLD

(Under the Direction of Eileen Kennedy)

ABSTRACT

Protein-protein interactions (PPIs) have critical roles in the regulation of signal transduction in the cell, and the dysregulation of these signaling pathways contributes to various disease states. As such, PPIs offer promising targets for the development of modulators of cell signaling and potential therapeutics. The design of constrained peptides is an attractive strategy for PPI disruption, as these molecules can mimic secondary structures contributing to PPIs. This strategy has primarily been used to target helix-mediated interactions; however, there are significantly fewer reports of peptides disrupting β-loop-mediated PPIs. One extensively studied and therapeutically relevant example of a β-loop-mediated PPI is the epidermal growth factor receptor (EGFR) dimer, which is largely stabilized by a β-loop termed the dimerization arm. Ligand-induced EGFR dimerization leads to activation of the kinase, which promotes signaling pathways involved in proliferation and survival in cancer. As such, disruptors that specifically target the dimerization interface may provide promising probes of EGFR dimerization while also suppressing tumor growth and survival. Thus, the aim of this research is to test highly stable chemical constraints to develop cyclic peptides mimicking the EGFR

dimerization arm as potential dimer disruptors. Using selenylsulfide and triazole chemistries, cyclic dimerization arm mimics were developed. Each of these constraints increased the resistance of the peptides to proteolytic degradation while also altering the conformation compared to unconstrained peptides. A 1,4-triazolyl-bridged peptide also demonstrated promise as a molecular probe of EGFR dimerization by disrupting EGFR phosphorylation and dimerization while reducing cell viability. Thus, this panel of constraints enables access to peptides with variety of conformations, increased stability, and the potential to disrupt dimerization. These approaches may have broad applications in the design of constrained peptides for the disruption of alternative β-loop mediated interactions. Furthermore, beyond the scope of this project, additional testing and optimization of these peptides and their analogs may lead to the development of potential anticancer therapeutics targeting EGFR dimerization.

INDEX WORDS: Epidermal growth factor receptor, Dimerization, Triazole, Selenylsulfide, Peptide, Macrocyclization, Protein-protein interaction

CYCLIZATION STRATEGIES TO STABILIZE EPIDERMAL GROWTH FACTOR RECEPTOR DIMERIZATION ARM MIMICS

by

LAURA ELIZABETH HANOLD

B.S., Sweet Briar College, 2010

A Dissertation Submitted to the Graduate Faculty of The University of Georgia in Partial Fulfillment of the Requirements for the Degree

DOCTOR OF PHILOSOPHY

ATHENS, GEORGIA

2016

CYCLIZATION STRATEGIES TO STABILIZE EPIDERMAL GROWTH FACTOR RECEPTOR DIMERIZATION ARM MIMICS

by

LAURA ELIZABETH HANOLD

Major Professor:	Eileen Kennedy
Committee:	Rajgopal Govindarajan
	Shelley Hooks
	Natarajan Kannan
	Jeffrey Urbauer

Electronic Version Approved:

Suzanne Barbour
Dean of the Graduate School
The University of Georgia
May 2016

DEDICATION

To my family

ACKNOWLEDGEMENTS

I would like to thank everyone who helped with the completion of this work. First, I would like to thank Dr. Eileen Kennedy for her mentorship during the completion of my doctoral research. Her support and guidance allowed me to explore the field of peptide science, develop new research skills and navigate through the peer review process, gaining experience that will be invaluable as I move forward in my career. I would also like to thank my committee members Dr. Raj Govindarajan, Dr. Shelley Hooks, Dr. Kannan Natarajan, and Dr. Jeffrey Urbauer for their guidance and insightful questions, which have helped me to critically evaluate my research. I thank Dr. Aaron Beedle, who provided training in fluorescence microscopy and western blot imaging and also collected the mouse serum used in these experiments. I would like to thank Dr. Ramona Bieber-Urbauer for her help and guidance on the circular dichroism experiments, Dr. Krishnadev Oruganty for all of his work on molecular dynamics simulations, and Dr. Samiksha Katiyar for her guidance in western blotting. I would like to thank Dr. Mandy Murph, Sterling Tran, and Wei Jia who helped with my training in viability assays.

I would also like to thank Megan Lewandowski, Yuxiao Wang, Sneha Patel and Melody Fulton for their discussions and support, which helped me to through the challenges of doctoral research. I want to thank the students who performed research under my supervision, maintaining stocks of peptides for all of the experiments performed in this research, including Viral Patel, Terran White, and Huong Pham. I also would like to thank Norman Ton who helped to optimize the proteolytic stability assay,

Chris Watkins for helping to synthesize TAMRA-labeled peptides for fluorescence microscopy, and Peter Liaw who helped with the early stages of the 1,5-EDA2 synthesis. I thank Parisa Darkhal and Melissa Young, who helped with peptide synthesis and western blot analysis for the earlier stages of this project during their rotations.

TABLE OF CONTENTS

Page

ACKNOWLEDGEMENTS v

LIST OF TABLES ix

LIST OF FIGURES x

LIST OF ABBREVIATIONS xii

CHAPTER

1 INTRODUCTION AND LITERATURE REVIEW 1

1.1 Statement of Purpose 1

1.2 Protein-Protein Interactions (PPIs) as Therapeutic Targets 3

1.3 EGFR Structure and Activation 6

1.4 Current EGFR Targeting Strategies 9

1.5 Peptides as EGFR Dimer Disruptors 11

1.6 Constraints for Stabilization of Peptides Targeting PPIs 13

2 INHIBITING EGFR DIMERIZATION USING TRIAZOLYL-BRIDGED DIMERIZATION ARM MIMICS 27

2.1 Abstract 28

2.2 Introduction 28

2.3 Results and Discussion 31

2.4 Conclusions 38

2.5 Materials and Methods 39

3 DESIGN OF A SELENYLSULFIDE-BRIDGED EGFR DIMERIZATION ARM MIMIC 63

3.1 Abstract 64

3.2 Introduction 64

3.3 Results and Discussion 67

3.4 Conclusions 71

3.5 Materials and Methods 72

3.6 Acknowledgements 79

4 SYNTHESIS OF A 1,5-DISUBSTITUTED TRIAZOLYL-BRIDGED EGFR DIMERIZATION ARM MIMIC 88

4.1 Abstract 89

4.2 Introduction 90

4.3 Results and Discussion 92

4.4 Conclusions 96

4.5 Materials and Methods 97

5 CONCLUSIONS 109

5.1 Summary of Results 109

5.2 Future Directions 113

REFERENCES 121

LIST OF TABLES

Page

Table 5.1: Summary of Constraint Synthesis, Stability and Conformation.....117

LIST OF FIGURES

Page

Figure 1.1: Development of Cyclic Peptides to Block Loop-Mediated PPIs 20

Figure 1.2: Small Molecule and Peptide Disruptors of p53-MDM2 21

Figure 1.3: EGFR Crystal Structures 22

Figure 1.4: Current FDA Approved EGFR Tyrosine Kinase Inhibitors 23

Figure 1.5: Binding of Gefitinib and Afatinib to the EGFR Kinase Domain 24

Figure 1.6: Binding of Fab Fragments of ErbB Targeted Monoclonal Antibodies 25

Figure 1.7: Chemical Constraints for Peptide Cyclization 26

Figure 2.1: Dimerization Arm Targeting Strategy for Inhibition of EGFR 50

Figure 2.2: Design and Synthesis of EDA Peptides 51

Figure 2.3: Molecular Dynamics Simulations of EDA Peptides 52

Figure 2.4: EDA Peptides are Resistant to Proteolytic Degradation 53

Figure 2.5: EDA2 is Stable in Tissue Culture Medium 54

Figure 2.6: EDA2 Down-Regulates Activated EGFR 55

Figure 2.7: The Effect of EDA1 and EDA3-6 on EGFR Phosphorylation 56

Figure 2.8: The Effect of EDA2 and Its Controls on Total EGFR Protein Levels 57

Figure 2.9: Disulfide Peptide Activity and Stability 58

Figure 2.10: EDA2 Reduces Cell Viability 59

Figure 2.11: EDA2 Down-Regulates EGFR Dimers 60

Figure 2.12: EGFR Dimerization Cross-linking Assay 61

Figure 2.13: EDA2 Co-localizes with EGFR 62

Figure 3.1: Design of EGFR Dimerization Arm Mimics 80

Figure 3.2: Disruption of Phosphorylation by Dimerization Arm Mimics.....81

Figure 3.3: Synthesis of Selenylsulfide Peptide **2c**.....82

Figure 3.4: Synthesis of Selenylsulfide Peptide **3c**.....83

Figure 3.5: The Selenylsulfide Peptide is Stable to Serum Proteases.....84

Figure 3.6: The Selenylsulfide-Bridged Peptide is Resistant to Reduction by DTT 85

Figure 3.7: Selenylsulfide **4c** is Non-Toxic 86

Figure 3.8: Selenylsulfide **4c** Reduces Cell Viability.....87

Figure 4.1: Sequence and Structure of the EGFR Dimerization Arm 104

Figure 4.2: Design of Triazolyl-Bridged Dimerization Arm Mimics.....105

Figure 4.3: Confirmation of Cyclization in Crude Peptide Products.....106

Figure 4.4: Circular Dichroism Spectra of Triazolyl-Bridged Peptides 107

Figure 4.5: Serum Stability of Triazolyl-Bridged Peptides 108

Figure 5.1: Selected Dimerization Arm Interactions for Optimization 118

Figure 5.2: Structure of the CD4-gp120 Interaction.....119

Figure 5.3: Oligomeric Protein Structures Showing High β-Strand Content 120

LIST OF ABBREVIATIONS

Aha	Azido-homoalanine
AKAP	A-kinase anchoring protein
Akt (PKB)	Protein kinase B / RAC serine/threonine-protein kinase
AM	Aminomethyl
Anl	Azido-norleucine
Anv	Azido-norvaline
ATP	Adenosine triphosphate
BAD	Bcl-2 associated agonist of cell death
BAK	Bcl-2 homologous antagonist/killer
BAX	Bcl-2-like protein 4
Bcl-2	B-cell CLL/lymphoma 2 protein
Bcl-9	B-cell CLL/lymphoma 9 protein
Bcl-X_L	Bcl-2-like protein 1
BID	BH3-interacting domain death agonist
BIM	Bcl-2-like protein 11
BOC	*tert*-Butyloxycarbonyl
BS^3	Bis(sulfosuccinimidyl) suberate
BSA	Bovine serum albumin
CD	Circular dichroism

CD4	T-cell surface glycoprotein CD4
cIAP	Cellular inhibitor of apoptosis protein
Cp*RuCl(COD)	Chloro(pentamethylcyclopentadienyl)(cyclooctadiene) ruthenium(II)
Cp*RuCl(PPh$_3$)$_2$	Chloro(pentamethylcyclopentadienyl)bis(triphenylphosphine) ruthenium(II)
CuAAC	Copper-catalyzed azide-alkyne cycloaddition
CYFIP1	Cytoplasmic FMR1-interacting protein 1
Dab	Diaminobutyric acid
DAPI	2-(4-Amidinophenyl)-6-indolecarbamidine dihydrochloride
DCM	Dichloromethane
DIC	Diisopropylcarbodiimide
DIEA (DIPEA)	Diisopropylethylamine
DMEM	Dulbecco's Modified Eagle Medium
DMF	Dimethylformamide
DMSO	Dimethyl sulfoxide
DTNP	2,2'-Dithiobis(5-nitropyridine)
DTT	Dithiothreitol
EDA	Epidermal growth factor receptor dimerization arm
EGF	Epidermal growth factor
EGFR	Epidermal growth factor receptor
ErbB	Avian erythroblastic leukemia viral oncogene homolog
Fab	Fragment antigen-binding

FAM	5(6)-Carboxyfluorescein
FBS	Fetal bovine serum
FITC	Fluorescein isothiocyanate
FGFR	Fibroblast growth factor receptor
Fmoc	9-Fluorenylmethoxycarbonyl
gp120	Surface glycoprotein 120
GPCR	G-protein-coupled receptor
Grb2	Growth factor receptor-bound protein 2
HB-EGF	Heparin-binding EGF-like growth factor
HCTU	O-(6-Chlorobenzotriazol-1-yl)-N,N,N′,N′-tetramethyluronium hexafluorophosphate
Her2 (ErbB2)	Human epidermal growth factor receptor 2
hDM2	Human double minute protein 2
HIV-1	Human immunodeficiency virus type 1
HPLC	High performance liquid chromatography
Kit	Mast/stem cell growth factor receptor Kit
LC/MS (LC-MS)	Liquid chromatography-mass spectrometry
MAPK	Mitogen activated protein kinase
MBHA	4-Methylbenzyhydrylamine
MDM2	Murine double minute protein 2
MIG6	Mitogen-inducible gene 6 protein
Mtt	4-Methyltrityl
MTT	Methylthiazolyldiphenyl-tetrazolium bromide

NMP	1-Methyl-2-pyrrolidinone
Npys	3-Nitro-2-pyridinesulfenyl
Notch	Neurogenic locus notch homolog protein
Orn	Ornithine
p53	Cellular tumor antigen p53
PBS	Phosphate buffered saline
PDB	Protein databank
PEG	Polyethylene glycol
Pg	Propargyl glycine
PKA	Protein kinase A
PLA	Proximity ligation assay
PMB	*para*-Methoxybenzyl
PI3K	Phosphoinositide 3-kinase
PLC-γ	Phospholipase C-gamma
PPI	Protein-protein interaction
PVDF	Polyvinylidene fluoride
RCM	Ring closing metathesis
RPMI	Roswell Park Memorial Institute medium
RuAAC	Ruthenium-catalyzed azide-alkyne cycloaddition
SD	Standard deviation
SDS-PAGE	Sodium dodecyl sulfate-polyacrylamide gel electrophoresis
Sec	Selenocysteine
SEM	Standard error of the mean

SH2	Src homology 2 domain
SHC1	SHC-transforming protein 1
SMAC	Second mitochondria-derived activator of caspases
STAT3	Signal transducer and activator of transcription 3
TAMRA	5(6)-Carboxytetramethylrhodamine
TFA	Trifluoroacetic acid
TGF-α	Transforming growth factor-alpha
THF	Tetrahydrofuran
TLC	Thin layer chromatography
TRITC	Tetramethylrhodamine isothiocyanate
TrkA	Tyrosine kinase receptor A / high affinity nerve growth factor receptor
VEGFR	Vascular endothelial growth factor receptor
WASF3	Wiskott-Aldrich syndrome protein family member 3
XIAP	X-linked inhibitor of apoptosis protein
YFP	Yellow fluorescent protein

CHAPTER 1

INTRODUCTION AND LITERATURE REVIEW

1.1 Statement of Purpose

Protein-protein interactions (PPIs) have critical roles in the regulation of signal transduction in the cell. As such, these interactions offer promising targets for the development of modulators of cell signaling. A variety of PPI disruptors are reported in the literature as molecular probes for studying signal transduction pathways or as potential therapeutic agents. While many strategies for disrupting PPIs are available, one attractive strategy is the design of constrained peptides targeting PPIs. The interaction between proteins is often stabilized by protein features with a defined secondary structure, and these secondary structures can serve as templates for the design of peptides to bind the interface.

Constrained peptides are suitable for mimicry of secondary structures that contribute to PPIs as they possess all of the functional groups that are present within the protein features. Further, constraints can be applied within the backbone, between side chains or between termini to help stabilize the desired binding conformation. Many of these stabilizing chemistries have been applied to the development of peptides targeting helix-mediated interactions by constraining helical structures. However, β-loop-mediated interactions offer promising templates for the design of PPI disruptors as well, yet there are significantly fewer reports of peptides disrupting β-loop-mediated PPIs in the literature.

The ectodomain of the epidermal growth factor receptor (EGFR) dimer is an extensively studied and therapeutically relevant example of a PPI largely stabilized by interactions of a β-loop. Ligand-induced EGFR dimerization leads to activation of the kinase, which promotes signaling pathways involved in proliferation and survival. While FDA approved inhibitors of EGFR are used in the clinic, these molecules function by blocking ligand or substrate binding. These sites are susceptible to resistance mutations and provide little insight into the role of dimerization in EGFR signaling. Thus, disruptors that specifically target the dimerization interface are promising probes of EGFR dimerization and may enable targeting of additional EGFR mutants.

Peptides targeting the ectodomain of EGFR have been reported; however, these peptides either lack structural constraints or possess a disulfide bridge which is prone to reduction. A variety of chemistries with greater stability may be incorporated into the peptide to constrain the structure while enhancing peptide stability. For example, the selenylsulfide bond, similar in structure and chemical nature to the disulfide, is less prone to reduction and may offer a more stable alternative to the disulfide bond. Alternatively, the triazole is an irreversible bond formed between azido- and alkynyl-amino acids. As these constraints differ greatly in size and structure, altering the constraints in a peptide may affect the overall conformation and stability of the cyclized peptide product. Thus, the aim of this research is to test highly stable chemical constraints to develop cyclic peptides mimicking a β-turn fold where the EGFR dimerization arm serves as a template. The results of this research may have broad applications in the design of constrained peptides for the disruption of β-loop mediated interactions, while also serving as molecular probes of EGFR dimerization (Figure 1.1). Furthermore, beyond the scope of

this project, additional testing and optimization of these peptides and their analogs may lead to the development of potential anticancer therapeutics.

1.2 Protein-Protein Interactions (PPIs) as Therapeutic Targets

Protein-protein interactions (PPIs) play critical roles in the regulation of cellular processes, functioning in transcriptional control, spatiotemporal regulation, and modulation of signal transduction [1-4]. As key regulators of signaling pathways, PPIs are attractive targets for the design of molecular probes to perturb protein function so as to elucidate their roles and regulation in the cellular environment. Additionally, signaling pathways may be dysregulated in various disease states through changes in expression or mutation of key proteins. Thus, modulation of signaling pathways by PPI disruption is a promising strategy for the development of potential therapeutics [5-11]. Numerous studies have focused on the development of molecular disruptors of protein-protein interactions that contribute to cancer phenotypes, including those involved in transcription, programmed cell death, and receptor mediated signal transduction [6-13].

Changes in transcriptional regulation, including alterations in expression or interactions of transcription factors, can lead to increased activation of oncogenes that promote cell proliferation and survival in cancer [14,15]. Thus, many efforts have focused on disruption of transcription factor interactions, including those of the estrogen receptor, STAT3 and tumor suppressor p53, so as to restore normal cellular function [16-19]. The estrogen receptor is a nuclear receptor that functions as a transcription factor upon activation [17]. Activation is driven by binding of ligands and coactivator proteins to promote transcriptional activity. Disruption of the interaction between coactivator proteins and the estrogen receptor has attracted interest as a potential strategy for

inhibition of estrogen receptor mediated transcription [16,17,20-25]. In contrast to the estrogen receptor, the tumor suppressor p53 functions as a transcription factor by activating genes involved in DNA repair and apoptosis [18,26-28]. However, the interaction of p53 with human double minute protein 2 (hDM2) or its homologs inhibits p53 and promotes its degradation, thereby blocking p53 tumor suppressor activity. Thus, the interaction between p53 and hDM2 proteins has received much attention as a target for anticancer therapeutics, resulting in the development of numerous disruptors of this interaction, some of which are currently in clinical trials [10,18,27-38].

In addition to aberrant transcriptional regulation, protein-protein interactions have significant roles in apoptosis evasion. The B-cell CLL/lymphoma 2 (Bcl-2) family of proteins includes both pro-apoptotic and anti-apoptotic proteins that regulate programmed cell death [39,40]. Anti-apoptotic proteins such as Bcl-2 and Bcl-X_L bind and inhibit pro-apoptotic proteins such as BAK or BAX. Other Bcl-2 members, such as BID, BAD and BIM, block this interaction and activate BAK or BAX. Dysregulation of Bcl-2 family members can lead to evasion of programmed cell death in cancer. Thus, disruptors of these interactions show promise in restoring pro-apoptotic pathways [9,39-44]. Caspase-9 also has a critical role in activation of apoptosis and is inhibited by interactions with X chromosome-linked inhibitor of apoptosis proteins (XIAPs) [45]. This PPI is blocked by second mitochondria-derived activator of caspases (SMAC), which binds to XIAP and prevents inhibition of caspase-9. Further regulation of SMAC proteins is achieved by binding of cellular IAPs (c-IAPs), which block the interaction between SMAC and XIAP. As dysregulation of IAPs contributes to apoptosis evasion in cancer, these interactions have received much attention as therapeutic targets [6,8-

10,45,46]. Several disruptors of the Bcl-2 and IAP families have reached Phase I and II clinical trials [9,10].

Protein-protein interactions of membrane bound receptors also play critical roles in cellular processes through activation of signal transduction cascades. The primary step in the activation of membrane receptors, such as G-protein-coupled receptors (GPCRs) and growth factor receptors, is binding of extracellular ligands, many of which have served as templates for the design of receptor antagonists [42]. However, further regulation of receptor signaling is accomplished through additional protein-protein interactions [8,10]. For example, receptor tyrosine kinases are regulated by binding of growth factors, oligomerization events and association of intracellular proteins [47-49]. Each interaction may be a potential target for the design of PPI disruptors. The ErbB family of receptor tyrosine kinases, including epidermal growth factor receptor (EGFR) and ErbB2, is extensively studied and currently targeted by several anticancer agents on the market [50,51]. Ligand activation of ErbB members promotes dimerization, in which both the receptor and intracellular kinase contribute interactions [48,49,52-55]. As ErbB dimerization is associated with kinase activation, these dimer interactions have become attractive targets for allosteric inhibition of kinase activity [56-61].

The aforementioned protein-protein interactions represent only a subset of the numerous interactions that are involved in oncogenic pathways. A variety of methods are used to target these interactions, including high throughput screening for small molecules, fragment based design, antibody development, and the rational design of small molecules and peptides to mimic secondary structures involved in the interactions [5,8,11,42,62-64]. Mimicry of secondary structures is a particularly attractive strategy

for the development of PPI disruptors as these structures provide well-defined templates for the design of molecules binding to the interface. Many PPIs, including those of the Bcl-2 family, hDM2, and estrogen receptor, are mediated by helix interactions and have been targeted with small molecules or peptides designed to mimic helices present at the interface (Figure 1.2) [4,63,65]. Nevertheless, protein-protein interactions can also be mediated by non-helical interactions, including those of strands, turns or loops [66-69]. Many non-helical interactions are contributed by receptor ligands, protease inhibitors, or epitope binding regions of antibodies [42,70-75]. However, one prime example of a β-loop that stabilizes a non-ligand PPI is the dimerization arm of the EGFR. The dimerization arm contributes a majority of the energy required for binding [54]. Disruption of this interface is reported to block EGFR activation, and an FDA approved monoclonal antibody targeting the same site on ErbB2 validates this approach [57,58,60,61,76]. Thus, development of dimerization arm mimics to disrupt the EGFR dimer may provide novel molecular probes of EGFR signaling pathways, promising anticancer therapeutics, and strategies to disrupt additional β-loop mediated interactions, such as CD4-gp120 in HIV-1 [62,77].

1.3 EGFR Structure and Activation

The Epidermal Growth Factor Receptor (EGFR) is a well-characterized example of a protein that is regulated by a β-loop-mediated dimerization event. Not only does this protein have significant contributions to signal transduction pathways that regulate cell growth and survival, but EGFR is also a validated target for anticancer therapeutics [51]. Thus, developing disruptors of EGFR dimerization may be a useful strategy for studying

its role in signal transduction pathways and cellular processes while also providing an alternative targeting strategy for the development of cancer therapeutics.

Epidermal growth factor receptor (EGFR), a member of the ErbB family of receptor tyrosine kinases, is composed of three major domains: the extracellular ligand binding domain, the transmembrane domain, and an intracellular kinase domain [78]. The extracellular ligand binding domain contains four subdomains, of which domain II and IV are cysteine rich domains. EGFR ligands, including epidermal growth factor (EGF), heparin-binding EGF-like growth factor (HB-EGF) and transforming growth factor alpha (TGF-α), make contacts with domains I and III in the activated receptor [50,52,55,79]. Ligand binding promotes and stabilizes a conformational rearrangement of the receptor from the inactive to the active state [52-54,80,81]. In the inactive conformation, the receptor is folded to bury the surface of domain II against domain IV, leaving domains I and III accessible to ligand binding (Figure 1.3a). Upon ligand binding, domains I and II pivot around domain III, exposing the surface of domain II (Figure 1.3b). Domain II is critical for the stabilization of the receptor dimer, contributing over 90% of the energy required for dimerization, with over 75% of the energy contributed by a β-loop structure termed the dimerization arm [54].

Receptor dimerization then promotes formation of the asymmetric kinase dimer. The kinase dimer is stabilized by interactions between the N-lobe of one kinase and the C-lobe of the other kinase and is further regulated by interactions of the juxtamembrane region (Figure 1.3c) [82-84]. Studies indicate that in the asymmetric kinase dimer, one kinase is catalytically active, while the other kinase receives the phosphorylation on C-terminal tyrosine residues [85,86]. These C-terminal tyrosine residues then serve as

docking sites for intracellular proteins that possess the Src homology 2 domain (SH2). Proteins such as growth factor receptor-bound protein 2 (Grb2) or SHC-transforming protein 1 (SHC1) can act as recruiters for additional signaling proteins, while other proteins such as phospholipase C-gamma (PLC-γ) can be directly phosphorylated by EGFR [87]. Phosphorylation of intracellular proteins associated with EGFR then activates various signaling cascades including the PI3K/Akt, PLC-γ, Ras/MAPK, and STAT3 pathways [51,88,89]. As these pathways have roles in cell growth and survival, increased activation by dysregulation of EGFR can promote proliferation and apoptosis evasion in cancer.

The regulation of EGFR activation and signaling is highly complex [78,90,91]. Recent studies suggest that the plasma membrane has a regulatory role in EGFR activation, as interaction of anionic lipids with basic juxtamembrane residues may help to stabilize and activate the kinase dimer [92]. Additionally, EGFR may form heterodimers with other ErbB family members, diversifying signaling through specific roles of individual kinase domains in the heterodimer [85,93]. Furthermore, EGFR can exist as inactive preformed dimers, higher order oligomeric clusters, or ligand-independent active dimers [92,94-100]. Regarding ligand binding, EGFR can have high or low affinity for ligands, and binding of two ligands may not be necessary for activation [101,102]. The variety of regulatory mechanisms, ligand binding affinities and oligomeric states reveal the complexity of EGFR modulation. This high complexity necessitates the development of molecular probes to perturb individual features involved in the allosteric control of EGFR activation and signaling. Current strategies primarily focus on blocking ligand or ATP binding to inhibit kinase activity, which may have limited applications in evaluating

the roles of the many PPIs involved in EGFR regulation. Thus, the development of PPI disruptors targeting features involved in the allosteric control of EGFR kinase activity may provide additional insight into their regulatory functions and role in EGFR signaling pathways.

1.4 Current EGFR Targeting Strategies

EGFR activates many signaling pathways contributing to cell proliferation, migration and programmed cell death, including pathways such as PLC-γ, PI3K/Akt, and Ras/MAPK pathways [51,88,89]. As such, normal levels of EGFR are required for healthy development and maintenance of epithelial and neuronal tissues, while dysregulation of EGFR is associated with disease, primarily cancer [50,51,89,103,104]. EGFR is overexpressed or mutated in a variety of cancers, including non-small cell lung, breast, pancreatic and colorectal cancers [51,105]. This increase in EGFR activity promotes oncogenic signaling pathways. As such, EGFR has become a well-validated target for the design of therapeutics to treat EGFR-overexpressing cancers.

FDA approved EGFR-targeted therapeutics fall within two classes: small molecule tyrosine kinase inhibitors, shown in Figure 1.4, and monoclonal antibodies. The first approved EGFR inhibitor, gefitinib (Iressa®), targets the ATP-binding site of EGFR (Figure 1.5), acting as a ATP-competitive inhibitor with a quinazoline core [106]. As a result of its success as an inhibitor of EGFR activation, gefitinib was approved in 2003 for treatment of metastatic non-small cell lung cancer (NSCLC) in patients who no longer respond to platinum therapies or docetaxel [107,108]. Although it was later withdrawn from the market due to a lack of perceived clinical benefit, gefitinib regained approval in 2015 for the treatment of metastatic non-small cell lung cancer in patients with exon 19

deletions or the L858R mutation [109]. Like gefitinib, the ATP-competitive EGFR inhibitors erlotinib (Tarceva®) and afatinib (Gilotrif®) and the dual EGFR/ErbB2 inhibitor lapatinib (Tykerb®) also possess a quinazoline core [110-115]. Erlotinib was approved in 2004 for the treatment of metastatic NSCLC after disease progression from platinum therapies or docetaxel, and in 2013, it gained a second approval for the treatment of metastatic NSCLC in patients with exon 19 deletions or L858R mutations [110,111]. Although lapatinib inhibits both EGFR and ErbB2, it was approved in 2007 for the treatment of ErbB2 overexpressing metastatic breast cancer [112,113]. Afatinib was approved in 2013 for the treatment of metastatic NSCLC with exon19 deletions or the L858R mutation activating mutation [114,115]. In contrast to gefitinib and erlotinib, afatinib is an irreversible inhibitor that binds the active site of EGFR and forms a covalent thioether bond with Cys797 (Figure 1.5). It has also demonstrated activity against ErbB2 and ErbB4. The efficacy of EGFR-targeted tyrosine kinase inhibitors suffers in patients with the T790M gatekeeper mutation, which occurs in approximately 50% of NSCLC patients with resistance to tyrosine kinase inhibitors [116,117]. However, in 2015, the FDA granted accelerated approval for osimertinib (Tagrisso®) in metastatic NSCLC with the EGFR T790M mutant [118,119].

In addition to targeting the EGFR kinase with small molecule tyrosine kinase inhibitors, the ectodomain of EGFR can be targeted with monoclonal antibodies. The first approved monoclonal antibody targeting a member of the ErbB family was trastuzumab (Herceptin®), an ErbB2 targeted therapy that received FDA approval for treatment of metastatic breast cancer in 1998 [120]. Trastuzumab binds to the juxtamembrane region of the ErbB2 receptor, thereby blocking dimerization (Figure1.6) [120,121]. In 2010,

trastuzumab received a second approval for the treatment of ErbB2 positive gastric or gastroesophageal junction adenocarcinoma [122]. With the success of trastuzumab in the clinic, the ErbB family emerged as promising targets for the development of novel anticancer therapeutics, leading to the development and approval of cetuximab (Erbitux®), the first EGFR targeted monoclonal antibody [120]. Cetuximab is a human/murine chimeric antibody that blocks ligand binding, conformational rearrangement and activation of EGFR [123]. In 2004, cetuximab was approved for the treatment of metastatic colorectal carcinoma (Figure1.6) [120]. In 2006, cetuximab was also approved for the treatment of squamous cell carcinoma of the head and neck [124]. Following the development of cetuximab, panitumumab (Vectibix®) and necitumumab (Portrazza®) emerged as humanized antibodies targeting ligand binding. Panitumumab was approved in 2006 for metastatic colorectal carcinoma, while necitumumab was approved in 2015 for metastatic non-small cell lung cancer [118,125]. Although, no antibodies are approved that target the EGFR dimer interface, pertuzumab (Perjeta®) targets the dimerization arm of domain II in ErbB2, thereby blocking the interface and preventing dimerization with members of the ErbB family (Figure1.6) [76]. Pertuzumab was approved in 2012 for the treatment of ErbB2 positive metastatic breast cancer [76,126]. The success of pertuzumab helped to establish the disruption of the ErbB dimer interface as a promising approach in anticancer therapeutic development.

1.5 Peptides as EGFR Dimer Disruptors

Although there are many EGFR-targeted therapies on the market, there is a need to develop alternative targeting strategies against EGFR mutants. As acquired resistance is observed in patients treated with anti-EGFR therapies [51,127], targeting alternative

surfaces for allosteric modulation of EGFR may provide additional means for blocking receptor signaling. These strategies may not necessarily be effective against acquired resistance from activation of alternative signaling pathways; however, they provide alternative therapies to target EGFR in patients with mutant forms of EGFR [127]. Thus, many efforts are underway to develop allosteric modulators of EGFR signaling. MIG6, an endogenously expressed peptide inhibitor of EGFR, binds to an allosteric site in the kinase domain of EGFR to inhibit activation [128]. MIG6 demonstrates that peptides targeting these allosteric sites are useful tools for the regulation of EGFR. Two other peptides have been developed to bind the intracellular domain of EGFR, both targeting juxtamembrane interactions. One peptide is an unconstrained peptide bearing a cell-penetrating TAT sequence, which was reported to disrupt dimerization and activation of EGFR [59]. Another constrained helical peptide was later developed to target the same region of EGFR [129].

The extracellular domain of EGFR is an attractive target, as cell penetration is not required for molecules targeting this surface. Since the receptor dimer is also reported to facilitate activation of the EGFR kinase, disruption of this interaction may modulate EGFR signaling activity [78]. As mutations are observed that cause resistance to ligand binding inhibitors such as cetuximab, dimer disruptors may also provide an alternative to ligand binding inhibition [105]. Several features of the EGFR ectodomain contribute interactions in the dimer, including loops of domain II and IV, which have served as templates for the design of peptides targeting the extracellular domain of EGFR. One study evaluates peptides mimicking domain IV of EGFR, which showed modest inhibition of EGFR activation [56]. However, domain IV was shown to have minor

contributions to dimer stabilization and may be a less effective targeting strategy [54]. The dimerization arm of domain II, on the other hand, is expected to contribute the most binding energy for dimerization, and may be a more favorable target. In two studies dendrimers bearing peptide sequences mimicking the ErbB3 dimerization arm and a loop in the EGFR dimerization arm binding site were reported [58,61]. Although these peptides displayed modest inhibitory activity against EGFR phosphorylation, the peptide conformation was not constrained, which may limit their activity and stability *in vivo*. In two additional studies a dimerization arm mimic constrained by a disulfide bond and a similar peptide bearing D-amino acids were developed [57,60]. Although these peptides were reported to have activity, disulfide bonds are prone to reduction, which may affect the stability of the peptides. Additionally, D-amino acids are more costly, and although they enhance proteolytic stability, they may not maintain the structural stability in the absence of the disulfide. Therefore, a more stable structural constraint offers a promising alternative to these peptide stabilization strategies.

1.6 Constraints for Stabilization of Peptides Targeting PPIs

The design of peptides mimicking critical features that stabilize PPIs is a promising strategy for PPI disruption. Peptides possess all of the functional groups that are present in these features, and with chemical modification, they can be constrained to mimic preferred binding conformations [63,130]. Furthermore, modifications may enhance cell penetration of these molecules, enabling targeting of intracellular PPIs that are inaccessible to antibodies [131].

One of the major disadvantages that initially slowed the development of peptide-based inhibitors and therapeutics was their instability. In solution, and out of the folded

protein context, peptides are highly flexible, exhibiting disordered structures that may be unfavorable for binding [40,132]. The flexible peptide backbone also becomes more accessible to proteases, decreasing their metabolic stability and creating an additional disadvantage for use *in vivo*. However, advances in peptide chemistry have led to the development of backbone modifications and cyclization chemistries that improve the resistance of peptides to proteolytic degradation and reduce the conformational freedom of the peptide backbone, potentially enabling the peptide to adopt preferred conformations for binding [130,132].

Although the focus of this research is on development of peptides mimicking a β-loop structure, it is important to highlight the chemistries that are used to stabilize additional secondary structures, as these strategies may be based on or applied to β-loop stabilization. A variety of modifications can be incorporated in the peptide to stabilize a helical conformation, thereby enabling the targeting of PPIs mediated by helix interactions [40,65,130,133,134]. The hydrogen bond surrogate has been used to stabilize the helical structure by mimicking the natural backbone hydrogen bonds of the helix [130]. In this strategy, a covalent bridge mimics the hydrogen bond between the amide nitrogen and the carbonyl oxygen at the i and i + 4 positions, respectively. Hydrazine, alkenyl, disulfide, or thioether bridges have been incorporated as hydrogen bond surrogates [130]. This strategy offers the advantage of stabilizing the helical structure without replacing potentially critical side chain residues. As an alternative, β-amino acids have been incorporated into the backbone to promote helicity [135]. Both the hydrogen bond surrogate and β-peptide strategies enable the stabilization of helical peptides without the loss of the side chain interactions. While the hydrogen-bond surrogate has

been applied to stabilizing helical turns, it may also have applications in mimicking hydrogen bonds of a β-loop or hairpin structure.

As an alternative, side-chains can also be modified to create a bridge between turns of the helix. This strategy often involves the incorporation of non-natural amino acids or the use of orthogonal protection schemes for selective formation of the bridge between amino acid side chains [132]. These bridges can be formed directly between side chains or by reactions of side chains with a bifunctional linker [133]. One of the most attractive examples of a helix stabilizing modification is the all-hydrocarbon staple [34,43,44,136,137]. This staple is formed between two alkenyl side chains by olefin ring closing metathesis using a ruthenium-based catalyst (Figure 1.7). An advantage of this modification is that it may help to promote uptake of the peptides into the cell, enabling the access to intracellular targets [131,136]. However, stapling alone may not be enough to promote uptake [40,130]. The hydrocarbon staple itself may also contribute binding interactions at the interface [138]. Some of the first examples of PPI disruptor peptides stabilized using this chemistry include a disruptor of the MDM2-p53 interaction and mimics of the BID-Bcl-2 and BID-BAX interaction [34,43,44]. This strategy was also applied to peptides targeting Notch, PKA-AKAP, and WASF3-CYFIP1 interactions [137,139,140]. Recently, the hydrocarbon staple was applied to a peptide targeting the juxtamembrane region of EGFR to prevent kinase activation [129].

Similar to the hydrocarbon staple, a triazolyl bridge can be incorporated between the i and i + 4 positions of the peptide to stabilize helices [41,133]. This strategy utilizes amino acids bearing azide and alkyne functionalities and can be performed on resin using a copper catalyst (Figure 1.7). The triazolyl staple has been incorporated into a helical

peptide targeting the β-catenin-BCL9 interaction [41]. In a similar strategy, peptides can be stabilized using a double stapling technique, in which an adaptor molecule bearing two alkyne functionalities, such as 3,5-diethynylbenzene or 1,5-hexadiyne, is reacted with two azido-amino acids in the peptide sequence [133]. The azido-amino acids can be incorporated at the i and i + 4 or the i and i + 7 positions. Triazolyl-stapled peptides may require additional modification in order to access intracellular targets.

Lactams can also be used to create a bridge between turns of a helix (Figure 1.7) [133]. This chemistry requires orthogonal deprotection schemes for the selective deprotection of side chains bearing the amino and carboxyl functionalities. One drawback of this method is that the lactam bridge may be susceptible to degradation. The disulfide bond has also been tested as a strategy for stabilizing helical structures (Figure 1.7) [132]. However, this bond is susceptible to reduction and disulfide exchange reactions, making it less ideal for targets in the reducing intracellular environment [133]. Although strategies replacing peptide side chains can potentially disrupt interactions with the protein interface, analysis of the binding interface can aid in positioning the bridge between non-critical residues.

In addition to helices, β-strands are also promising templates for the development of peptide-based PPI disruptors; however, a single linear peptide strand is inherently more difficult to stabilize [134,141]. Chemistries have been developed, such as tetrahydropyridazinedione, 1,6-dihydro-3(2*H*)-pyridinone and piperidine-piperidinone backbones, that help to promote β-strand conformations [42,141,142]. However, interactions between β-strands and the interface may include hydrogen-bonding between backbone atoms. Thus, backbone modifications stabilizing the strand structure may alter

this hydrogen-bonding network. As an alternative, strands may be stabilized by side-chain-to-side-chain macrocyclization [130,141]. Since these chemistries help to stabilize the β-strand conformation, they may also be useful modifications for the stabilization of the strands within a β-loop or hairpin.

Loop stabilizing chemistries also have a variety of applications in the design of peptides targeting protein-protein interactions. These chemistries are similar to helix chemistries and may be applied to macrocyclic peptides mimicking β-loops or hairpins [42,133]. These chemistries can be used in head-to-tail cyclization, side-chain-to-side-chain cyclization or dimerization [132]. A common strategy that does not require non-natural amino acids or catalytic reactions is macrocyclization via disulfide bond formation (Figure 1.7). [132]. Cysteine residues can be incorporated at different positions within the peptide sequence, and the disulfide bond is formed using oxidative conditions. This strategy has been incorporated into a peptide targeting EGFR dimerization as well as cyclotides, conotoxins and peptide therapeutics such as oxytocin and desmopressin [57,60,132,143]. However, disulfides are susceptible to reduction and are thus less stable in reducing environments. As an alternative, selenylsulfide and diselenide chemistries can be applied to the cyclization of peptides with enhanced stability in reducing conditions (Figure 1.7) [143-145].

The amide bond is also easily formed on resin using orthogonal protection schemes such as those listed for helical peptides bearing a lactam staple [133,146]. This strategy can also be employed for head-to-tail cyclization. Head-to-tail cyclization is typically performed off-resin, thus it is necessary to select resins that allow for cleavage of a fully protected peptide upon cleavage [146]. Conditions for the reaction must also be

selected to reduce dimerization of peptides, which typically requires low concentrations that may hinder the reaction progress [146].

The triazolyl-bridge is another cyclization strategy that can either be formed via side-chain-to-side-chain cyclization, head-to-tail cyclization or side-chain-to-tail cyclization [147,148]. There are two types of triazolyl-bridges that are formed using azide-alkyne cycloaddition chemistry. The 1,4-disubstituted triazole can be selectively formed using a copper catalyst, while the 1,5-disubstituted triazole is selectively formed using a pentamethylcyclopentadienyl ruthenium chloride catalyst (Figure 1.7) [149,150]. The pentamethylcyclopentadiene group is critical for the regioselectivity of the ruthenium catalysts [150]. An alternative method for 1,5-triazole formation was reported using azide and phosphorane chemistry [147,151-153]. Triazolyl bridges have been applied to the macrocyclization of antimicrobial peptides and protease inhibitors with loop or hairpin structures [154,155]. As an alternative to the triazole, olefin metathesis has also been employed in the stabilization of macrocyclic peptides; however, the efficiency of this reaction is dependent on the length of the side chain [156-160].

Although there are numerous macrocyclization chemistries that can be used to stabilize β-loop structures, triazole and selenylsulfide chemistries were selected for the stabilization of the EGFR dimerization arm mimics in this research. The selenylsulfide chemistry was selected because it is similar in structure and chemical nature to the previously described disulfide [57,60]; however, it is more stable to reducing conditions [144]. The triazole was selected as an irreversible macrocyclization technique to offer greater stability while also increasing solubility. Furthermore, by varying the positions of the amino acids and the number of methylene units in the azido-amino acid side chains, a

panel of structures could be developed. For future perspectives, the hydrocarbon staple is also a promising alternative, yet the hydrophobic nature of the bridge may reduce solubility.

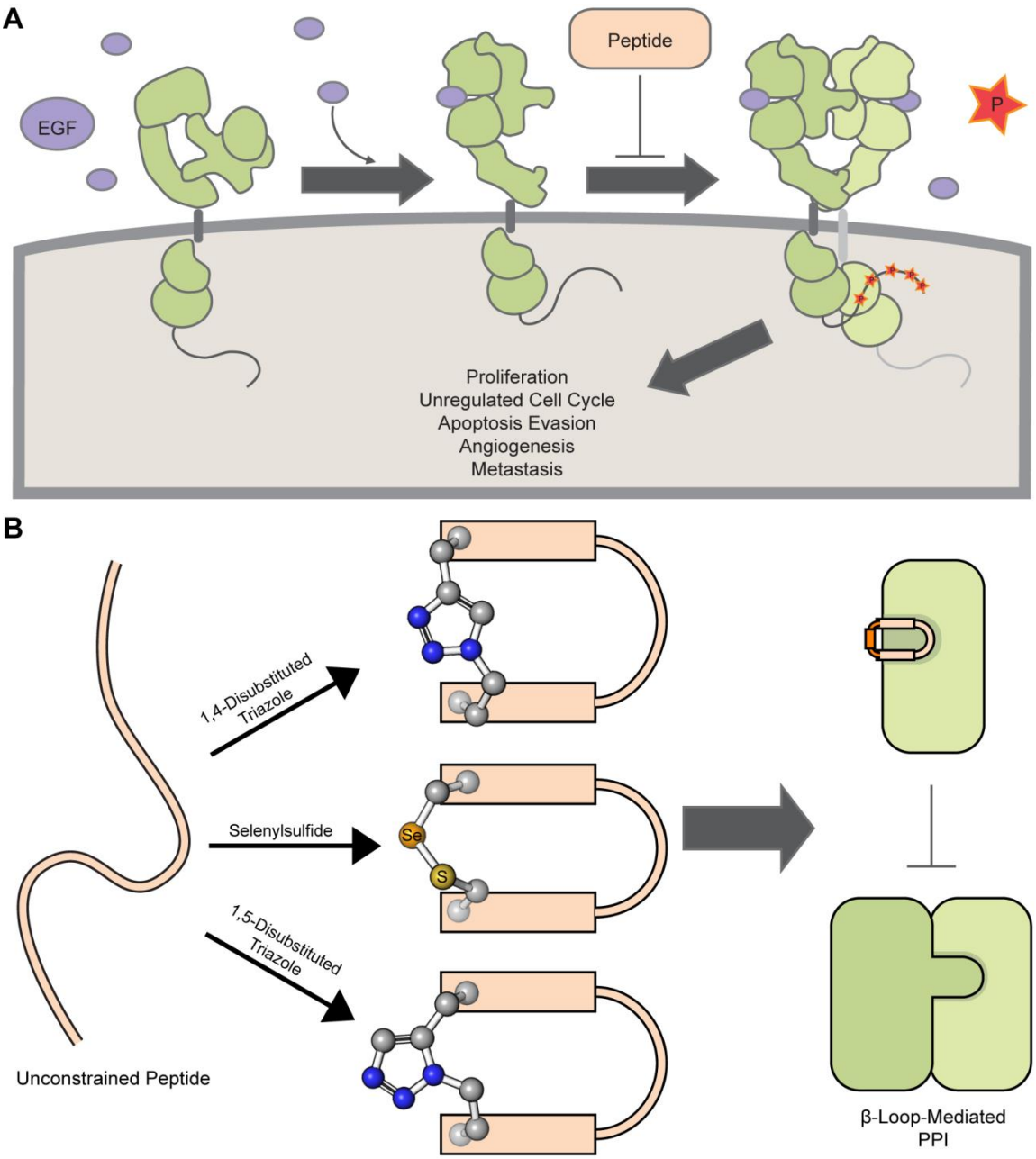

FIGURE 1.1 Development of Cyclic Peptides to Block Loop-Mediated PPIs
(a) Epidermal growth factor receptor (EGFR) signaling contributes to proliferative and survival pathways in the cell. Ligand binding promotes dimerization, which activates the kinase domain to initiate signaling cascades. Disruption of dimerization with peptides may be a promising strategy for blocking EGFR activation and signaling. (b) Peptides blocking beta-loop mediated PPIs can be designed using the beta-loop feature as a template. Different chemical constraints can be incorporated into the peptide sequence to stabilize the beta-loop fold of the peptide. These peptides may then occlude the interface and block the protein-protein interaction.

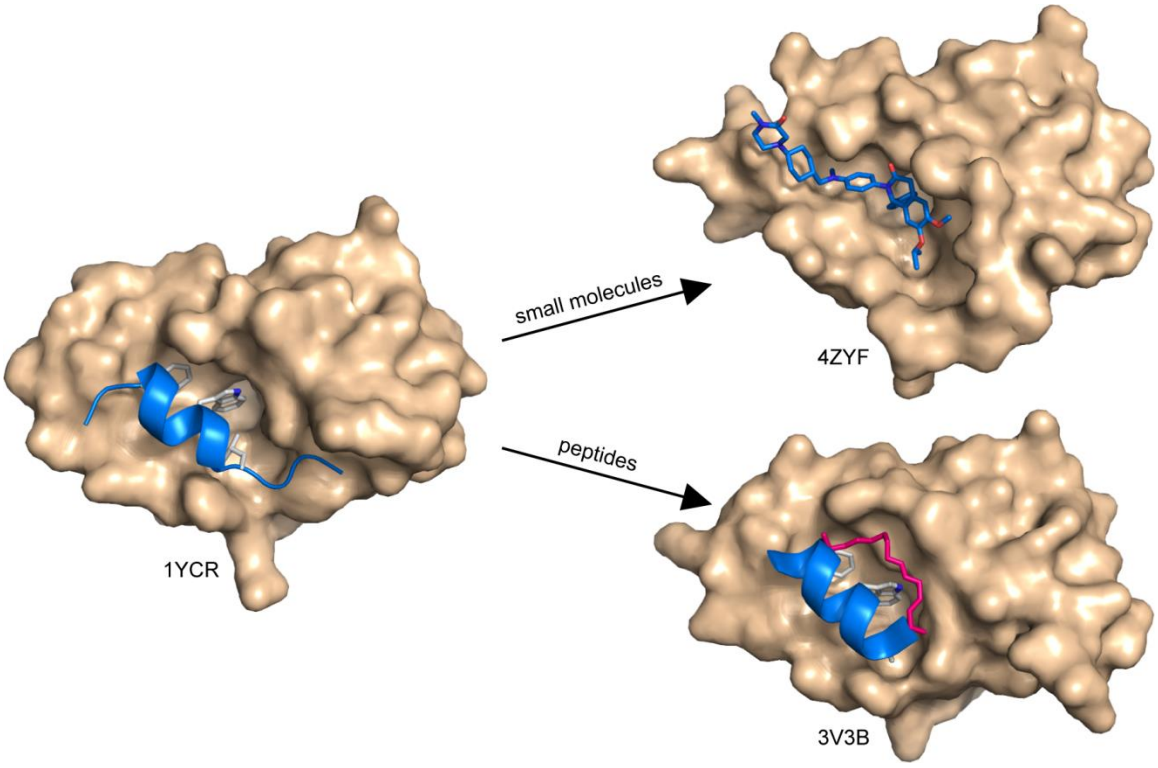

FIGURE 1.2 Small Molecule and Peptide Disruptors of p53-MDM2
The helical region of p53 (PBD: 1YCR), small molecule CGM097 (PDB: 4ZYF) and stapled peptide SAH-p53-8 (PDB: 3V3B) are shown in blue, bound to MDM2. CGM097 is currently in Phase I clinical trials (NCT01760525) demonstrating the therapeutic potential of PPI disruption.

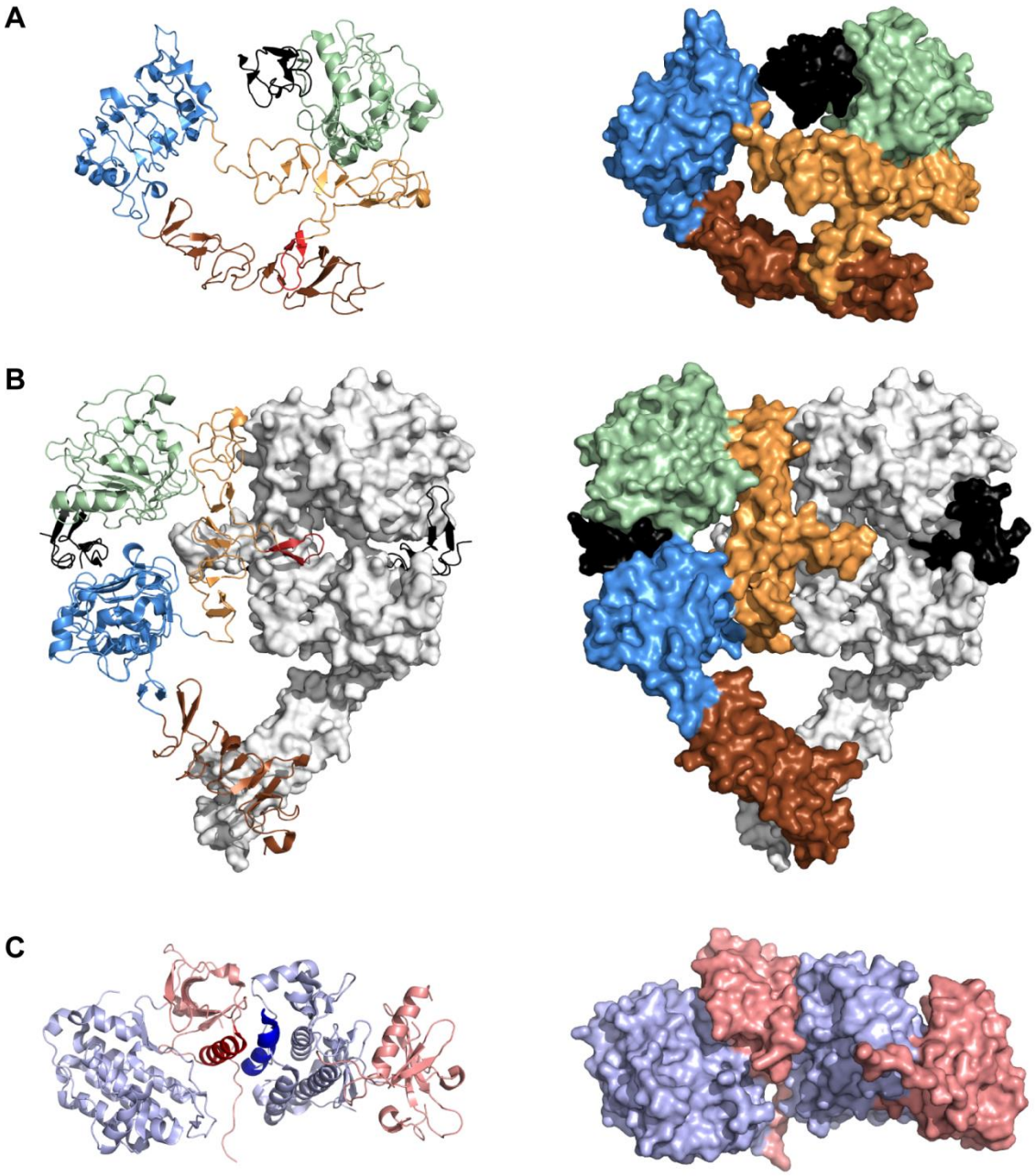

FIGURE 1.3 EGFR Crystal Structures
(a) The inactive EGFR ectodomain (PDB: 1NQL). Domain I (green), domain II (orange), domain III (blue), and domain IV (brown) and EGF (black) are shown. The dimerization arm is highlighted in red in the cartoon representation. (b) The EGFR dimer is shown using the same color scheme, with one monomer in cartoon representation, and the surface representation of the other is shown in white (PDB: 3NJP). (c) The EGFR kinase domain is shown with the N-lobes colored pink and the C-lobes in light blue (PDB: 2GS6). The H-helix (blue) and interacts with the C-helix (red) in the asymmetric dimer.

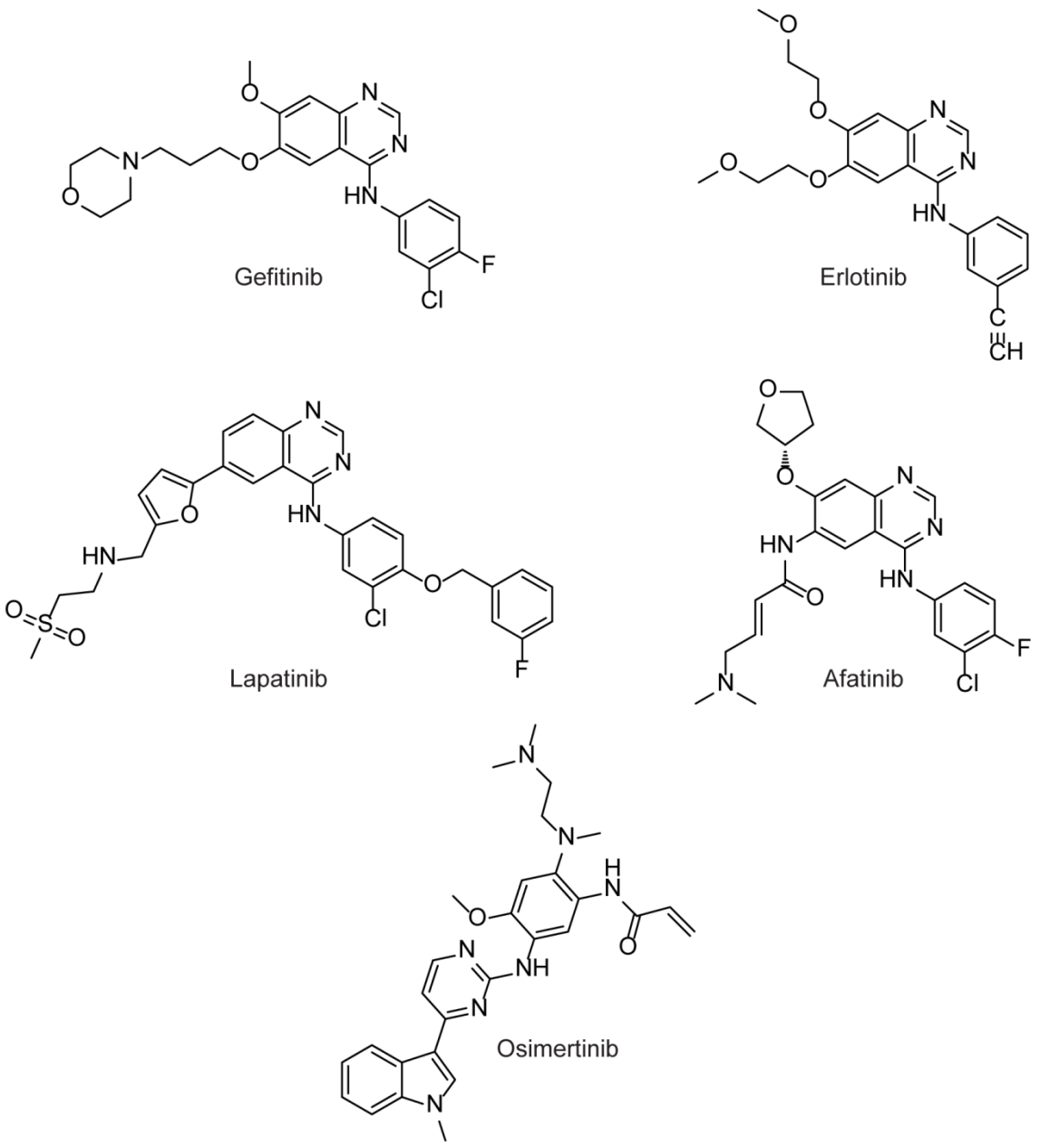

FIGURE 1.4 Current FDA Approved EGFR Tyrosine Kinase Inhibitors
The structures of current FDA approved EGFR-targeted tyrosine kinase inhibitors are shown. Osimertinib is the first approved inhibitor targeting the EGFR T790M mutant.

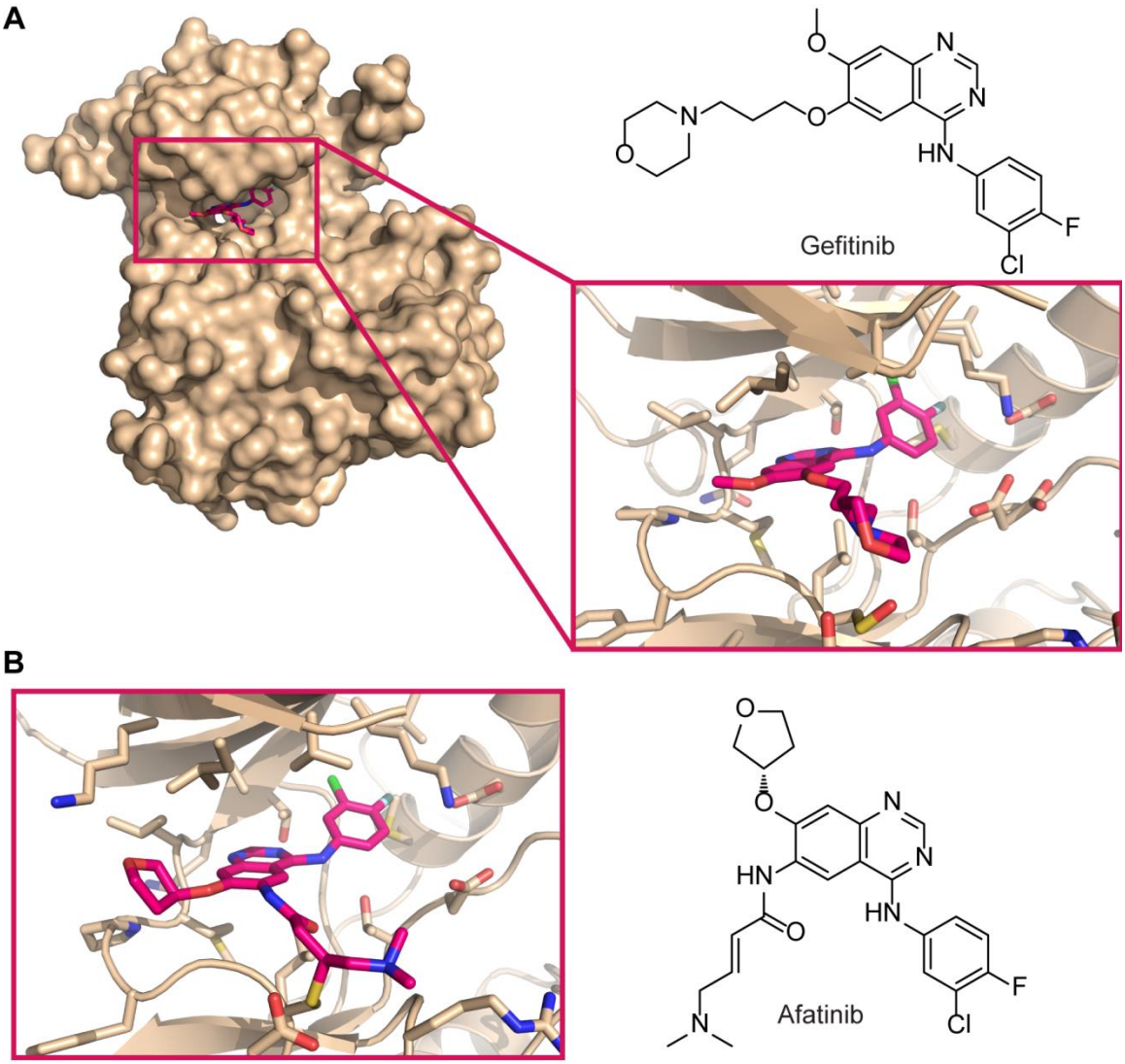

FIGURE 1.5 Binding of Gefitinib and Afatinib to the EGFR Kinase Domain
(a) Structure of gefitinib bound to the active site of the EGFR kinase (PDB: 4WKQ). (b) Structure of afatinib bound to the active site of the kinase (PDB: 4G5J). Unlike gefitinib, afatinib forms a covalent bond in the EGFR active site. The thioether is shown between afatinib and Cys797 of the kinase.

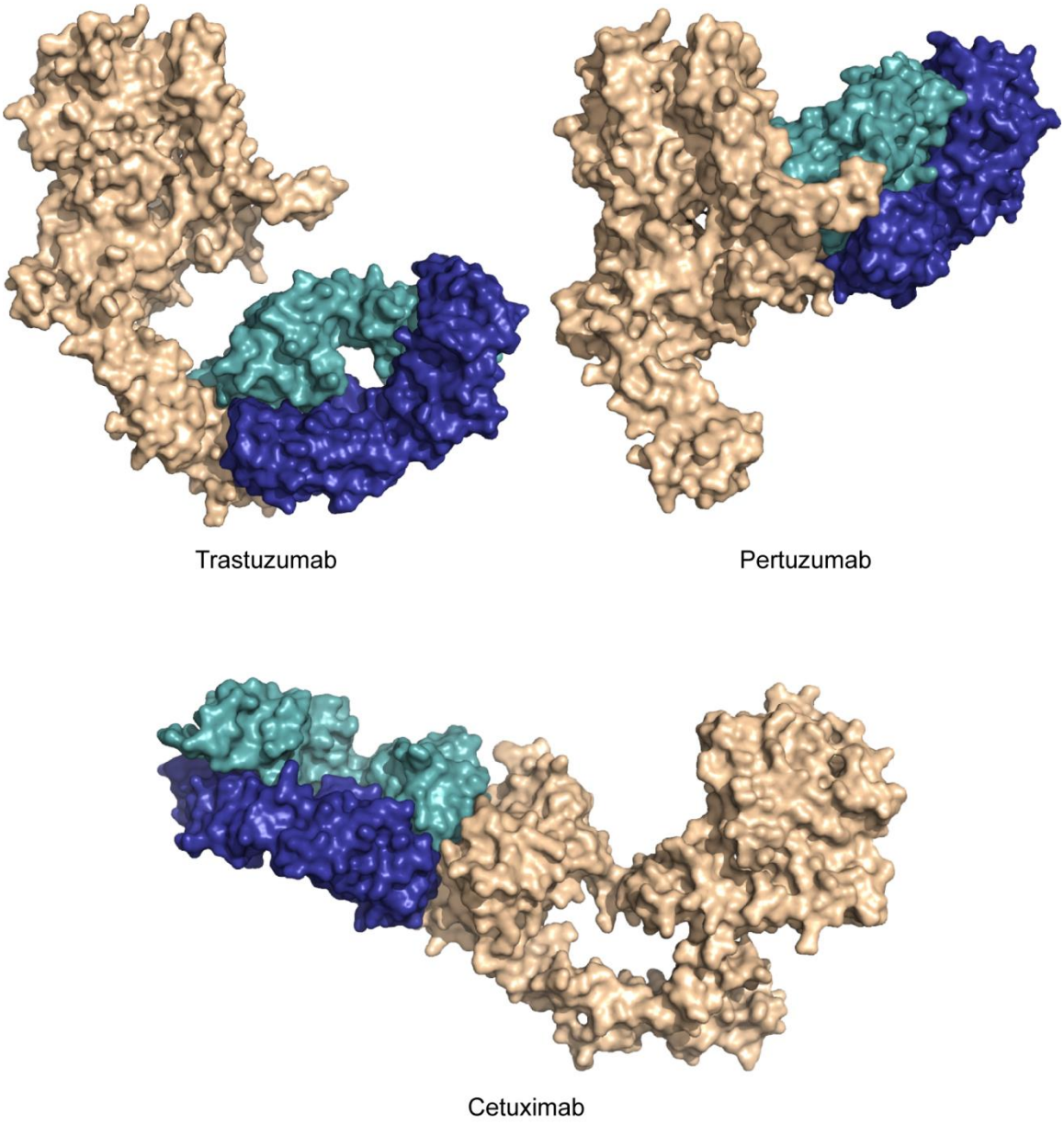

FIGURE 1.6 Binding of Fab Fragments of ErbB Targeted Monoclonal Antibodies
The Fab fragments of trastuzumab and pertuzumab (teal and blue) are shown bound to the Her2 receptor (beige). The Fab fragment of cetuximab (teal and blue) is shown bound to the extracellular domain of EGFR receptor (beige). Images were generated in Pymol from PDB files 1N8Z, 1S78, and 1YY9.

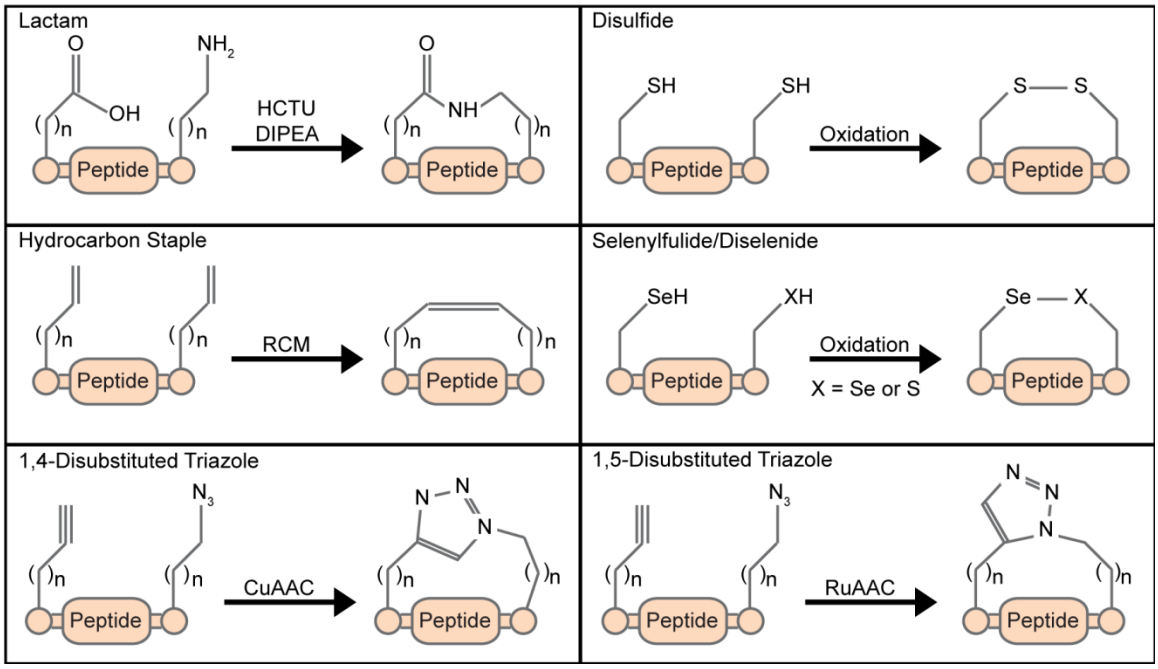

FIGURE 1.7 Chemical Constraints for Peptide Cyclization
Synthetic strategies for peptide stabilization through cyclization are shown. The lactam bridge requires orthogonal protection strategies for on-resin cyclization using standard solid phase peptide synthesis coupling techniques. The bridge may be formed between residues bearing a terminal amine (e.g. lysine) and a carboxylic acid (e.g. aspartate or glutamate). The disulfide, selenylsulfide, and diselenide may be formed between cysteines and selenocysteines using oxidative conditions. Cleavage conditions containing dithiobisnitropyridine may also promote formation of these bridges. The hydrocarbon staple is typically used for stabilization of helical peptides, yet it also may be applied to macrocycles. The hydrocarbon staple is formed between alkenyl amino acids using olefin ring closing metathesis (RCM) in the presence of a ruthenium catalyst. The triazoles may be formed on resin between an alkynyl and an azido amino acid. The 1,4-disubstituted triazoles are selectively formed during copper-catalyzed azide-alkyne cycloaddition (CuAAC). The 1,5-disubstituted triazoles are selectively formed during ruthenium-catalyzed azide-alkyne cycloaddition (RuAAC) using pentamethylcyclopentadienyl ruthenium chloride catalysts.

CHAPTER 2

INHIBITING EGFR DIMERIZATION USING TRIAZOLYL-BRIDGED DIMERIZATION ARM MIMICS[1]

[1] L.E. Hanold, K. Oruganty, N.T. Ton, A.M. Beedle, N. Kannan, and E.J. Kennedy. 2015. *PLoS ONE*. 10(3): e0118796.

Reprinted here with permission of the publisher

2.1 Abstract

The epidermal growth factor receptor (EGFR) is overexpressed in multiple carcinomas and is the focus of a variety of targeted therapies. Here we report the design of peptide-based compounds that mimic the EGFR dimerization arm and inhibit allosteric activation of EGFR. These peptides are modified to contain a triazolyl bridge between the peptide strands to constrain the EGFR dimerization arm β-loop. In this study, we demonstrate that these peptides have significantly improved proteolytic stability over the non-modified peptide sequence, and their inhibitory effects are dependent on the number of the methylene units and orientation of the introduced triazolyl bridge. We identified a peptide, EDA2, which downregulates receptor phosphorylation and dimerization and reduces cell viability. This is the first example of a biologically active triazolyl-bridged peptide targeting the EGFR dimerization interface that effectively downregulates EGFR activation.

2.2 Introduction

The Epidermal Growth Factor Receptor (EGFR) is a transmembrane receptor tyrosine kinase and member of the ErbB receptor family that performs key roles in cell regulation, including proliferation and differentiation [161]. As such, tight regulation of EGFR activity is essential to normal cell growth and function. There are several factors involved in EGFR regulation including ligand binding, conformational changes, dimerization, kinase activation, and internalization for downregulation, degradation or recycling [48,49,53,54,82,162]. Upon ligand binding, the extracellular receptor portion of EGFR undergoes considerable conformational changes between the inactive and active states [53,54]. In its inactive form, the receptor is folded so as to bury the dimerization

arm. Once activated, EGFR undergoes a significant rearrangement that projects the dimerization arm outward to engage in receptor dimerization (Figure 2.1). Dimerization of the extracellular receptor is largely dependent on dimerization arm interactions, and this allosteric change is followed by intracellular kinase domain dimerization and phosphorylation [48,49,53,54,82]. The phosphorylated tyrosine residues of the active kinase domain serve as docking sites for downstream proteins and promote signaling cascades involved in cell growth, proliferation, and migration. As an additional layer of regulation, the receptor can be internalized and degraded or recycled back to the membrane for continued signaling.

In addition to EGFR homodimerization, there are alternative modes of receptor oligomerization contributing to regulation of the EGFR signaling pathway, including heterodimerization, formation of ligand-free inactive dimers, and formation of higher order oligomeric clusters [92,95-98]. The various modes of oligomerization contribute to EGFR regulation and signaling complexity and may prime EGFR for ligand binding, provide spatial regulation for EGFR signaling, diversify signaling, and promote internalization of EGFR [92,97-99]. While it is known that these oligomeric structures can form, little is known about allosteric regulation governing some of these complexes. Thus, disruption of these various protein-protein interaction interfaces is necessary in order to evaluate their role in EGFR signaling. Since the vast majority of EGFR inhibitors target either the EGF binding site or the active site of EGFR [89,163], we sought to develop ligands that directly disrupt the dimerization interface. Previous studies showed that the dimerization arm of EGFR forms a large part of the dimer interface and contributes a substantial share of the driving energy for dimerization of the extracellular

receptor (Figure 2.1) [52,54]. The dimerization arm is a promising target for the design of ErbB disruptors and has been validated by the development of various compounds including pertuzumab, a monoclonal antibody that targets the dimerization arm of ErbB2, as well as a peptide dendrimer that targets this site on EGFR [61,76]. Additionally, an unconstrained peptide mimicking the ErbB3 dimerization arm and a disulfide-bridged peptide mimicking the EGFR dimerization arm were both shown to inhibit EGFR dimerization and phosphorylation [57,58,60]. However, non-modified peptides are inherently unstable to proteases, and disulfide bonds are sensitive to redox conditions and may become reduced in the acidic tumor microenvironment or endosomal compartments where EGFR signaling may occur [162,164,165]. As an alternative approach, we sought to introduce a covalent cross-linker into a dimerization arm mimic as a strategy to inhibit dimerization and downregulate EGFR activation.

Triazole crosslinks have been introduced into peptide-based scaffolds for diverse purposes. Previous work includes incorporating triazoles into peptide backbones or side chains [166] so as to either cyclize peptides [167-169], serve as the turn residues in β-turn mimics [170,171], replace disulfide bonds within β-hairpin structures [155], or to mimic β-strand configurations [172,173]. However, this chemistry had not previously been applied to the cyclization and stabilization of EGFR dimerization arm mimics. Thus, we sought to incorporate a triazolyl-bridge to covalently link the β-strands of the dimerization arm in an effort to improve the stability and inhibitory properties of the peptide mimic.

2.3 Results and Discussion

2.3.1 Peptide Design

Since the dimerization arm plays a major role in the stabilization of the extracellular receptor dimer, multiple mimics were previously designed [57,58,60,61,76]. As an alternative strategy to covalently constrain the dimerization arm, we utilized cycloaddition chemistry to introduce a 1,4-disubstituted [1,2,3]-triazolyl-containing bridge between the terminal residues of the sequence. A panel of EGFR Dimerization Arm (EDA) peptides was designed using the native sequence of human EGFR (residues 269–278, Figure 2.2a). The β-strand and turn residues were conserved from the original amino acid sequence since the majority of these residues make extensive contacts with the other receptor half-site.

Using this strategy, the dimerization arm was covalently cross-linked while on solid support to link the terminal residue side chains using copper (I)-catalyzed azide-alkyne [3+2] Huisgen cycloaddition chemistry (Figure 2.2b) [166,174,175]. The azide- or alkyne-containing amino acids were incorporated into terminal positions of the sequence to minimize modifications within the dimerization arm itself. Since the optimal bridge length was not known, we modified this length by incorporating different azido-amino acid derivatives (Figure 2.2c) that were synthesized as previously described [176]. The methylene units of the azido-amino acids were varied from 2 to 4 units (azido-L-homoalanine, azido-norvaline, or azido-norleucine) to alter the overall length of the triazole linker while the alkyne (propargylglycine) remained fixed. Since the linker asymmetrically connects the triazole, the peptides were synthesized in pairs by exchanging the positions of the azido- and alkynyl-amino acids. This was performed to

evaluate the effects of the triazole position on inhibitory activity. In addition, two peptide controls were designed: one containing the non-modified sequence of the dimerization arm, and the other containing a scrambled sequence of the dimerization arm (Figure 2.2a) [57].

2.3.2 Molecular Dynamics Simulation of Triazolyl-Bridged Peptides[2]

In order to predict the impact of the introduced triazolyl bridges on the overall structure of the dimerization arm, molecular dynamics simulations were performed. The effect of the linker length was studied in relation to the hydrogen-bonding network and the overall structure of the cyclized peptides (Figure 2.3). In the native structure, a hydrogen bond is present between Asn271 and Tyr275 and supports the β-loop structure. A query of the number of molecular dynamics (MD) frames containing the native H-bond for the triazolyl-bridged peptides predicts that EDA2 and EDA4 largely retain the hydrogen bond throughout the duration of the simulation, however, the H-bond is nearly absent in EDA3 and is only moderately retained in EDA1, EDA5 and EDA6 (Figure 2.3a). This suggests that the structures of EDA2 and EDA4 may not significantly perturb the β-loop structure. However, cluster analysis predicts that EDA4 will adopt a more splayed conformation with a distance of 8.5 Å between the Cα carbon of Tyr270 and Nle277 of the terminal ends of the peptide strands (Figure 2.3b), which is nearly twice the measured distance of 4.5 Å in the structure of the native sequence. On the other hand, EDA2 appears to have less perturbation to the β-loop conformation with a moderate width of 5.9 Å that more closely resembles the native structure. EDA1, EDA5 and EDA6 were found to resemble the crystal structure most closely by maintaining a β-loop

[2] Molecular dynamics simulations were performed by Krishnadev Oruganty and are cited here to support the rational for the testing of multiple triazolyl bridges.

conformation with widths of 4.3 Å, 4.4 Å and 4.3 Å, respectively, while also maintaining the β-loop hydrogen bond in approximately 30-50% of the MD frames. Further, the triazolyl bridge of EDA1, 5 and 6 appears to project outward from the β-strands and may cause steric hindrance with binding contacts on domain II of the receptor. On the other hand, the triazolyl bridge of EDA2 and EDA4 adopts a more planar conformation relative to the β-strands and may allow for more extensive contacts with the receptor surface. Additionally, EDA2 appears to have less conformational flexibility as only a single cluster was identified, whereas 2–3 clusters were identified for EDA4 and EDA5. Overall, the MD simulations demonstrate that EDA2 maintains the native H-bond to support β-loop formation, is not significantly perturbed in terms of distance between the β-strands, contains a triazolyl crosslink that does not significantly project outward, and has reduced conformational flexibility as indicated by cluster analysis. Taken together, the simulations suggest that the conformation of EDA2 is relatively stable as compared to the other peptides and may more closely mimic the native binding conformation of the dimerization arm.

2.3.3 The Triazolyl-Bridge Enhances Peptide Stability

To determine whether the addition of a covalent constraint promoted proteolytic stability, degradation of the EDA peptides was measured in the presence of purified proteases[3], serum, and culture media (Figure 2.4 and 2.5). The rate of peptide degradation was first measured using purified proteases (Figure 2.4a). EDA peptides were incubated with a cocktail of immobilized trypsin and chymotrypsin over a time course of four hours. The amount of remaining peptide was quantified by LC/MS relative to an internal

[3] Stability assays using purified proteases were performed by Norman T. Ton and are cited here to provide evidence for the resistance of all cyclic peptides to proteolytic degradation.

standard. While the non-modified control peptide was rapidly degraded with 50% lost within one hour, all of the triazolyl-linked peptides showed significantly enhanced proteolytic resistance with little to no degradation over the 4-hour time course, demonstrating that introduction of the linker appears to provide substantial resistance to proteolytic degradation.

Peptide stability was also assessed using fresh mouse serum since multiple proteases are present in serum (Figure 2.4b). Since there were not significant differences in stability between the panel of triazolyl-linked peptides and EDA2 was predicted to have minimal structural perturbations relative to the native dimerization arm, subsequent stability experiments were performed using EDA2 and a non-modified control. After incubation with plasma proteases over a sixteen-hour time course, the non-modified peptide was almost completely degraded within two hours, however, EDA2 showed nominal degradation during the entire time course tested. These results demonstrate that EDA2 is resistant to serum proteases over an extended time course. As another parameter of stability, peptide hydrolysis was also measured in tissue culture media (RPMI) over a four-hour time course (Figure 2.5). Both EDA2 and the non-modified control remained intact throughout the time course, illustrating that the peptide sequence is inherently stable in cell culture media beyond the duration of time courses used in subsequent cell-based assays.

Another physical parameter that was assessed was secondary structural characteristics at different pH values. This was addressed since the peptide may be exposed to acidic conditions such as the extracellular space of the tumor microenvironment and the endosomal compartments where internalized EGFR is sorted.

Thus, structural stability of EDA2 and the non-modified control were measured at pH 7.4 and 6.5 using circular dichroism (Figure 2.4c and d) [162,164,165]. Across both pH conditions tested, EDA2 largely retained its secondary structural characteristics as indicated by a broad minimum at approximately 205 nm. The non-modified control contains a more disordered structure with the representative minimum at approximately 195 nm. These results demonstrate that the secondary structure of EDA2 is not significantly altered between physiologic and slightly acidic pH conditions.

2.3.4 Disruption of EGFR Phosphorylation and Cell Viability by EDA2

The EDA peptides were first tested to see if they could downregulate EGFR activation. Receptor activation was monitored as a function of EGFR autophosphorylation on Tyr1068 in intact MDA-MB-231 cells (Figures 2.6 and 2.7). The receptor was stimulated with EGF for 5 min following a 30 min peptide pretreatment. As predicted, EDA2 effectively downregulated EGFR activation while all the remaining EDA peptides (EDA1 and EDA3–6) showed little to no activity (Figure 2.7). EDA2 was found to reduce EGFR phosphorylation by greater than 60% as compared to untreated cells at a dose of 5 μM (Figure 2.6b). In contrast, the non-modified and EDA2 scramble (EDA2-Scr) controls had no inhibitory effect on EGFR phosphorylation, indicating that this effect is dependent on both sequence and cyclization. To further demonstrate that this effect was not due to changes in EGFR expression, an independent assay showed that total EGFR levels were not affected (Figure 2.8). The serum stable disulfide peptide also displayed modest activity, yet circular dichroism analysis indicated alterations in conformation at the mildly acidic pH of 6.5 (Figure 2.9). [4]

[4] Previously unpublished data.

Since EDA2 appeared to downregulate EGFR phosphorylation, we sought to determine whether this activity could also lead to a decrease in cell viability (Figure 2.10). Three diverse, EGFR-expressing cell lines (MDA-MB-231, PC-3, and BxPC-3) were dosed daily with EDA2 over a 0-50 μM concentration range over a five-day time course, after which cell viability was quantified using the Cell Titer Blue assay. The small molecule inhibitor gefitinib was used as a viability control. At higher concentrations (10 μM or higher), viability was reduced to less than 25% in both MDA-MB-231 and PC-3 cells. At the lower dose of 6.25 μM, EDA2 reduced viability by 50% and 72% in MDA-MB-231 and PC-3 cell lines, respectively. On the other hand, BxPC-3 was less sensitive, where viability was only reduced by 34% at the same dose. Thus, while some cells display considerable sensitivity to EDA2 over the five-day period, others have less sensitivity and this may be due to additional mutational factors such as a mutant *TP53* gene in the case of BxPC-3 [177].

2.3.5 EDA2 Disrupts Dimerization

While EDA2 downregulates receptor phosphorylation, we also wanted to investigate whether EGFR dimerization itself was inhibited. As a strategy to measure the number of detectable EGFR dimers in intact cells, a quantitative Proximity Ligation Assay (PLA) was performed (Figure 2.11). Cells were stimulated with EGF in the presence or absence of EDA2 or its scramble control (EDA2-Scr). The cells were then fixed and probed with equivalent amounts of the plus and minus PLA probes conjugated to an anti-EGFR monoclonal antibody to illuminate EGFR dimers. Fluorescence microscopy was used to visualize the DAPI and PLA signals. EDA2-treated cells displayed a notable decrease in EGFR dimers, expressed as orange punctate signals, as

compared to the untreated and EDA2-Scr control. Quantification of the fluorescent signals in individual cells (n=500 cells) indicates that EDA2 caused a significant reduction in EGFR dimers by 33% (Figure 2.11b). To verify that EDA2 did not simply reduce overall EGFR expression levels, total EGFR was measured under the conditions tested. EDA2 and the control peptides were found to have no effect on EGFR expression (Figure 2.8). Overall, these results show that EDA2 reduces EGFR dimerization and demonstrates the potential of EDA2 for downregulating EGFR activation and signaling.

EGFR dimerization in cells was also examined using a crosslinking assay (Figure 2.12).[5] MDA-MB-231 cells were treated with peptide or vehicle for 30 min, then stimulated with 10 ng/mL EGF for 7 min, after which EGFR dimers were crosslinked in intact cells using bis(sulfosuccinimidyl)suberate. Western blot analysis revealed a decrease in EGFR dimers compared to the stimulated control. There was also a decrease in EGFR monomers, which is suspected to be an artifact of the extended duration of the crosslinking assay. During the cross-linking and quenching steps, activated EGFR may be internalized and degraded.

In a separate co-localization experiment, cells stably transfected with EGFR-YFP were treated with TAMRA-labelled peptide for 1 hour.[6] The cells were then stimulated with EGF for 15 min, fixed and stained with DAPI. Fluorescence microscopy indicated that EDA2 was co-localized with EGFR in the presence or absence of EGF, while the scrambled control was not (Figure 2.13). Upon stimulation, there appeared to be a slight increase in internalized EGFR in the presence of EDA2 compared to the vehicle and scrambled controls, suggesting that EDA2 may increase internalization.

[5] Previously unpublished data.
[6] Previously unpublished data.

2.4 Conclusions

In summary, we developed a triazolyl-bridged peptide mimicking the EGFR dimerization arm. This peptide was found to have increased proteolytic resistance and maintained secondary structural characteristics in an acidic environment. EDA2 was further shown to downregulate EGFR dimerization, phosphorylation and cell viability, while co-localizing with EGFR in the cell. Although the native sequence of the dimerization arm was used in this study, this represents a starting point for sequence optimization so as to improve target inhibition and optimize binding interactions. These compounds can be used to probe homo- and heterodimerization of ErbB members. By targeting the dimer interface, analogous peptides can also be engineered to specifically target other members of the EGFR family so as to probe dimerization. Further, the peptides can be applied to study the effects of oligomerization on EGFR regulation. While peptide-based therapeutic candidates are generally characterized by high clearance and low bioavailability as compared to small molecules, chemical modifications may help to increase their half-life and uptake as demonstrated by stapled peptides currently in clinical trials [178-181]. The EDA peptides demonstrate resistance to proteolytic degradation, yet further improvements upon their ADME characteristics such as circulatory half-life may be achieved by additional modification such as PEGylation. Thus, further optimization of the EDA2 scaffold may lay the foundation for novel therapeutic treatment strategies of EGFR-overexpressing tumors. Ultimately, this study demonstrates novel utility of intrastrand triazole crosslinking to generate proteolytically stable, biologically active peptide-based macrocycles for targeted EGFR inhibition.

2.5 Materials and Methods

2.5.1 General Information

All protected amino acids, Rink amide MBHA resin and PAL-NovaPEG resin were purchased from Novabiochem unless otherwise noted. HCTU was purchased from Peptides International. All synthesis reagents and solvents were purchased from Fisher, Sigma-Aldrich, or Acros and used without further purification. Cell culture media and phosphate buffer saline were obtained from Lonza, fetal bovine serum from Thermo, penicillin/streptomycin and bovine serum albumin from Amresco, trypsin EDTA from Cellgro, and EGF from Abcam. Antibody to EGFR p-Y1068 was purchased from Abcam or Pierce, total EGFR from Santa Cruz Biotech, and α-tubulin from the University of Iowa. PVDF membrane was purchased from Millipore. Immobilized chymotrypsin was obtained from Proteochem, and chemiluminescent substrate and immobilized trypsin were obtained from Pierce. Peptide characterization and purification were performed on a Zorbax SB-C18, 5 μm HPLC column using an Agilent 1200 series HPLC system coupled to the Agilent 6120 quadrupole LC/MS. Peptides and viability assays were quantified using the Biotek Synergy 2 microplate reader. C57BL/6J mice obtained from Jackson Laboratories were maintained in a local breeder colony. All mouse housing and handling procedures were approved by the University of Georgia Institutional Animal Care and Use Committee.

2.5.2 Cell Culture

MDA-MB-231, PC-3, BxPC-3 and MDA-MB-435 cells purchased from ATCC were cultured in Roswell Park Memorial Institute-1640 (RPMI) with L-glutamine (Lonza) and supplemented with 10% fetal bovine serum (Thermo Scientific) and

penicillin/streptomycin (Amresco). Cells were grown at 37°C with 5% CO_2. HeLa Kyoto cells stably transfected with YFP-EGFR [182], generously provided by Dr. Carsten Schultz of European Molecular Biology Laboratory in Heidelberg, Germany, were cultured in DMEM with glucose and L-glutamine, 10% fetal bovine serum and penicillin/streptomycin. All cells were grown at 37°C with 5% CO_2

2.5.3 Synthesis of Azido Amino Acids

Azido derivatives of amino acids were synthesized as previously described.[176] Fresh triflic azide was prepared immediately before the azido transfer reaction. Briefly, 1M solution of triflic anhydride in dichloromethane (DCM) (6 ml, 6 mmol, 3 equiv.) was added to a solution of sodium azide (0.781 g, 12 mmol, 6 equiv.) in 5 ml water at 0°C. The solution was stirred for 2.5 hours at 0°C, after which saturated sodium bicarbonate was added until the evolution of CO_2 stopped. The solution was transferred to a separatory funnel and the organic layer was collected. The aqueous layer was washed two times with DCM. The organic layers were returned to the separatory funnel to be added dropwise to the amino acid.

An aqueous solution containing zinc chloride (18.5 mg, 0.14 mmol) and 1 equivalent (2 mmol) of either Fmoc-Dab-OH (Bachem), Fmoc-Orn-OH (Bachem) or Fmoc-Lys-OH (CHEM-IMPEX) was added to a round bottom flask. The solution was stirred and triethylamine (0.837 ml, 6 mmol, 3 equiv.) was slowly added. Methanol (40 ml) was added dropwise to create a final ratio of water/methanol/DCM at 3:10:3. After complete addition of methanol, the freshly prepared triflic azide solution was added dropwise from the separatory funnel. The solution was stirred at ambient temperature for 2–3 hours and the reaction was monitored by TLC. The organic solvents were removed

by rotary evaporation, and the remaining aqueous solution was acidified with 1% (w/v) citric acid (20 ml). The aqueous layer was extracted with DCM and the combined organic layers were purified by silica gel chromatography using a 0.5–7% (v/v) methanol gradient in DCM. Final products were confirmed by NMR and mass spectrometry.

2.5.4 Peptide Synthesis

Peptides were prepared using Fmoc-based solid-phase peptide synthesis. The non-modified peptide control was synthesized on Rink amide MBHA resin. Peptides that were engineered to contain a triazole cross-link were synthesized on PAL-NovaPEG resin. Resin (25 µmol) was loaded into a fritted peptide synthesis column and equilibrated in N-methylpyrrolidinone (NMP). Deprotections were performed using a solution of 25% (v/v) piperidine in NMP. Amino acid couplings were performed using a 0.5 M solution of amino acid (0.5 ml, 0.25 mmol, 10 equiv) along with 0.5 M solution of HCTU (0.495 ml, 0.248 mmol, 9.9 equiv) and DIEA (87 µL, 0.5 mmol, 20 equiv). All couplings containing the azido-amino acids or propargyl glycine (Peptech) were performed using 4 equiv of 0.5 M amino acid (0.1 mmol, 0.2 ml), 3.96 equiv of 0.5 M HCTU (0.099 mmol, 0.25 ml), and 8 equiv of DIEA (0.2 mmol, 43.5 ml).

2.5.5 On-Resin Cyclization of EDA Peptides

The 1,4-disubstituted-[1,2,3]-triazolyl cross-link was formed on-resin using copper(I)-catalyzed azide-alkyne cycloaddition chemistry. The resin (25 µmol) was suspended in a 1:2 solution of t-butanol (Alfa Aesar) and water. Sodium ascorbate (160 mg, 750 µmol, 30 equiv.) and copper sulfate (55 mg, 375 µmol, 15 equiv.) were added, causing the mixture to turn bright orange. The mixture was left to stir overnight. The mixture was then returned to a synthesis column, washed with 1:2 solution of t-

butanol/water, and dried for a test cleavage. Cyclization was confirmed by a shift in retention time using LC/MS.

2.5.6 N-terminal Fluorescein Labeling

Unless otherwise stated, all peptides used in this study were labeled with 5(6)-carboxyfluorescein (Acros) after on-resin cyclization or after the addition of β-Ala. After equilibrating the resin in DMF, 5(6)-carboxyfluorescein (19 mg, 50 μmol, 2 equiv), HCTU (19 mg, 45 μmol, 1.8 equiv) and DIEA (20 μL, 115 μmol, 4.6 equiv) were dissolved in 1 mL DMF. The solution was added to the resin and bubbled overnight while protected from light.

2.5.7 N-terminal 5(6)-Carboxytetramethylrhodamine Labeling

EDA2 and EDA2-Scr were labelled with 5(6)-carboxytetramethylrhodamine (Novabiochem) after on-resin cyclization. After equilibrating the resin in DMF, 5(6)-carboxytetramethylrhodamine (22 mg, 50 μmol, 2 equiv), HCTU (19 mg, 45 μmol, 1.8 equiv) and DIEA (20 μL, 115 μmol, 4.6 equiv) were dissolved in 1 mL DMF. The 5(6)-carboxytetramethylrhodamine solution was added to the resin and bubbled overnight while protected from light.

2.5.8 Peptide Cleavage

Resin cleavage was performed by incubating the resin for 4–5 hours in a cleavage solution containing 95:2.5:2.5 trifluoroacetic acid/water/triisopropylsilane. After cleavage, the peptide was filtered through glass wool into ice cold methyl t-butyl ether. The precipitate was collected by centrifugation at 4 °C. The supernatant was decanted and the pellet was air-dried. The peptide product was dissolved in methanol and products were confirmed by LC/MS. Non-modified control molecular weight = 1568.6 (expected

1569.62); Disulfide Control = 1632.6 (expected 1631.74); EDA1 = 1648.0 (expected 1648.68); EDA2 = 1648.0 (expected 1648.68); EDA3 = 1662.2 (expected 1662.71); EDA4 = 1662.2 (expected 1662.71); EDA5 = 1676.2 (expected 1676.74); EDA6 = 1676.2 (expected 1676.74); EDA2-Scr = 1647.6 (expected 1648.68); TAMRA-EDA2 = 1701.6 (expected 1702.8); TAMRA-EDA2-Scr = 1702.0 (expected 1702.8)

The peptides were purified by reverse phase HPLC on a Zorbax SB-C18 column using a flow rate of 4 ml/min and a gradient of 10%–100% (v/v) acetonitrile containing 0.1% (v/v) TFA over 24 minutes. Fluorescein labeled peptides were quantified using the extinction coefficient of 68,000 L mol^{-1} cm^{-1} for fluorescein and 85,000 L mol^{-1} cm^{-1} for carboxytetramethylrhodamine in 10 mM Tris pH 8.

2.5.9 Modeling of EDA Peptides and Molecular Dynamics Simulation

The peptide coordinates corresponding to EDA wild-type were taken from the EGFR dimer structure 3NJP (residues 270–277). Avogadro was used to model the triazolyl linker between the terminal ends of the peptide before Tyr270 and after Met277. The geometry of the cross-linked peptide was minimized using the GAFF force-field implemented within Avogadro. The topological parameters, partial charges and other force field parameters were estimated with programs in the AmberTools 13 suite [41]. The amber generated force field values were converted to gromacs format using acpype [42]. Molecular dynamics simulations were carried out using Gromacs v4.6.2.

The peptide structures were solvated in a periodic dodecahedron box with at least 1nm space on all sides of the peptide. Energy minimization using steepest descent was carried out until Fmax reached 10 kJ/mol/nm. An NVT simulation with position restraints on the peptide atoms were performed with a V-rescale thermostat used for temperature

equilibration. Long range electrostatics were treated using PME, with a short range cutoff of 0.9 nm. Pressure equilibration was done under similar conditions (including position restraints) with an additional Berendsen pressure coupling algorithm. Production runs for 40ns were carried out under the NPT conditions after removing the position restraints. The frames of the trajectory were saved to disk every 2ps.

The g_hbond program in the Gromacs suite was used to query the number of frames in which the hydrogen bond between Asn271 and Tyr275 was observed. The hydrogen bond between Asn271 and Gln276 was seen in all peptides with equal occupancy and hence is not discussed in the text. Cluster analysis of the trajectories was carried out with the g_cluster program in the Gromacs suite with a RMSD cutoff of 1.0 angstrom. The cluster centers were written to a PDB file and analyzed.

2.5.10 Proteolytic Degradation of Peptides

Immobilized trypsin and chymotrypsin were added to 5 µg peptide in digestion buffer (100 mM Tris, 200 mM NaCl, 100 mM $CaCl_2$, pH 8.2) where E/S for each protease was ~375. Benzyl alcohol was used as an internal standard. Peptides were incubated at 37 °C for 0, 0.5, 1, 2 and 4 hours with gentle agitation, after which methanol was added to a final concentration of 50% (v/v). The immobilized protease was pelleted by centrifugation at 15,000 rpm, and the supernatant was collected and analyzed by LC/MS. After incubation with protease, the disulfide and triazole peptide spectra displayed a peak with a mass equivalent to the methylated peptide. Data represents the combined absorbance of both methylated and unmethylated peptides. Peptide absorbance at 220 nm was normalized relative to the benzyl alcohol peak. Data was plotted in GraphPad Prism as percentage of parent peptide relative to T0. Normalized curves

represent one phase decay where Y0 equals 100, the plateau equals 0, and K is greater than 0.

2.5.11 Peptide Stability in Tissue Culture Media

A solution of 0.2 mM peptide and 0.1% benzyl alcohol in RPMI-1640 supplemented with 0.1% (w/v) BSA was incubated at 37°C with mixing at 300 rpm. Aliquots were collected in duplicate and quenched with an equal volume of acetonitrile with 0.1% (v/v) TFA. The samples were centrifuged at 14,000 rpm and the supernatant was analyzed by LC/MS. The peptide absorbances at 220 nm were normalized relative the benzyl alcohol standard and the percent of remaining peptide was calculated relative to T0. The resulting data was plotted in GraphPad Prism.

2.5.12 Serum Stability of Peptides

Blood for serum was collected from mice under the following University of Georgia Animal Use Protocols: A2010 08-153 and A2013 07-016. Fresh blood was obtained from isoflurane-anesthetized C57BL/6J male or female mice by terminal cardiac puncture according to standard procedures. Serum was separated from clotted blood by 5 min centrifugation at 10,000 g. A solution of 70% (v/v) fresh mouse serum, 0.1% (v/v) benzyl alcohol, and 0.2 mM peptide in PBS was incubated at 37°C in a thermomixer with shaking at 300 rpm. Aliquots were collected in duplicate at 0, 2, 4, 8 and 16 hours and quenched by the addition of an equal volume of acetonitrile and 0.1% (v/v) TFA. The proteins were pelleted by centrifugation at 14,000 rpm. The supernatant was collected and analyzed by LC/MS. Peptide and benzyl alcohol absorbance at 220 nm was recorded, and the percent parent peptide remaining was calculated relative to the benzyl alcohol internal standard. Data was plotted in GraphPad Prism as percent parent peptide relative

to T0. Normalized curves represent one phase decay where Y0 equals 100, the plateau equals 0, and K is greater than 0.

2.5.13 Circular Dichroism

CD spectra were obtained on a Jasco J-710 CD Spectrometer at 25°C using a 0.1 mm cuvette. Solutions of the non-modified control, disulfide control, and EDA2 in 10 mM sodium phosphate buffer at pH 6.5 and pH 7.4 were prepared. Spectra were recorded over 190–260 nm at 0.5 nm intervals using a 2 nm bandwidth, 100 ms time constant, 50 nm/min scanning speed, and 3 responses. The units were converted to molar ellipticity in Jasco Spectra Manager after baseline subtraction. The Savitzky-Golay smoothing filter was applied with a convolution width of 21.

2.5.14 EGFR Phosphorylation in MDA-MB-231 Cells

MDA-MB-231 cells cultured on non-tissue culture-treated plates were seeded in 24 well tissue culture-treated plates in RPMI-1640 supplemented with 10% FBS and penicillin/streptomycin. Cells were incubated at 37°C until approximately 80% confluent. The media was then replaced with RPMI 1640 supplemented with 0.1% (w/v) BSA, and the cells were incubated overnight. Serum starved cells were then pretreated with 0.05, 0.5, or 5 µM peptide for 30 min, followed by a 5 min stimulation with 50 ng/mL EGF. Cells were immediately lysed in 1x Laemmli buffer.

Proteins were separated by 8% SDS-PAGE then transferred onto PVDF membrane. Identical membranes were probed for EGFR p-Tyr1068 and α-Tubulin. Bands were visualized by chemiluminescence and quantified using Licor Image Studio Lite. Results were normalized to the corresponding α-Tubulin and reported as a ratio relative to EGF-stimulated cells in the absence of peptide. The average of at least three

experiments was plotted in GraphPad Prism, where error bars represent SEM. Significance values were calculated using two-way ANOVA with Bonferonni multiple-comparison test. Evaluation of total EGFR levels upon treatment with the non-modified peptide, EDA2, and EDA2-Scr was performed in separate experiments as described above. Total EGFR is reported as the average of two experiments performed in at least duplicate, where error bars represent SEM. Significance values were calculated using one-way ANOVA with Bonferonni multiple-comparison test.

2.5.15 Cell Viability Assays

MDA-MB-231, PC-3, or Bx-PC3 cells were seeded at 7,500 cells/well in a 96 well plate and allowed to adhere in RPMI-1640 containing 1% FBS. Media was then replaced with RPMI-1640 containing 0.1% FBS and peptide or gefitinib at concentrations ranging from 1.56 to 50 µM. Treatment solutions were refreshed daily for a total of five days of treatment. After 5 days of treatment, the media was replaced with 100 µL serum free RPMI and 10 µL of Cell Titer Blue reagent (Promega) was added. Cells were incubated at 37 °C for 5 hrs. Fluorescence was quantified using 530 nm excitation and 590 nm emission filters. Data is plotted in GraphPad Prism as the average percent viability relative to the vehicle control, where error bars represent SEM.

2.5.16 EGFR Dimerization Duolink Fluorescence Assay

MDA-MB-231 cells were seeded into 8 well chamber slides in RPMI-1640 supplemented with 10% FBS and 1x penicillin/streptomycin. The cells were grown to 80–90% confluence then serum starved for 24 hours in RPMI-1640 supplemented with 0.1% (w/v) BSA. The cells were then treated with 5 µM peptide for 30 minutes and stimulated for 5 minutes with 10 ng/mL EGF. The cells were then washed with PBS and

fixed with 2% paraformaldehyde and permeabilized in Triton-X 100. The Duolink In Situ Assay was performed according to the manufacturer's instructions. Wells were blocked using the Duolink Blocking Solution. Equal volumes of the Plus and Minus PLA probes conjugated to the EGFR monoclonal antibody (Millipore) were added to the wells and incubated at 4 °C overnight. The probes were then ligated and amplified using the Duolink Orange Detection Kit. The slide was mounted using Permafluor mounting medium with Dapi. Images were obtained at 40x magnification using TRITC and DAPI filters on an IX71 inverted fluorescent microscope with Cell Sens software (Olympus). Fluorescent signals per cell were counted from five representative 40X magnification microscope fields per condition. The averages from a single experiment performed in duplicate were plotted using GraphPad Prism. Error bars represent SEM. Significance values were calculated in GraphPad Prism using the D'Agostino-Pearson normality test, which demonstrated a non-Gaussian distribution, followed by a non-parametric ANOVA with Kruskal-Wallis and Dunn's multiple-comparison tests.

2.5.17 EGFR Dimerization Crosslinking Assay[7]

MDA-MB-231 cells were seeded into 24 well plates in RPMI 1640 containing 10% FBS and penicillin/streptomycin. Cells were grown to approximately 80% confluency, then they were washed and serum starved in RPMI 1640 containing 0.1% BSA. After 24 hours, the cells were pretreated with 0.05, 0.5, or 5 µM peptide for 30 minutes. Cells were then stimulated with 10 ng/mL EGF for 7 minutes, washed with PBS, then incubated with 3.5 mM BS^3 (Thermo Scientific) at 4°C for 30 minutes. The crosslinking reaction was quenched by incubating the cell solution with 20 mM Tris at

[7] Previously unpublished data

room temperature for 15 minutes. Cells were washed with PBS then lysed in 1X Laemmli buffer for immunoblotting.

Proteins were separated on 5%-8% gradient gels by SDS-PAGE then transferred onto PVDF membranes. The membranes were probed using anti-EGFR. Bands were visualized by chemiluminescence and quantified using Licor Image Studio. Results were normalized to α-Tubulin and reported as a ratio relative to EGF-stimulated cells in the absence of peptide. The averages of two experiments performed in triplicate were plotted using GraphPad Prism. Error bars represent SEM.

2.5.18 Co-localization of TAMRA-labelled Peptides to EGFR-YFP[8]

HeLa Kyoto cells stably transfected with EGFR-YFP were seeded into 8 well chamber slides in DMEM supplemented with 10% FBS and 1x penicillin/streptomycin. The cells were grown to 80-90% confluence then serum starved for 24 hours in DMEM. The cells were then pretreated with or 5 μM peptide for 1 hour then stimulated with 50 ng/mL EGF for 15 minutes. The cells were then washed with PBS and fixed with 2% paraformaldehyde, and the nucleus was stained with DAPI. The slide was mounted using Permafluor. Images were obtained at 40x magnification using FITC, TRITC and DAPI filters on an IX71 inverted fluorescent microscope with Cell Sens software (Olympus).

[8] Previously unpublished data

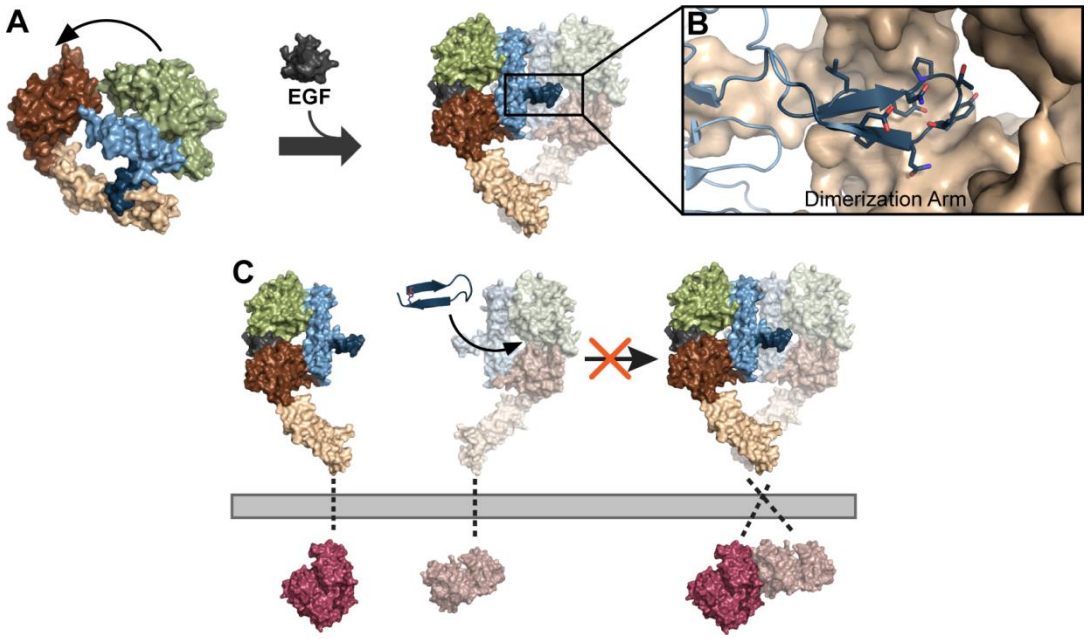

FIGURE 2.1 Dimerization Arm Targeting Strategy for Inhibition of EGFR
(a) EGF-induced activation of the extracellular receptor of EGFR. In the inactive state, the dimerization arm (dark blue) of the extracellular receptor is buried within domain IV (beige). In the active state, the receptor undergoes a conformational change to promote intermolecular interactions of the dimerization arm for receptor dimerization. Other features of the receptor include domain I (green), domain II (blue), domain III (brown) and EGF (dark grey). (b) The dimerization arm (dark blue) makes extensive contacts with domain II of the receptor binding partner (beige). (c) Triazolyl-bridged peptides were designed to mimic the dimerization arm, thereby blocking receptor dimerization and activation of the kinase (violet) through occlusion of the dimerization arm binding pocket. Additional features include the transmembrane domain (grey dashed lines). Structures were rendered using PyMol (PDB files: 1NQL, 3NJP, and 2GS6).

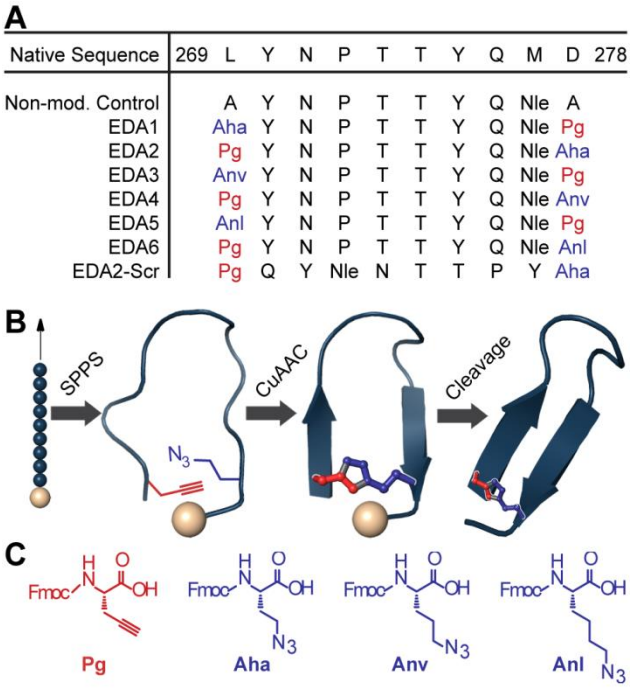

FIGURE 2.2 Design and Synthesis of EDA Peptides
(a) Peptide sequences were derived from the dimerization arm sequence of EGFR. The overall linker length and positioning of the azide and alkyne amino acids were varied. Non-natural amino acids are show in red and blue. (b) Dimerization arm mimics were synthesized by incorporating non-natural amino acids into the peptide sequence using solid phase peptide synthesis (SPPS). Peptides were cyclized on solid support via copper (I)-catalyzed azide-alkyne cycloaddition prior to resin cleavage. (c) Non-natural amino acids used for the triazole cross-link: N-Fmoc-L-propargylglycine (Pg), N-Fmoc-4-azido-L-homoalanine (Aha), N-Fmoc-5-azido-L-norvaline (Anv), N-Fmoc-6-azido-L-norleucine (Anl).

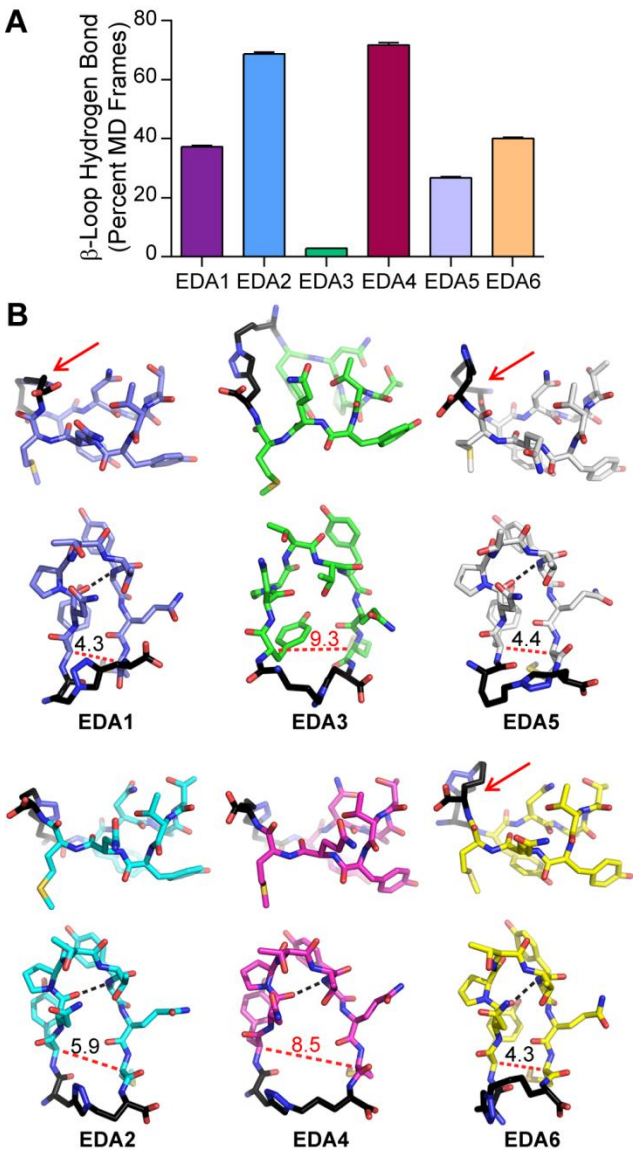

FIGURE 2.3 Molecular Dynamics Simulations of EDA Peptides
(a) Molecular dynamics simulations were performed and the g_hbond program in Gromacs suite was used to determine the stability of the hydrogen bond characteristic of the β-loop conformation. A query of the number of frames in which the hydrogen bond between Asn271 and Tyr275 is present predicts that this hydrogen bond is largely maintained in EDA2 and EDA4. Data is plotted as the percent of molecular dynamics trajectory frames in which the hydrogen bond between Asn271 and Tyr275 is present. (b) Molecular dynamics simulations were performed to predict the overall structure of the EDA peptides and the cluster centers for EDA1-6 are shown. Red arrows indicate linkers that fold over the non-binding surface of the peptide. The black dashed line indicates the hydrogen bond between Asn271 and Tyr275. Widths between the β-sheets were measured between the Cα carbon of residues Tyr270 and Nle277 (red dashed line).

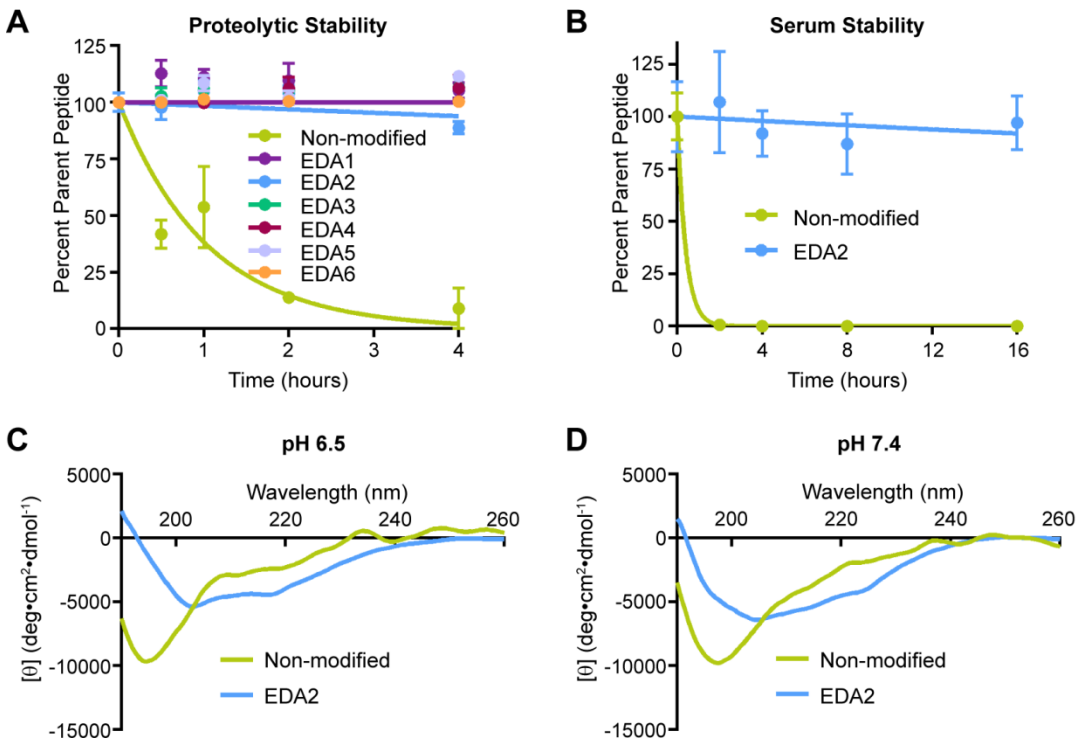

FIGURE 2.4 EDA Peptides are Resistant to Proteolytic Degradation
Proteolytic stability was measured in the presence of (a) a cocktail of immobilized chymotrypsin and trypsin over a time range of 0-4 hours and (b) 70% mouse serum over a time range of 0–16 hours. (c,d) CD spectra of the non-modified and EDA2 peptides were obtained on a Jasco J-710 CD Spectrometer at 25 °C in 10 mM sodium phosphate buffer at pH 6.5 and 7.4. EDA2 maintains its structure under both conditions.

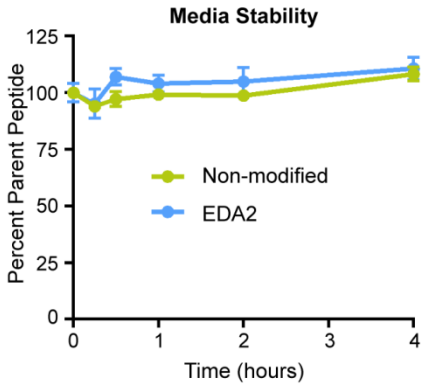

FIGURE 2.5 EDA2 is Stable in Tissue Culture Medium
Peptide stability was measured in the presence of RPMI-1640 tissue culture medium over a time range of 0-4 hours at 37 °C. The relative amount of loss as compared to that of the parent peptide at t=0 was quantified by LC/MS using an internal standard. Data is plotted in GraphPad Prism as the average of duplicates, where error bars represent SEM.

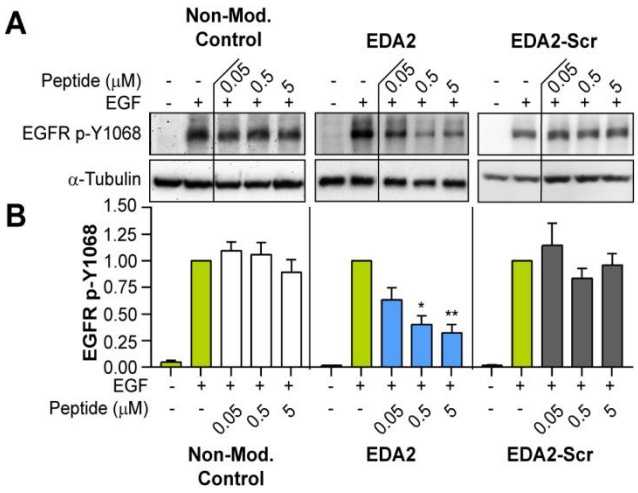

FIGURE 2.6 EDA2 Down-Regulates Activated EGFR
(a) Cells were stimulated with 50 ng/mL EGF for 5 min in the presence or absence of EDA peptides, followed by western blotting. An apparent decrease in phosphorylated EGFR was observed when treated with EDA2. Vertical lines indicate non-adjacent samples from the same western blot. (b) Quantification of EGFR phosphorylated at Tyr1068, normalized to tubulin, shows that EDA2 reduces phosphorylated EGFR by greater than 60%, while the non-modified and scrambled controls do not. Data is plotted as the average of at least three experiments, where error bars represent SEM. * $p < 0.05$, ** $p < 0.01$ relative to the EGF-stimulated control. All remaining means are not significant ($p > 0.05$) relative to the EGF-stimulated control.

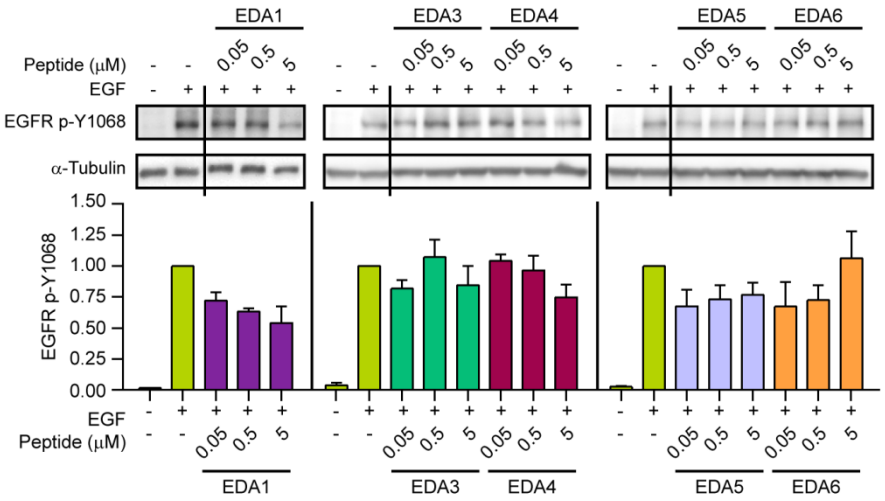

FIGURE 2.7 The Effect of EDA1 and EDA3-6 on EGFR Phosphorylation
Serum starved MDA-MB-231 cells were treated with peptide or vehicle for 30 minutes, after which cells were stimulated for 5 minutes with 50 ng/mL EGF. Cells were immediately lysed following stimulation and proteins were separated by 8% SDS-PAGE. Western blot analysis showed that EDA1 and EDA3-6 do not inhibit EGFR phosphorylation at Tyr1068. Vertical lines indicate non-adjacent samples from the same western blot. Data is plotted as the average of three experiments, where error bars represent SEM. All peptide means did not significantly differ ($p > 0.05$) from the EGF-stimulated control.

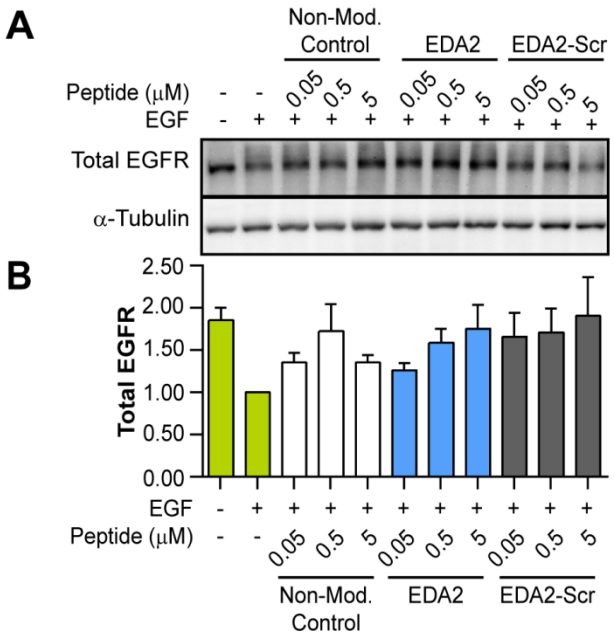

FIGURE 2.8 The Effect of EDA2 and Its Controls on Total EGFR Protein Levels
(a) Serum starved MDA-MB-231 cells were treated with peptide or vehicle for 30 minutes then stimulated with 50 ng/mL EGF for 5 minutes. Cells were immediately lysed and total EGFR levels were analyzed by western blotting. (b) Total EGFR was quantified and normalized to the tubulin loading control. Data is plotted as the average of two experiments performed in duplicate and triplicate, where error bars represent SEM. The means did not significantly differ ($p > 0.05$), indicating that the peptides do not affect total EGFR protein levels in the cell.

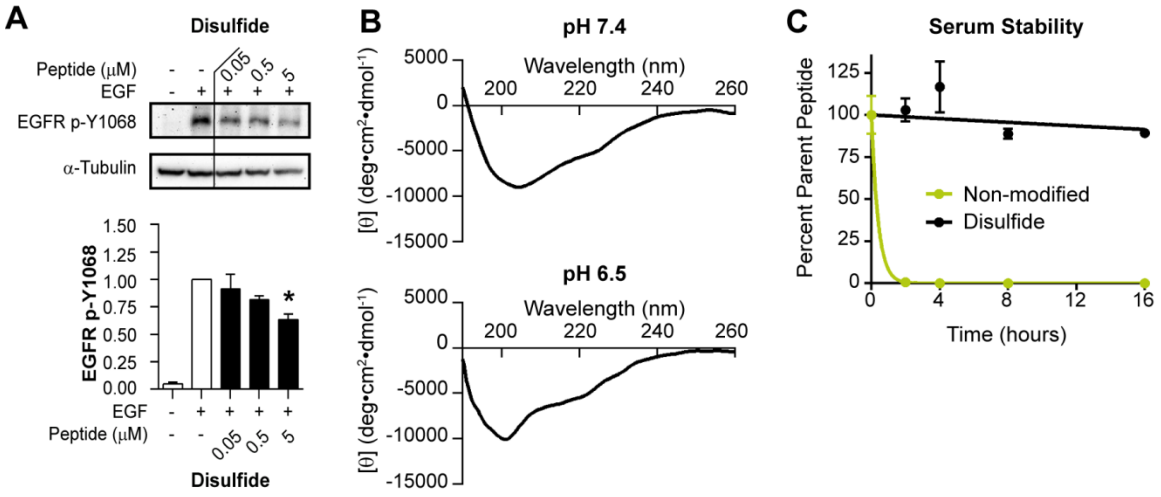

FIGURE 2.9 Disulfide Peptide Activity and Stability[9]

(a) Serum starved MDA-MB-231 cells were treated with disulfide peptide or vehicle for 30 minutes then stimulated with 50 ng/mL EGF for 5 minutes. Cells were immediately lysed and phospho EGFR levels were analyzed by western blotting. EGFR phosphorylation was quantified and normalized to the tubulin loading control. Data is plotted as the average of four replicates from two experiments, where error bars represent SEM. A reduction of 37% was observed at 5 μM. One-way ANOVA with Tukey's multiple comparison test was performed. * $p < 0.05$. (b) Circular dichroism analysis of the disulfide peptide indicated a shift in the minimum from 204 nm to 201 nm at pH 7.4 and pH 6.5, respectively. This shift indicates potential alterations in conformation under mildly acidic conditions. (c) Proteolytic stability was measured in the presence of 70% mouse serum over a time course of 0-16 hours. The disulfide was resistant to degradation.

[9] Previously unpublished data

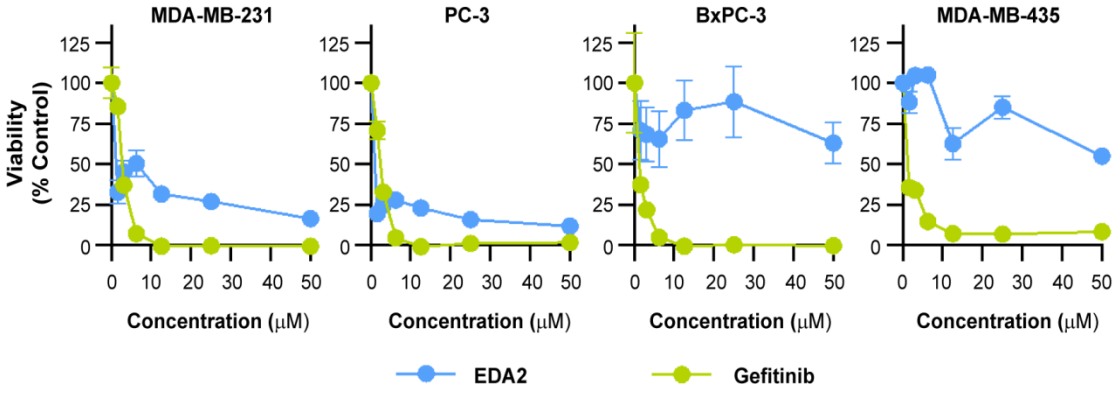

FIGURE 2.10 EDA2 Reduces Cell Viability

A panel of cell lines was dosed daily with EDA2 or gefitinib for 5 days, and viability was quantified using the Cell Titer Blue assay. 6.25 μM EDA2 reduced viability by 50%, 72%, and 34% in MDA-MB-231, PC-3, and Bx-PC-3 cells, respectively. EDA2 did not reduce viability in EGFR negative MDA-MB-435[10] cells at 6.25 μM. Data is plotted as the average of quadruplicates, where error bars represent SEM.

[10] Previously unpublished data.

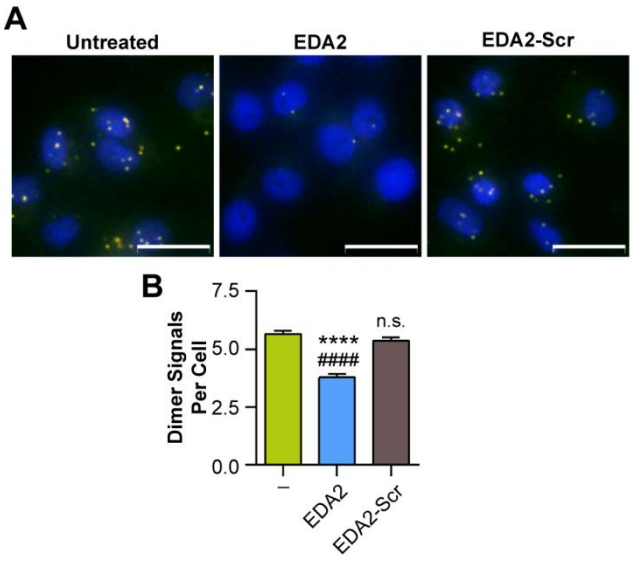

FIGURE 2.11 EDA2 Down-Regulates EGFR Dimers
(a) MDA-MB-231 cells were stimulated with 10 ng/mL EGF for 5 min in the presence or absence of 5 µM EDA2 and the scrambled control peptide (EDA2-Scr). The dimer species of EGFR was detected using a fluorescent Duolink assay and is shown as an overlay of the PLA signal (orange) and DAPI (blue). When dimerized, one EGFR molecule may bind the plus probe while the other may bind the minus probe. The close proximity of the plus and minus PLA probes then allows for ligation and amplification, which can be detected as a punctate fluorescent signal. Images were obtained with a 40x objective and scale bars represent 25 µm scale. (b) The dimer signals of individual cells were measured for each condition tested (n=500 cells per condition). Data is plotted as the average signal count per cell, where error bars represent SEM. **** $p < 0.0001$ relative to the stimulated control, #### $p < 0.0001$ relative to the scrambled control. Remaining comparisons do not differ significantly ($p > 0.05$).

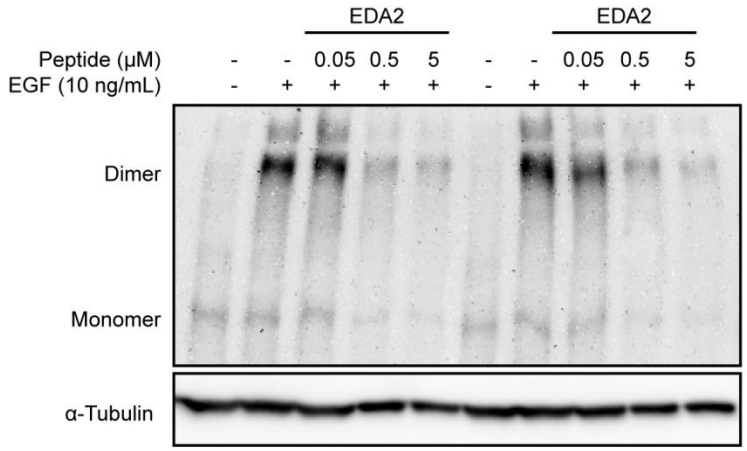

FIGURE 2.12 EGFR Dimerization Cross-linking Assay[11]
MDA-MB-231 cells were pretreated with increasing concentrations of EDA2, then stimulated with 10 ng/mL EGF for 7 min. Dimers were then cross-linked using bis(sulfosuccinimidyl) suberate. The dimer species of EGFR was detected using western blot analysis. Two replicates are represented here, illustrating the decrease in EGFR dimers and monomers compared to the controls.

[11] Previously unpublished data

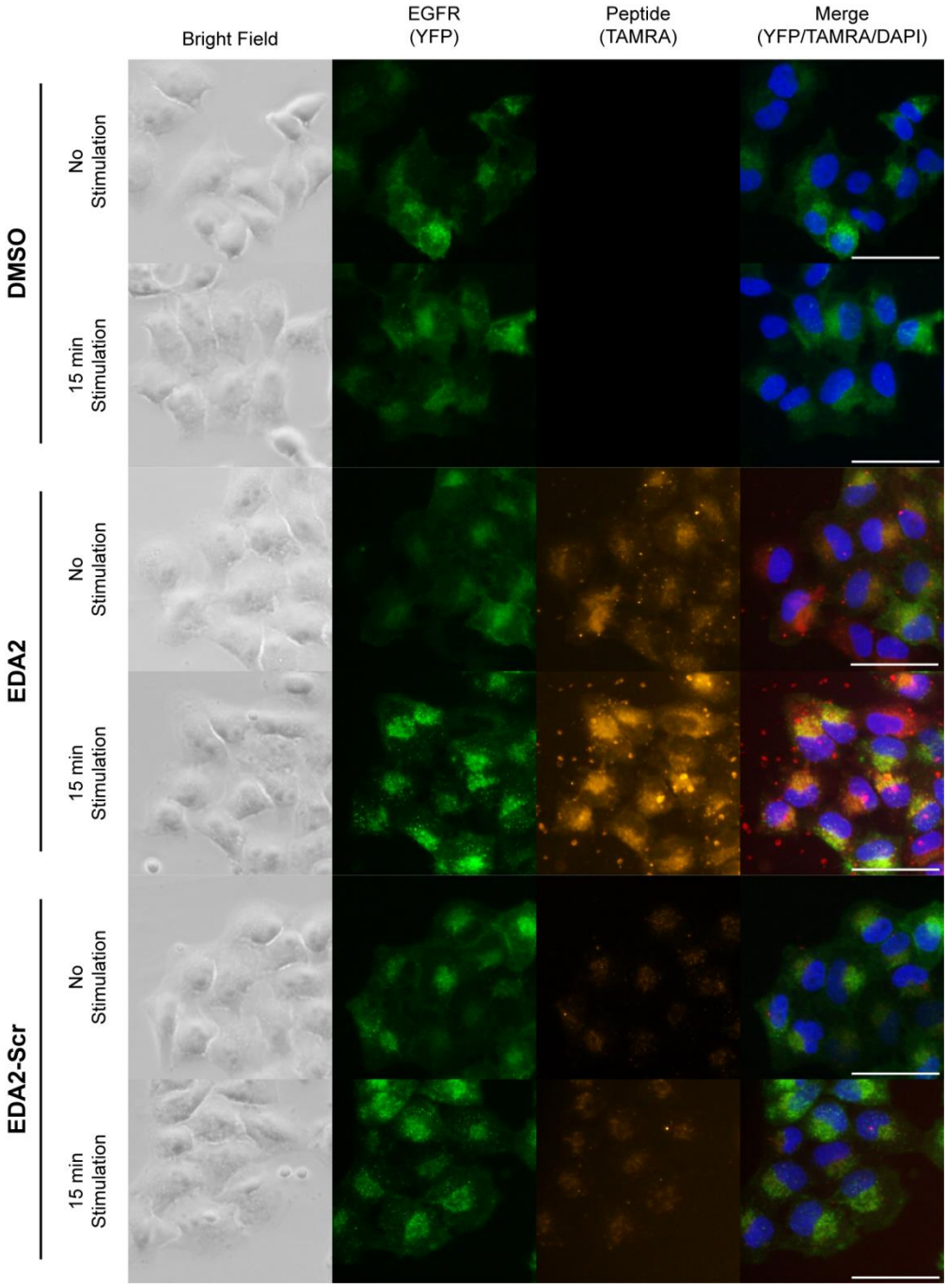

FIGURE 2.13 EDA2 Co-localizes with EGFR[12]

Hela-Kyoto cells stably transfected with EGFR-YFP were treated with vehicle or TAMRA-labeled peptide for 1 hr. Cells were then stimulated with 50 ng/mL EGF for 15 min. EDA2 appears to be co-localized with EGFR in the absence and presence of stimulation, while the scrambled does not. Scale bar = 25 µm.

[12] Previously unpublished data.

CHAPTER 3

DESIGN OF A SELENYLSULFIDE-BRIDGED EGFR DIMERIZATION ARM MIMIC[13]

[13] L.E. Hanold, C.P. Watkins, N.T. Ton, P. Liaw, A.M. Beedle, E.J. Kennedy. 2015. *Bioorganic & Medicinal Chemistry*. 23:2761-2766.

Reprinted here with permission of the publisher

3.1 Abstract

The epidermal growth factor receptor (EGFR) dimerization arm is a key feature that stabilizes dimerization of the extracellular receptor, thereby mediating activation of the tyrosine kinase domain. Peptides mimicking this β-loop feature can disrupt dimer formation and kinase activation, yet these peptides lack structural constraints or contain redox sensitive disulfide bonds which may limit their stability in physiological environments. Selenylsulfide bonds are a promising alternative to disulfide bonds as they maintain much of the same structural and chemical behavior, yet they are inherently less prone to reduction. Herein, we describe the synthesis, stability and activity of selenylsulfide-bridged dimerization arm mimics. The synthesis was accomplished using an Fmoc-based strategy along with C-terminal labeling for improved overall yield. This selenylsulfide-bridged peptide displayed both proteolytic stability and structural stability even under reducing conditions, demonstrating the potential application of the selenylsulfide bond to generate redox stable β-loop peptides for disruption of protein-protein interactions.

3.2 Introduction

Peptides are gaining increased momentum as disruptors of protein-protein interactions (PPIs) due to the development of diverse chemical modifications that enhance the structural and proteolytic stability of the peptide-based scaffold. Various modifications such as disulfides, lactams, triazolyl-bridges and hydrocarbon staples can be utilized to reinforce peptide secondary structural characteristics including beta-turns and helices [130,153,183,184] These constraints can be applied to stabilize the spatial orientation of key features for PPI interfaces, thereby enhancing the ability of a peptide to

occlude a binding surface and ultimately disrupt critical interaction surfaces for protein function or signaling events. The study of alpha-helical peptide mimics has led to the development of diverse PPI disruptors including p53-Mdm2, BID-BCL-2, and AKAP-PKA interactions [35,43,65,137,139]. However, β-loop/turn structures also play a significant role in various PPIs. Although there are many examples of constrained β-loop/turns, including backbone-disulfide-stabilized mimetics [185], linkage of two β-strands via a triazole bridge [170], cyclization of a linear precursor using a triazole bridge [186,187], and hydrocarbon-linked turns [188], design of β-loop mimics as PPI disruptors remains a challenge.

One example of PPI-mediated dimerization stems from a key β-loop structure on the epidermal growth factor receptor (EGFR) dimerization interface (Figure 3.1) [48,49,53,54,82]. EGFR dimerization is an essential step for kinase domain activation. Once activated, EGFR initiates multiple signaling pathways to regulate various cellular processes including proliferation. The dimerization of the extracellular receptor is largely stabilized by interactions involving the dimerization arm, a β-loop structure within domain II, that binds a shallow pocket on the opposing monomeric receptor surface [54]. Further, the dimerization arm is divergent among the ErbB family since it shares only 30%, 40%, and 60% sequence identity with ErbB2, ErbB3 and ErbB4, respectively (Figure 3.1b), thereby serving as a potential site for selective targeting [189,190].

Recent efforts have focused on developing peptide disruptors that target the dimerization arm interface on EGFR [57,58,60,187]. One example is a disulfide bridged peptide that maintains the β-loop conformation as found in the dimerization arm of the protein [57,60]. The disulfide bridge is a common peptide modification due to the ease

of cysteine incorporation into a protein or peptide sequence, yet the disulfide bond is inherently susceptible to reducing conditions such as those present in intracellular compartments and the tumor microenvironment [132,191,192]. In contrast, a selenylsulfide bond has a lower reduction potential, thereby making it less susceptible to reduction and therefore more stable than the disulfide bond [144,193-195]. Selenocysteine has been applied to various synthetic strategies including native chemical ligation [196,197] and in selenoconotoxin synthesis to stabilize complex peptide structures [143,145,198-200]. Since EGFR is a highly relevant target for inhibition, we sought to utilize selenylsulfide chemistry to generate a redox-stable dimerization arm mimic.

The synthesis of selenopeptides is often accomplished using Boc-based strategies since piperidine used in Fmoc-synthesis promotes β-elimination of the *p*-methoxybenzyl-protected selenium [144]. However, due to the harsh cleavage conditions and specialized equipment required for handling hydrofluoric acid that are required for Boc synthesis, we sought to utilize the more facile Fmoc-based approach. Although pentafluorophenyl ester derivatives of amino acids do not require the use of base during coupling reactions, current Fmoc-based strategies require the use of base during deprotection steps [144]. Thus, we explored different strategies so as to improve the overall yield of a selenocysteine-containing peptide using Fmoc chemistry. Herein, we describe the synthesis, stability and toxicity of a selenylsulfide-bridged EGFR dimerization arm mimic.

3.3 Results and Discussion

3.3.1 Peptide Design and Synthesis

Peptides were designed using residues 270-277 (UniProtKB P00533) of the native hEGFR dimerization arm sequence as a template (Figure 3.1c and 3.2). All peptide sequences were modified with a short polyethylene glycol linker (PEG) to increase solubility and a 5(6)-carboxyfluorescein label. Peptides were prepared using Fmoc-based solid phase peptide synthesis. Disulfide peptide controls were designed by inserting cysteine at the C- and N-terminus of the peptide, while the uncyclized peptide control**s** were similarly designed with alanine residues at these positions. Since *p*-methoxybenzyl (PMB)-protected selenocysteine has a propensity to undergo β-elimination in the presence of piperidine and diisopropylethylamine (DIPEA) during deprotection and coupling, we designed the selenylsulfide peptides with selenocysteine at the N-terminus so as to minimize exposure of the protected selenol to additional coupling and deprotection steps. Selenylsulfide peptides were cleaved in a solution of trifluoroacetic acid (TFA) and thioanisole, using 2,2'-dithiobis(5-nitropyridine) (DTNP) to remove the PMB-protecting group from selenocysteine [201,202].

Selenylsulfide peptide **1b** (Figure 3.2) was first synthesized using standard coupling procedures. However, the synthesis resulted in a mixture of side products including methylated products and the dehydroalanine-containing peptide, which was present to a large extent. This indicates that the addition of PEG and fluorescein after selenocysteine coupling is sufficient to cause elimination of the PMB-protected selenol. However, an initial screening of disulfide **1a** and selenylsulfide **1b** mixture demonstrated that both peptides were capable of inhibiting phosphorylation in a dose-dependent

manner (Figure 3.2). Thus, replacement of the disulfide bond does not appear to interfere with the ability of the peptide to inhibit EGFR phosphorylation. Further, it appears that the selenylsulfide-bridged compound is stabilized in a favorable conformer for targeting the dimerization arm binding pocket.

To improve peptide yield, formation of dehydroalanine was prevented by minimizing the use of bases such as piperidine and diisopropylethylamine during and after selenocysteine coupling (Figure 3.3). Oxyma Pure and diisopropylcarbodiimide (DIC) were used as coupling reagents as a means to circumvent addition of piperidine during coupling of PMB-protected selenocysteine [203]. After coupling the selenocysteine residue, two brief 5-minute deprotections were performed using 25% piperidine to remove the Fmoc group. $(PEG)_3$ and 5(6)-carboxyfluorescein were then coupled using similar conditions to minimize exposure to base. Although selenopeptide **2c** was observed, the dehydroalanine product was also present to a large extent (approximately 1-2 times that of the selenylsulfide product). The elimination of the selenol also resulted in a molar increase for the ratio of DTNP to selenocysteine during the cleavage step. Thus, the excess DTNP resulted in Npys-protected selenol and thiol side chains as illustrated in Figure 3.3. The overall yield of the synthesis was <1%.

Since the two additional deprotections after incorporation of the selenocysteine contributed to elimination of the selenol group, we redesigned the peptide so that $(PEG)_3$ and 5(6)-carboxyfluorescein moieties were incorporated at the C-terminus of the peptides prior to selenocysteine coupling (Figure 3.4) so as to reduce exposure of PMB-protected selenocysteine to piperidine and DIEA. This was accomplished by first coupling Fmoc-Lys(Mtt)-OH directly to the resin followed by a short $(PEG)_3$ linker and the peptide

sequence preceding selenocysteine. While the N-terminus of the peptide remained Fmoc-protected, the Mtt group of lysine was selectively removed using 1% trifluoroacetic acid in DCM to expose the ε-amine, and 5(6)-carboxyfluorescein was coupled to the lysine side chain. To prevent reactivity of the hydroxyls present in the 5(6)-carboxyfluorescein, these hydroxyl groups were first protected with trityl chloride [204]. The peptide was then deprotected with piperidine prior to addition of the selenocysteine. To minimize exposure of PMB-protected selenocysteine to piperidine, the final Fmoc group was removed with three brief 5-minute exposures to piperidine.

Since an excess of DTNP resulted in Npys-protected selenol and thiol side chains and since the DTNP may be recycled during the deprotection reaction, DTNP was reduced from 0.4 to 0.25 mol. equiv to deprotect the selenocysteine during cleavage [201]. Further, the selenol was found to readily oxidize to form the selenylsulfide bridge, therefore an additional oxidation reaction was unnecessary. Peptide **3c** was synthesized in an improved overall yield that was greater than 20 times that of peptide **2c**.

3.3.2 Peptide Structure and Stability

Next, proteolytic stability was measured. Peptides **3a-c** were incubated with fresh mouse serum over a time course of 12 hours (Figure 3.5). Degradation was quantified as the change in percent composition of the degradation products. After 12 hours, uncyclized peptide **3a** was degraded by 70%, while disulfide **3b** and selenylsulfide **3c** were less than 15% degraded. Additionally, chromatographic peaks corresponding to cleavage between $(PEG)_3$ and Ala278 at the C-terminus and between N-terminal residues Ala269, Tyr270 and Asn271 of the uncyclized peptide **3a** were observed. In contrast, minimal peaks corresponding to the degradation of disulfide **3b** and selenylsulfide **3c**

peptides were observed. Interestingly, the dehydroalanine product of selenylsulfide **3c** was observed after incubation with the serum. The significant reduction of degradation products at the end of the time course demonstrates that the selenylsulfide-bridge appears to prevent proteolytic cleavage due to incorporation of the structural constraint.

Peptide stability was also measured in the presence of the reducing reagent dithiothreitol (DTT). Circular dichroism spectra were obtained over a 0-400 μM concentration range of DTT (Figure 3.6). The uncyclized peptide **3a** maintained a minimum at 198 nm. However, an apparent shift in the minimum to 198 nm for selenylsulfide **3c** was not observed until 32 equiv of DTT was added (400 μM), demonstrating the stability of the secondary structure of the constrained peptide to this reducing agent over a broader concentration range.

3.3.3 The Effect of Peptides on Cell Viability

Although selenium is an essential trace nutrient, higher concentrations are toxic [205]. To measure whether the selenopeptide was toxic to cells, a variety of diverse cell lines were treated with unlabeled peptides **4a-c** for 6 hours at three concentrations ranging from 1 to 10 μM. Viability was measured for peptides **4a-c** using an MTT assay (Figure 3.7). No toxicity was observed over the concentration range tested, demonstrating that the selenylsulfide-bridged peptide is not toxic over this concentration range.

While the selenylsulfide peptide was not toxic after 6 hours of treatment, it may affect cell viability after an extended treatment period. A variety of cell lines were treated with peptides **4b-c** or gefitinib for 5 days at concentrations ranging from 1 to 25 μM. Viability was recorded using the CellTiter Blue assay (Figure 3.8)[14]. Selenylsulfide

[14] Previously unpublished data

peptide **4c** reduced viability by 59%, 42%, and 51% in MDA-MB-231, PC-3, and BxPC-3 cells, respectively. However, disulfide **4b** appeared to have greater activity, reducing viability by 71%, 59.5%, and 76% in MDA-MB-231, PC-3, and BxPC-3 cells, respectively.

3.4 Conclusions

In conclusion, we have synthesized a selenylsulfide-bridged peptide mimicking the EGFR dimerization arm using Fmoc chemistry. By labeling the peptide at the C-terminus prior to selenocysteine coupling, we were able to overcome elimination of the PMB-protected selenol during Fmoc-based solid phase peptide, thereby dramatically improving the yield of the synthesis. Although Boc-based synthesis is often used to prepare selenylsulfide-containing peptides to circumvent the acidic conditions of deprotection that cause elimination of PMB-protected selenium, Fmoc-based synthesis provides a more facile approach for peptide synthesis by eliminating the need for harsh cleavage conditions and specialized equipment for handling hydrofluoric acid [144]. Additionally, pentafluorophenyl esters have been used in selenopeptide synthesis to eliminate the use of base in coupling steps, yet these amino acids are more costly and do not eliminate the use of base during subsequent deprotection steps [144,145]. The synthetic design strategy shown in this study provides a useful alternative for efficient Fmoc-based synthesis of labeled selenylsulfide-bridged peptides. This peptide also demonstrated resistance to proteolytic degradation as well as structural stability in the presence of the reducing agent DTT. Thus, this redox stable bond may act as a useful tool for the generation of β-loop peptides to target PPIs.

3.5 Materials and Methods

3.5.1 General Information

All resins and amino acids were purchased from Novabiochem. 2-(6-chloro-1H-benzotriazole-1-yl)-1,1,3,3-tetramethylaminium hexafluorophosphate (HCTU) and Fmoc-11-amino-3,6,9-trioxaundecanoic acid were purchased from ChemPep. All solvents and chemical reagents were purchased from Sigma, Fisher, or Acros and used without further purification. Cell culture media and PBS was obtained from Lonza, trypsin EDTA from Corning, fetal bovine serum and horse serum from Fisher, and penicillin/streptomycin from Amresco.

All high-performance liquid chromatography and LC-MS were performed on an Agilent 1200 series HPLC coupled to an Agilent 6120 quadrupole mass spectrometer. Absorbance measurements were acquired using a Biotek Synergy 2 microplate reader.

3.5.2 Cell Culture

Cells were cultured at 37 ºC with 5% carbon dioxide. MDA-MB-231, PC-3 and BxPC-3 cells were cultured in RPMI-1640 (Lonza) with 10% fetal bovine serum (Fisher) and penicillin/streptomycin (Amresco). HCT-116 cells were cultured in DMEM (Lonza) with glucose and L-glutamine, 10% fetal bovine serum, and penicillin/streptomycin. Mia Paca-2 cells were cultured in DMEM with glucose and L-glutamine, 10% fetal bovine serum, 2.5% horse serum (Fisher), and penicillin/streptomycin.

3.5.3 General Peptide Synthesis Procedure

Peptides were synthesized on rink amide MBHA resin on a 25 μmol scale. The resin was deprotected with a solution of 25% piperidine in *N*-methyl-pyrrolidinone (NMP) for 25 min and washed three times with NMP. Fmoc-protected amino acids were

then coupled using 0.5 M amino acid (0.5 mL, 250 μmol, 10 equiv.), 0.5 M HCTU (0.495 mL, 247.5 μmol, 9.9 equiv.) and DIPEA (87 μL, 0.5 mmol, 20 equiv.) in NMP for at least 45 min. Fmoc protecting groups were removed in a solution of 25% piperidine in NMP for 25 min. Peptides were labeled with 5(6)-carboxyfluorescein (19 mg, 50 μmol, 2 equiv.), HCTU (19 mg, 46 μmol, 1.8 equiv.) and DIPEA (20 μL, 115 μmol, 4.6 equiv.) in DMF overnight. Peptides were cleaved in a solution of 95% TFA, 2.5% water, and 2.5% triisopropylsilane for 4 h. The solution was then filtered through glass wool into ice cold *tert*-butyl-methyl-ether and the precipitate was pelleted by centrifugation at 4 ºC. The supernatant was discarded and the pellet was dried and dissolved in methanol. The peptide was the characterized by LC-MS using a Zorbax SB-C18, 5μm column. Purification was performed using reverse-phase HPLC with a 10-100% gradient of acetonitrile in water containing 0.1% TFA. The absorbance of 5(6)-carboxyfluorescein at 495 nm was measured using a Biotek Synergy 2 microplate reader and the quantity of peptide was calculated from the molar extinction coefficient of 68000 M^{-1}. Uncyclized **2a** molecular weight = 1687.0 (expected = 1687.8); disulfide **2b** molecular weight = 1750.6 (expected = 1749.9).

*3.5.4 Synthesis of Peptides **1a-b***

Peptides were synthesized on a 25 μmol scale using rink amide MBHA resin. Deprotections were performed in 25% piperidine in NMP for 25 min. All Fmoc-protected amino acids were coupled using 0.5 M amino acid (0.5 mL, 250 μmol, 10 equiv.), 0.5 M HCTU (0.495 mL, 247.5 μmol, 9.9 equiv.) and DIPEA (87 μL, 0.5 mmol, 20 equiv.) for at least 45 min. unless otherwise noted. Fmoc-Sec(PMB)-OH and Fmoc-12-amino-4,7,10-trioxadodecanoic acid were coupled using 0.5 M amino acid (0.2 mL, 0.1 mmol, 4

equiv.), 0.5 M HCTU (0.248 mL, 124 μmol, 4.96 equiv) (Peptides International), and DIPEA (43.5 μL, .250 μmol, 10 equiv.) for at least 1 hr. Peptides were labeled with 5(6)-carboxyfluorescein (19 mg, 50 μmol, 2 equiv.), HCTU (19 mg, 45 μmol, 1.8 equiv.) and DIPEA (20 μL, 115 μmol, 4.6 equiv.) in DMF overnight. The disulfide peptide was cleaved in a solution of 95% TFA, 2.5 % triisopropylsilane, and 2.5% water for 4 hours. The selenylsulfide was cleaved in a solution of 97.5% TFA, 2.5% thioanisole, and DTNP (4 mg, 12.5 μmol, 0.5 equiv.) for 1.5 hr. Peptides were characterized by LC-MS and purified using reverse-phase HPLC with a gradient of 10-100% acetonitrile in water with 0.1% TFA. Disulfide **1a** molecular weight = 1765.4 (expected = 1763.9). Selenylsulfide **1b** products: selenylsulfide **1b** molecular weight = 1806.6 (expected 1810.8), methylated, reduced peptide molecular weight = 1827.6 (expected = 1826.8) and methylated dehydroalanine peptide = 1744.6 (expected = 1744.9).

*3.5.5 Synthesis of Selenylsulfide Peptide **2c** with Oxyma Pure*

The peptide sequence was synthesized on a 25 μmol scale using general coupling and deprotection procedures. Fmoc-Sec(PMB)-OH and Fmoc-11-amino-3,6,9-trioxaundecanoic acid were coupled using 0.5 M amino acid (0.2 mL, 0.1 mmol, 4 equiv.) and 0.2 mL of a pre-activated solution of Oxyma Pure (14 mg, 0.1 mmol, 4 equiv), DIC (15.5 μL, 0.1 mmol, 4 equiv.) in DMF for at least 2 h. Deprotections were performed using two 5 min. reactions with 25% piperidine in NMP. The peptide was labeled using a pre-activated solution of 5(6)-carboxyfluorescein (19 mg, 50 μmol, 2 equiv.), Oxyma Pure (7 mg, 50 μmol, 2 equiv.) and DIC (7.7 μL, 50 μmol, 2 equiv.) in 1 mL DMF. The peptide was cleaved in a solution of 97.5% TFA, 2.5% thioanisole and DTNP (3 mg, 10

μmol, 0.4 equiv.) for 1.5 h. The peptide was collected and purified using general procedures. Overall yield: 0.2%. Molecular weight = 1797.6 (expected = 1796.8).

*3.5.6 Synthesis of Peptides **3a-c***

Peptides **3a-c** were synthesized on a 25 μmol scale using rink amide MBHA resin. The resin was deprotected in 25% piperidine in NMP. Fmoc-Lys(Mtt)-OH and Fmoc-11-amino-3,6,9-trioxaundecanoic acid were coupled using a solution containing 0.5 M amino acid (0.2 mL, 0.1 mmol, 4 equiv.), 0.5 M HCTU, (0.248 mL, 124 μmol, 4.96 equiv.) and DIPEA (43.5 μL, 250 μmol, 10 equiv.) in NMP for at least 1.5 h. The peptide sequence preceding the final alanine, cysteine, or selenocysteine was then synthesized using general procedures. With the N-terminus Fmoc-protected, the Mtt-protecting group of lysine was removed by performing multiple washes with 1% TFA in DCM for a total of 30 min. The peptide was then labeled overnight using a solution of 5(6)-carboxyfluorescein (19 mg, 50 μmol, 2 equiv.), HCTU (19 mg, 45 μmol, 1.8 equiv.) and DIPEA (20 μL, 115 μmol, 4.6 equiv.) in DMF. The fluorescein was then tritylated using two overnight reactions of 12.5 μmol peptide with a solution of trityl chloride (21 mg, 75 μmol, 6 equiv.) and DIEA (13 μL, 75 μmol, 6 equiv.) in 1.5 mL DCM. The N-terminus was then deprotected using 25% piperidine in NMP for 25 min. Fmoc-Sec(PMB)-OH was then coupled using 0.5 M amino acid (0.25 mL, 0.125 mmol, 5 equiv.), 0.5 M HCTU (0.248 mL, 124 μmol, 4.96 equiv.) and DIPEA (43.5 μL, 250 μmol, 10 equiv.) in NMP, while cysteine and alanine were coupled using standard procedures. Three 5 min reactions or a 25 min reaction with 25% piperidine in NMP were used to deprotect the final residue of the selenylsulfide or uncyclized/disulfide peptides, respectively. Peptides were cleaved using general procedures. The PMB-protecting

group of the selenylsulfide was removed using 97.5% TFA, 2.5% thioanisole, and DTNP (1.9 mg, 6.25 μmol, 0.25 equiv.) for 1.5 hr. The peptides were characterized, purified, and quantified using general procedures. Uncyclized **3a** molecular weight = 1815.0 (expected = 1815.9). Disulfide **3b** molecular weight = 1879.0 (expected = 1878.0). Selenylsulfide **3c** overall yield: 5.1%; molecular weight = 1925.6 (expected = 1924.9).

*3.5.7 Synthesis of Peptides **4a-c***

Unlabeled peptides **4a-c** were synthesized by coupling Fmoc-11-amino-3,6,9-trioxaundecanoic acid directly to the resin using a solution containing 0.5 M amino acid (0.2 mL, 0.1 mmol, 4 equiv.), 0.5 M HCTU (0.248 mL, 124 μmol, 4.96 equiv.) and DIPEA (43.5 μL, 250 μmol, 10 equiv.) in NMP for at least 1.5 h. The peptide sequence was completed using standard procedures and Fmoc-Sec(PMB)-OH was coupled and deprotected using the conditions above. Uncyclized and disulfide peptides were cleaved in 95% TFA, 2.5% water, and 2.5% triisopropylsilane for 4 h. The selenylsulfide peptide was cleaved in a solution of 97.5% TFA, 2.5% thioanisole and DTNP (1.94 mg, 6.25 μmol, 0.25 equiv.) for 2.5 h. Peptides were characterized and purified according to general procedures. The peptides were quantified in 6 M guanidine HCl using the molar extinction coefficient of Tyrosine (1280 M^{-1}) and cysteine (120 M^{-1}) [206]. Uncyclized **4a** overall yield: 11%; molecular weight = 1328.6 (expected = 1329.5). Disulfide **4b** overall yield: 12%; molecular weight = 1392.6 (expected = 1391.6). Selenylsulfide **4c** overall yield: 5.1%; molecular weight = 1439.2 (expected = 1438.5).

*3.5.8 EGFR Phosphorylation Assay with Peptides **1a-b***

MDA-MB-231 cells were seeded into 24 well plates in RPMI-1640 supplemented with 10% FBS and penicillin/streptomycin. Cells were allowed to adhere and grow to

approximately 70% confluence then serum starved in RPMI-1640 containing 0.1% BSA and penicillin/streptomycin for 23.5 hours. Cells were pretreated with peptide for approximately 30 min. then stimulated with 50 ng/mL EGF for 5 min. Cells were immediately lysed in 1x Laemmli. Lysates were boiled 10 min. and proteins were separated by SDS-PAGE on an 8% gel. Western blotting was performed using PVDF membrane, and membranes were probed for EGFR p-Y1068 (Abcam) and α-Tubulin (University of Iowa). Bands were quantified using Licor Image Studio Lite.

3.5.9 Serum Stability

Fresh mouse serum was collected from pooled blood obtained by terminal cardiac puncture from isoflurane-anesthetized C57BL/6J mice; blood collection and mouse husbandry procedures were approved by the University of Georgia IACUC committee. Peptides **3a-c** were incubated at a concentration of 0.2 mM in a solution containing 50% mouse serum, 0.4% benzyl alcohol, and 15% DMSO in PBS, pH 7.2 at 37 ºC. Aliquots were drawn in triplicate at 0, 1.5, 3, 6, and 12 h and proteins were precipitated with an equal volume of acetonitrile containing 0.1% TFA. The precipitate was pelleted by centrifugation at 14,000 rpm for 5 min, and the supernatant was collected. Degradation was monitored at 280 nm by LC-MS using a Zorbax Eclipse XDB-C18, 5 μm column, with a gradient of 0-100% acetonitrile in water containing 0.1% TFA and a 1.0 mL/min flow rate at 45 ºC. Absorbance was integrated between 9 and 10.75 min using the ChemStation software to determine absorbance of degradation products. The parent peptide peak was also integrated. The percent composition of degradation products was calculated relative to the combined absorbance of degradation products and parent peptide. The percent composition at T_0 was subtracted from all values to determine the

increase in percent composition and is plotted over time, where error bars represent SD of triplicate experiments.

3.5.10 Circular Dichroism

Circular dichroism spectra were obtained for peptides **3a-c** with a C-terminal label in 10 mM sodium phosphate buffer, pH 7.0 at concentrations of approximately 10-20 μM, using a Jasco J-710 CD Spectrometer. Peptides were treated with 16, 80, or 400 μM DTT for 10 min prior to reading. Blanks were obtained for each concentration of DTT and subtracted from the spectra. Spectra were obtained with a 0.1 cm path length using 100 mdeg sensitivity, 1 nm data pitch, continuous scanning mode with a speed of 50 nm/min, 4 sec response, 2 nm bandwidth, and 3 accumulations. Savitzky-Golay smoothing was applied with a convolution width of 17. Mean residue ellipticity was calculated for the peptides using the equation [207,208]:

$$[\theta] = (\theta * 0.1 * \text{MRW})/P * C$$

where θ is the theta machine units in mdeg, MRW is the mean residue weight (molecular weight of the peptide/total number of residues), P is the path length in cm, and C is the concentration in mg/mL. The final concentration of peptide was confirmed following the experiment using the Biotek Synergy 2 microplate reader.

3.5.11 MTT Toxicity Assay

Cells were seeded at 10,000 cells per well in a 96 well plate in complete media and allowed to grow for 48 hours at 37 ºC. The media was replaced with a 0, 1, 5 or 10 μM solution of unlabeled peptide **4a-c** in complete media and incubated for 6 hours. Following treatment, the media was replaced with 110 μL media containing 0.45 mg/mL MTT and incubated for 2 hours at 37 ºC. The solution was removed and 100 μL DMSO

was added and rocked on an orbital shaker for 15 minutes protected from light. The absorbance was measured at 570 nm. Percent viability was calculated relative to the vehicle control. The average of quadruplicates was plotted in GraphPad Prism, where error bars represent SEM. For each peptide, a two-way ANOVA was performed across all cell lines with Tukey's multiple comparison test.

*3.5.12 Cell Viability Assay with Peptides **4b** and **4c***[15]

MDA-MB-231, PC-3, or BxPC-3 cells were seeded at 7,500 cells per well in a 96 well plate using RPMI-1640 supplemented with 1% FBS and penicillin/streptomycin. After the cells adhered, the cells were treated in quadruplicate with increasing peptide or gefitinib concentrations, 0-25 µM, in RPMI supplemented with 0.1% FBS and penicillin/streptomycin. The solutions were refreshed daily for a total of five days of treatment. The solution was then replaced with 100 µL of serum free RPMI and 10 µL of CellTiter Blue reagent. The cells were incubated for 3 hours at 37°C, after which, fluorescence was measured using a 530 nm excitation filter with a 25 nm bandwidth and a 590 nm emission filter with a 35 nm bandwidth. The fluorescence of the blank containing media and CellTiter Blue but no cells was subtracted from the fluorescence values of the samples. Viability is reported as percent relative to the vehicle control, where error bars represent SEM.

3.6 Acknowledgements

The authors thank the NIH (1K22CA154600 to E.J.K.) for their generous financial support. We would also like to thank Jeffrey Urbauer and Ramona Bieber-Urbauer for their assistance with circular dichroism.

[15] Previously unpublished data

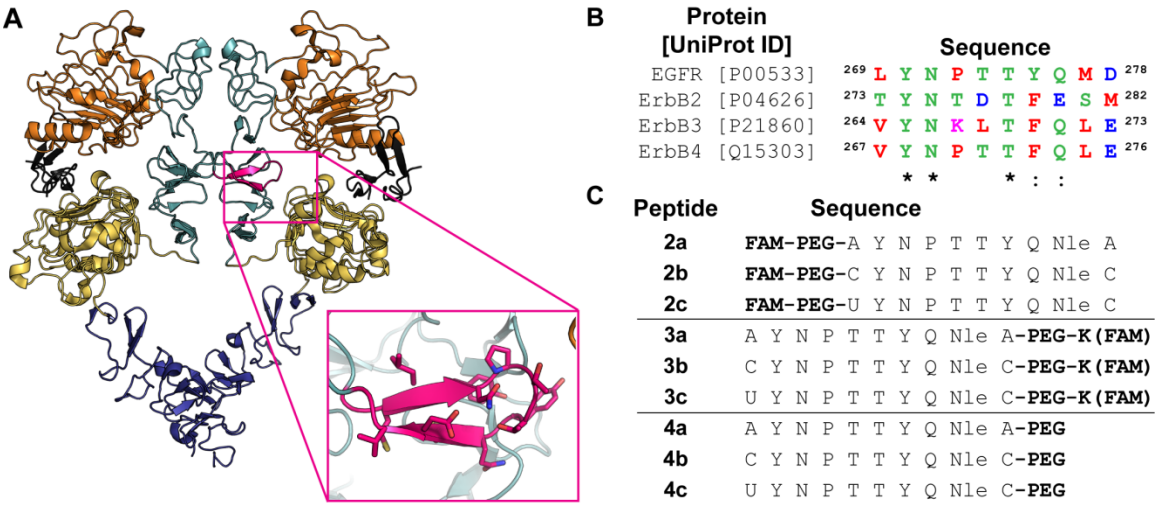

FIGURE 3.1 Design of EGFR Dimerization Arm Mimics
(a) In the active conformation, the dimerization arm (magenta) of the receptor is exposed and forms contacts with domain II (light teal) of the second receptor half-site. Domain I is shown in orange, domain III in yellow, domain IV in purple, and EGF in black. Images were rendered in Pymol using PDB ID 3NJP. (b) Sequence alignment of the ErbB dimerization arms. Polar amino acids are shown in green, acidic in blue, basic in magenta, and nonpolar in red. An asterisk represents conserved residues, while a colon represents residues with high similarity. (c) Peptide sequences were designed from the native EGFR dimerization arm with cysteine or selenocysteine added to the termini for cyclization. Cysteine and selenocysteine were replaced with alanine in the uncyclized control. U = Selenocysteine; FAM = 5(6)-carboxyfluorescein; PEG = 11-amino-3,6,9-trioxaundecanoic acid

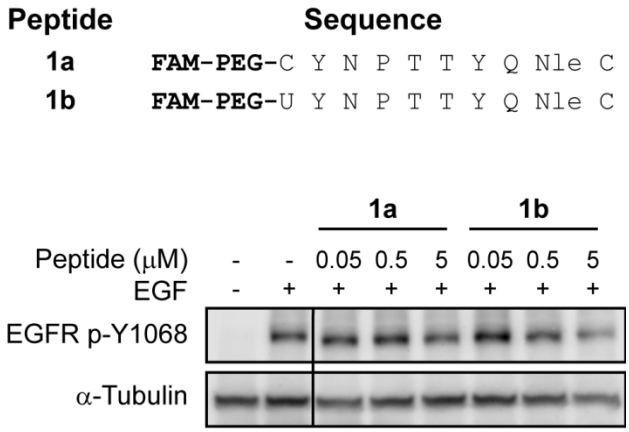

FIGURE 3.2 Disruption of Phosphorylation by Dimerization Arm Mimics
Sequences of peptides **1a** and **1b** are listed in the top panel (U = selenocysteine, FAM = 5(6)-carboxyfluorescein, and PEG = 12-amino-4,7,10-trioxadodecanoic acid). Serum-starved MDA-MB-231 cells were pretreated with peptide **1a** or **1b** for 30 min, then stimulated with 50 ng/mL EGF for 5 min. Proteins were separated by SDS-PAGE on an 8% gel and western blot analysis was performed. Treatment with both the disulfide and selenylsulfide products resulted in a notable decrease in phosphorylated EGFR. Vertical lines indicate non-adjacent bands from the same membrane image. Images are representative of three experiments.

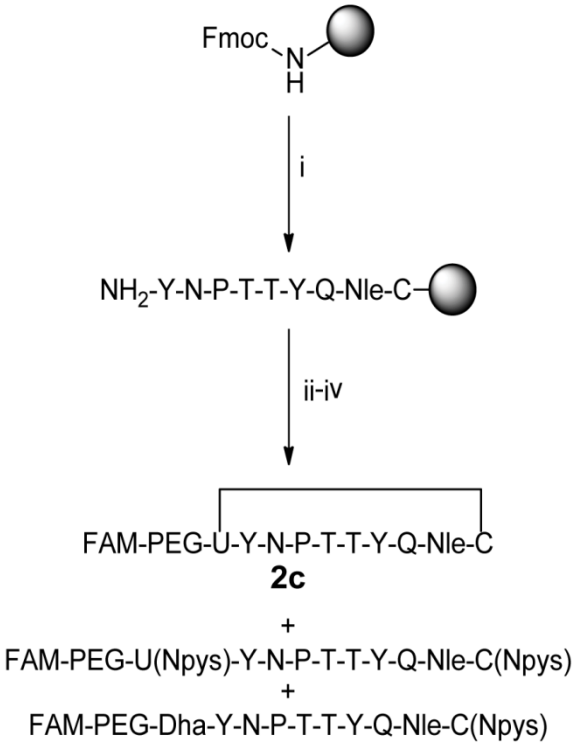

FIGURE 3.3 Synthesis of Selenylsulfide Peptide 2c
(i) Fmoc-based solid phase peptide synthesis on rink amide MBHA resin. Deprotection: 25% piperidine in NMP, 25 min. Coupling: 10 equiv amino acid, 9.9 equiv HCTU, 20 equiv DIPEA in NMP, ≥45 min. (ii) Deprotection: 25% piperidine in NMP, 2 x 5 min. Coupling: 4 equiv amino acid, 4 equiv Oxyma Pure, 4 equiv DIC in DMF, 135-160 min. (iii) 2 equiv. 5(6)-carboxyfluorescein, 2 equiv. Oxyma Pure, 2 equiv. DIC in DMF, overnight. (iv) 97.5% TFA, 2.5% thioanisole, 0.4 equiv. DTNP, 1.5 h. FAM = 5(6)-carboxyfluorescein, U = selenocysteine, Dha = dehydroalanine.

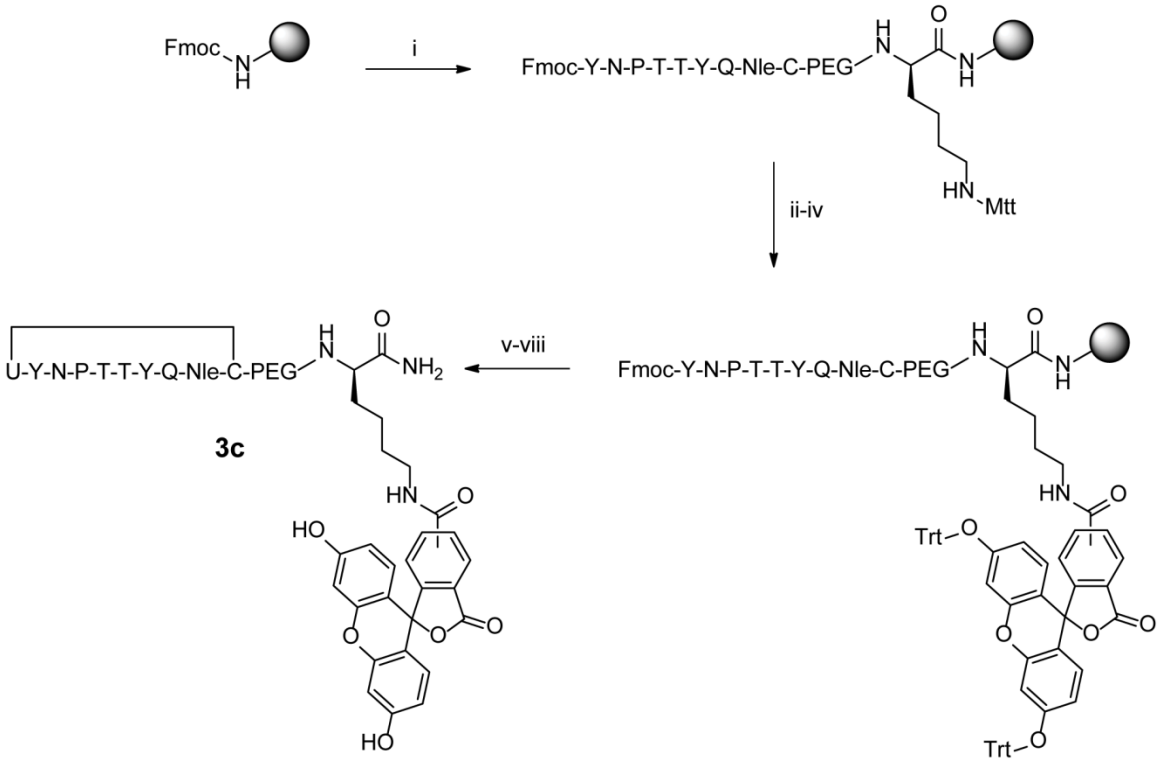

FIGURE 3.4 Synthesis of Selenylsulfide Peptide 3c
(i) Fmoc-based solid phase peptide synthesis on rink amide MBHA resin. Deprotections: 25% piperidine in NMP, 25 min. Couplings: 10 equiv amino acid, 9.9 equiv HCTU, 20 equiv DIPEA in NMP, ≥45 min. (ii) 1% TFA in DCM, 30 x 2 min. (iii) 2 equiv 5(6)-carboxyfluorescein, 1.8 equiv HCTU, and 4.6 equiv DIPEA in DMF, overnight. (iv) 6 equiv Trityl chloride and 6 equiv DIPEA in DCM, overnight. (v) Deprotection: 25% piperidine in NMP 25 min. Coupling: 5 equiv Fmoc-Sec(PMB)-OH, 4.95 equiv HCTU, 10 equiv DIPEA in NMP, 95 min. (vi) 25% piperidine in NMP, 3 x 5 min. vii) 95% TFA, 2.5% water, 2.5% Triisopropyl silane, 3 h. (viii) 97.5% TFA, 2.5 % thioanisole, 0.25 equiv DTNP, 1.5 h.

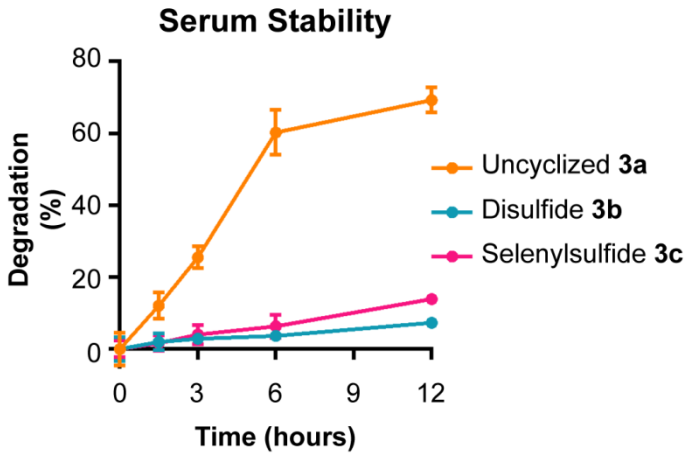

FIGURE 3.5 The Selenylsulfide Peptide is Stable to Serum Proteases
Peptides **2a-c** were incubated in the presence of 50% mouse serum over a time course of 12 h. Degradation was monitored by LC-MS. The 280 nm absorbance of each peptide and their corresponding degradation products was measured. Degradation was measured as compared to the initial time point. Error bars represent SD.

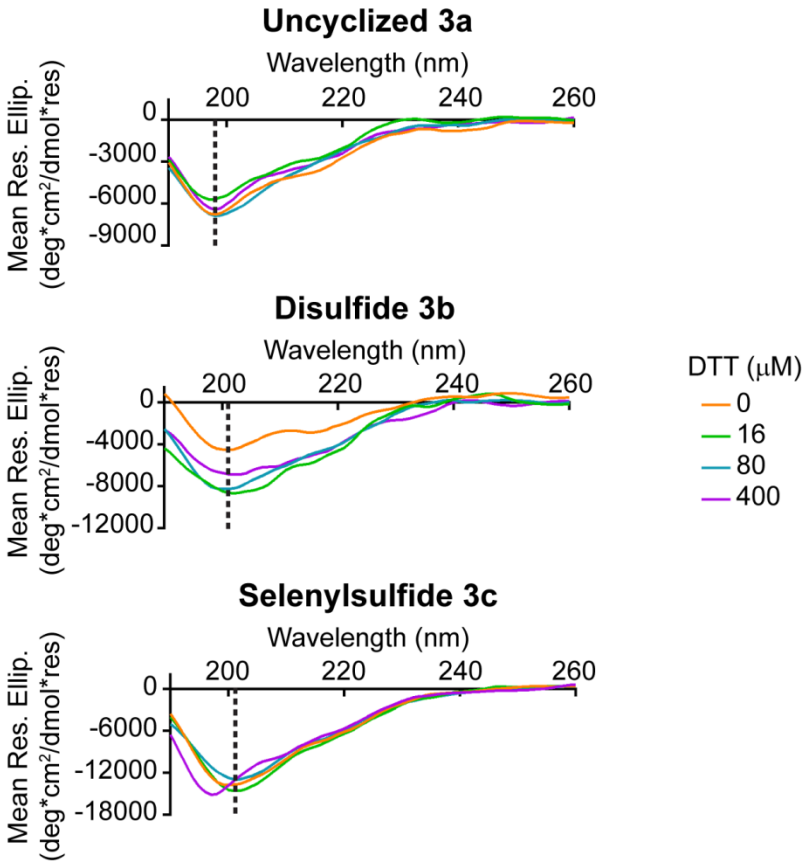

FIGURE 3.6 The Selenylsulfide-Bridged Peptide is Resistant to Reduction by DTT By circular dichroism analysis, the selenylsulfide showed a notable shift in the minimum from 201 nm to 198 nm after the addition of 400 μM DTT (32 equiv), demonstrating the stability of the peptide in the presence of a reducing agent. The dashed line indicates the minima at 0 μM DTT.

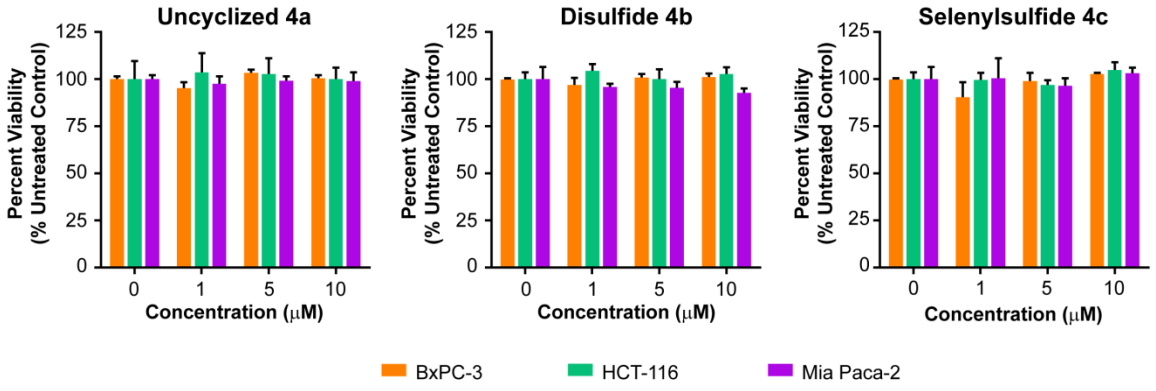

FIGURE 3.7 Selenylsulfide 4c is Non-Toxic
Cells were incubated with unlabeled peptide for 6 h, followed by cell viability analysis using an MTT assay. Percent viability relative to the untreated control is reported as the average of quadruplicates, where error bars represent SEM. A two-way ANOVA was performed for all cell lines with Tukey's multiple comparison test. For all conditions, $p > 0.5$ as compared to the untreated control.

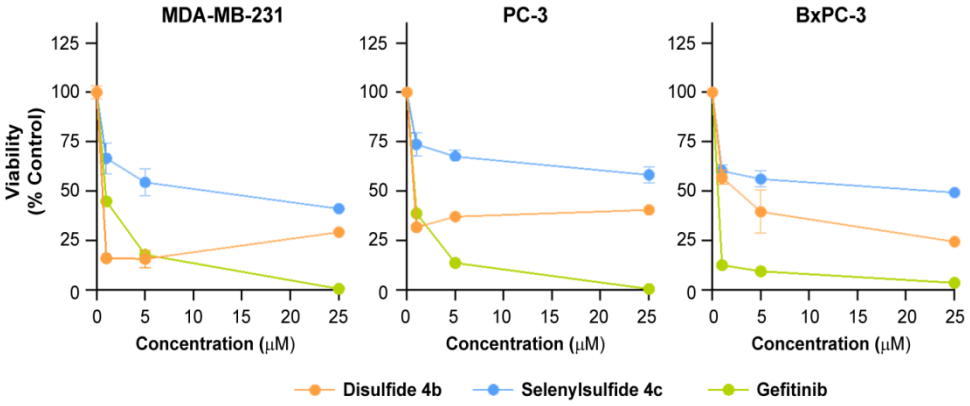

FIGURE 3.8 Selenylsulfide 4c Reduces Cell Viability[16]
Cells were incubated with peptide or gefitinib for 5 days, after which viability was measured using the CellTiter Blue assay. Fluorescence was recorded using 530/25 nm excitation, and 590/35 emission filters. Selenylsulfide **4c** reduced viability by 59%, 42%, and 51% in MDA-MB-231, PC-3, and BxPC-3 cells, respectively. Data is plotted as average percent viability of quadruplicates relative to the vehicle control, where error bars represent SEM.

[16] Previously unpublished figure

CHAPTER 4

SYNTHESIS OF A 1,5-DISUBSTITUTED TRIAZOLYL-BRIDGED EGFR DIMERIZATION ARM MIMIC[17]

[17] L.E. Hanold, P. Liaw, A.M. Beedle, E.J. Kennedy. To be submitted to *ChemBioChem*.

4.1 Abstract

Protein-protein interactions are attractive targets for the development of allosteric modulators of kinase activity. Features present at the interface of these interactions can provide templates for the development of peptide-based PPI disruptors. These features may be composed of a variety of secondary structures, including well-defined helices, strands and loops. The epidermal growth factor receptor (EGFR) dimer is an extensively studied example of a PPI that is stabilized by a β-loop structure called the dimerization arm. Peptides mimicking the dimerization arm may disrupt the dimer interface, enabling the study of this interaction and its contribution to EGFR activation and signal transduction. These mimics can be constrained and stabilized using cyclization strategies, including the triazolyl-bridge. The [1,2,3]-triazolyl-bridge offers a highly stable, irreversible and unreactive modification that can be incorporated between amino acid side chains using azide-alkyne cycloaddition. The regioselectivity of the reaction depends on the catalyst used, with copper promoting the 1,4-substitution pattern, while ruthenium catalysts promote the 1,5-substitution. The differences in the structure of these two bridges may affect the overall conformation of the peptides, which may alter their affinity for the target. Thus, we sought to develop a 1,5-triazolyl-bridged analog of our previously reported dimerization arm mimic, EDA2, for future comparison of structure and activity. Testing various reaction conditions with ruthenium based catalysts, we synthesized a 1,5-disubstituted triazolyl-bridged dimerization arm mimic, 1,5-EDA2. The structure and stability of this peptide were compared to 1,4-EDA2 using circular dichroism and serum stability assays, which demonstrated that differences between the two bridges affected the overall secondary structure without compromising stability. This is one of the first

reported examples of a 1,5-triazolyl-bridged peptide designed to mimic a β-loop that stabilizes a protein-protein interaction.

4.2 Introduction

Protein-protein interactions have significant roles in a variety of cellular processes, including signal transduction pathways and spatiotemporal regulation [1-4]. In signal transduction cascades, PPIs can serve as allosteric modulators of enzymes or function as scaffolds to recruit elements of a signaling cascade to a signaling event [1-4]. Disrupting these interactions presents a promising strategy for studying the kinases without alterations in gene expression or the potential off-target effects of small molecules that target the highly conserved kinase active site [132]. Additionally, disease relevant PPIs represent promising targets for therapeutic development [10,11]. One extensively studied example of a therapeutically relevant PPI is the EGFR dimer [48,49,53,54,82]. EGFR, a receptor tyrosine kinase, is a well validated target for anti-cancer therapeutic development. Receptor dimerization is primarily stabilized by a β-loop called the dimerization arm (Figure 4.1a) and leads to activation of the kinase domains [49,54]. Sequence of alignment of the EGFR dimerization arm illustrates that the turn residues of this loop are conserved in multiple species (Figure 4.1b), suggesting the importance of these residues in the interactions with the PPI interface. Secondary structures, such as the EGFR dimerization arm, that contribute to “hot-spot” binding in PPIs provide a template for the design of PPI disruptors.

Constrained peptides are promising protein-protein interaction disruptors. Peptides can be designed to mimic key protein features that are critical to interactions at the PPI interface [42,130]. Although an unmodified peptide sequence is highly flexible in

aqueous solution, a chemical constraint can help to stabilize the preferred secondary structure and reduce the conformational flexibility of the peptide, lowering the entropic barrier that the peptide must overcome for binding [132]. A chemical constraint can also improve proteolytic stability by reducing the accessibility of the peptide backbone to proteases. Furthermore, some constraints as well as peptide modifications may help to improve cell penetration, enabling the design of peptides for intracellular targets [131]. The triazolyl-bridge is a promising constraint that has been reported to stabilize hairpins and helices [41,153,155,170]. Although additional modifications may be necessary to improve uptake, the triazole is suitable for extracellular targets and has the advantage of being irreversible and hydrophilic, enhancing both stability and solubility [149].

While the incorporation of a 1,4-triazole is extensively reported in the literature as a peptide bond surrogate, a cyclization strategy or a side chain modification, there are fewer examples of peptides bearing a 1,5-triazolyl bridge [148,155,166-173]. Similar to the 1,4-triazole, the 1,5-triazole has applications in the synthesis of peptide bond surrogates or in peptide macrocyclization [153,209]. Cyclization may be performed off-resin, yet this approach may result in a lower purity as oligomeric peptides may be formed [210]. The 1,5-triazole can also be formed on-resin, yet there are fewer examples of this method. A transition metal-free cyclization strategy was reported for peptides bearing a 1,5-triazole [151,152]. However, this strategy was reported for cyclic peptides bearing a head-to-tail constraint rather than side-chain-to-side-chain, which prevents modification of the peptide termini. In an alternative strategy, a sunflower trypsin inhibitor peptide was synthesized using ruthenium catalyzed azide-alkyne cycloaddition, resulting in formation of the triazolyl-bridge between side chains [154]. In the same

report, the structures of the 1,4- and 1,5-disubstituted triazolyl-bridges were compared to that of the disulfide bridge, demonstrating that these regioisomers affected the distance between peptide strands. Due to these differences, the substitution patterns of the triazolyl bridge may contribute to the overall conformation of the peptide, affecting the affinity of the peptide for its target.

Previously, we developed a 1,4-triazolyl-bridged dimerization arm mimic for EGFR dimerization disruption, referred to here as 1,4-EDA2 [187]. As the 1,5-disubstituted triazolyl bridge may have a different effect on the overall conformation of the peptide, we sought to develop a 1,5-triazolyl-bridged dimerization arm mimic for further evaluation. Here we describe the development of 1,5-EDA2 using on-resin ruthenium-catalyzed azide-alkyne cycloaddition. The structure and stability of 1,5-EDA2 relative to 1,4-EDA2 are also discussed.

4.3 Results and Discussion

4.3.1 Peptide Design and Synthesis

Using 1,4-EDA2 as a template, a peptide bearing the 1,5-disubstituted triazolyl-bridge was developed (Figure 4.2). Azido-homoalanine was incorporated at the C-terminus, while propargyl glycine was incorporated at the N-terminus. Peptides were synthesized on solid support using standard Fmoc methods. Two different pentamethylcyclopentadienyl ruthenium chloride catalysts were selected for the reaction: a bis(triphenylphosphine) substituted catalyst ($Cp^*RuCl(PPh_3)_2$) and a cyclooctadiene substituted catalyst ($Cp^*RuCl(COD)$). The $Cp^*RuCl(PPh_3)_2$ catalyst is stable to high temperatures, while the cyclooctadiene is more easily displaced in the $Cp^*RuCl(COD)$ catalyst [211]. Thus, each catalyst offers different advantages.

Ruthenium catalyzed azide-alkyne cyclization was performed using conditions previously described on rink amide MBHA resin, with 0.2 equiv Cp*RuCl(COD) in DMF in a 60°C oil bath for 5.5 hours [154]. However, cyclization was undetected using these conditions. To improve the yield of the cyclized peptide, we tested different conditions, altering catalyst, solvent and reaction time. Preliminary experiments were designed to select the solvent for future experiments. Three solvents with varying polarity were selected: dimethylformamide (DMF), tetrahydrofuran (THF) and toluene. As the resin showed poor swelling capacity in toluene, DMF and THF were selected for additional experiments. Cyclization was performed using 0.2 equiv. Cp*RuCl(PPh_3)$_2$ in either DMF or THF for up to 24 hours at 60°C. A low loading resin was selected in order to reduce interstrand crosslinking. The reaction was performed on a 10 µmol scale in vented polypropylene vials. While a small amount of cyclization was observed in the first replicate of this synthesis, with the most cyclization observed at 24 hours, cyclization was not detected in subsequent syntheses. Although there was little difference in the amount of cyclization in DMF or THF, the swelling capacity of the resin seemed improved in DMF. For future experiments we sought to reduce evaporation, maintain anhydrous conditions, and increase catalyst concentration in order to improve cyclization.

As there seemed to be little difference between cyclization in the presence of DMF or THF, DMF was used for further testing due to improved resin swelling and higher boiling point. Cyclization was next tested in the presence of two different catalysts, Cp*RuCl(COD) and Cp*RuCl(PPh_3)$_2$. The reaction was performed on a 25 µmol scale using 0.5 equiv. of catalyst under inert gas and anhydrous conditions for 24 hours at 60°C. Cyclized product was detected under these conditions, with little to no

starting material remaining after 24 hours. The purified yield of fluorescein labelled peptide was less than 1%, and there seemed to be little difference between cyclization using Cp*RuCl(PPh_3)$_2$ and Cp*RuCl(COD). However, an impurity was observed in the crude product of peptide cyclized with Cp*RuCl(PPh_3)$_2$, which was difficult to separate from the cyclized peptide during RP-HPLC. This impurity had a mass of approximately 14 amu less than the expected peptide mass. As reactions with Cp*RuCl(PPh_3)$_2$ did not appear to improve the yield of cyclized peptide, and the impurities in the crude product of this peptide were difficult to separate from the cyclized peptide, Cp*RuCl(COD) was used in future experiments.

Although the no starting material was detected after the 24 hour cyclization in the presence of Cp*RuCl(COD), the overall yield of the peptide after cyclization and labeling was low. To determine if the reaction time could affect the purity and yield of the peptide, peptide was reacted with catalyst for 6, 12 and 25 hours. There was a dramatic decrease in purity of the crude product following the ruthenium catalyzed cyclization, with a purity of approximately 65% and 16-18% for the starting material and cyclized product, respectively (Figure 4.3). There was little difference in the purity between 6 and 25 hours, with a percent purity of 16 ± 2, 17 ± 3, and 18 ± 2 at 6 hours, 12 hours and 25 hours, respectively. These results indicate that the reaction can proceed for longer times without an effect on the overall purity. However, little to no starting material was observed after 6 hours, indicating that all material had reacted, and the extended reaction times did not improve yield of the peptide. The overall yields were approximately 2.0%, 1.2% and 1.1% for the 6, 12 and 25 hour reactions, respectively. These results demonstrate that there is no advantage to extending the reaction time, which

may reduce the yield. Under these conditions, the yield is fairly comparable to that of the previously reported synthesis using microwave synthesis [154]. Since all of the starting material had reacted by 6 hours, and longer reaction times appeared to reduce the yield, it may be necessary to terminate the reaction before 6 hours so as to improve the yield and purity of the peptide.

4.3.2 Circular Dichroism

Circular dichroism experiments were performed to determine if the 1,5-disubstituted triazolyl-bridge affected the overall secondary structure of the dimerization arm peptide. Spectra were obtained in 10 mM phosphate buffer, pH 7, for the uncyclized parental peptide, 1,4-EDA2 and 1,5-EDA2 (Figure 4.4). The parental peptide displayed a representative random coil spectrum with a minimum at approximately 198 nm. A broad minimum was observed at approximately 209 nm for 1,4-EDA2, with a minor minimum at 220 nm. The spectrum of1,5-EDA2 displayed a minimum at approximately 200 nm, with a shoulder at approximately 218 nm. Interestingly, the spectra of 1,5-EDA2 closely resembled that of the parental peptide. The variations between the spectra of 1,4-EDA2 and 1,5-EDA2 suggest that the regiochemistry of the triazole moiety in the bridge may affect the overall structure of the peptide.

4.3.3 Serum Stability of the Cyclic Peptides

To determine if the two bridges affect the overall stability of the peptide in the presence of serum proteases, serum stability experiments were performed over a 24 hour time course using 75% mouse serum. Peptide was quantified using LC-MS, measuring absorbance at 280 nm and normalizing the absorbance of the parent peptide to that of the internal standard (Figure 4.5). After 3 hours, no peaks corresponding to the mass of the

uncyclized peptide were observed, indicating complete degradation of the uncyclized control. A peak corresponding to the mass of 1,4-EDA2 and 1,5-EDA2 was observed at each time point, demonstrating that the bridged peptides are more resistant to degradation than the uncyclized peptide. The 1,5-triazolyl bridged peptide appears to be slightly more stable than the 1,4-triazolyl-bridged peptide, with 34% 1,5-EDA2 and 56% 1,4-EDA2 degraded after 24 hours. Interestingly, 1,5-EDA2 was resistant to proteolytic degradation despite the similarities in the circular dichroism spectra compared to the rapidly degraded uncyclized peptide.

4.4 Conclusions

The 1,5-disubstituted triazolyl-bridged EGFR dimerization arm mimic was synthesized. Multiple conditions were tested for the ruthenium-catalyzed azide-alkyne cycloaddition. Reaction with 0.5 equiv. Cp*RuCl(COD) at 60°C for 6 hours appeared to be favorable conditions for formation of the 1,5-EDA2, with an overall yield approximately two-fold greater than 25 hour reactions. Additional testing of reaction conditions at different temperatures and shorter reactions times may improve the yield and purity. Circular dichroism spectra indicate that the secondary structural content of 1,5-EDA2 may more closely resemble that of the uncyclized peptide than that of 1,4-EDA2. Interestingly, despite this similarity, 1,5-EDA2 was resistant to proteolytic degradation, while the uncyclized peptide was rapidly degraded, suggesting that the shift in the minimum was a result of increased secondary structure stabilization. Further analysis of the structure using NMR techniques may elucidate the effects of the two bridges on the overall structure and flexibility of the peptide. Future cell-based experiments will determine if these differences between the bridges affect the overall

activity of the peptide. This is one of the first reported examples of a 1,5-triazolyl-bridged peptide designed to mimic a critical feature of the PPI interface.

4.5 Materials and Methods

4.5.1 General Information

Resins and Fmoc-protected amino acids were purchased from Novabiochem unless otherwise noted. O-(6-Chlorobenzotriazol-1-yl)-N,N,N′,N′-tetramethyluronium hexafluorophosphate (HCTU) and Fmoc-11-amino-3,6,9-trioxaundecanoic acid (Fmoc-PEG3) were purchased from ChemPep. All solvents and chemical reagents were purchased from Sigma, Fisher, or Acros and used without further purification. Phosphate buffered saline (PBS) was obtained from Lonza.

High-performance liquid chromatography (HPLC) and liquid chromatography-mass spectrometry (LC-MS) were performed on an Agilent 1200 series HPLC coupled to an Agilent 6120 quadrupole mass spectrometer using ChemStation software version B.04.02 SP1. The Biotek Synergy 2 microplate reader and the Gen5 software version 2.00.18 were used to obtain absorbance measurements. Circular dichroism spectra were obtained using a JASCO J-710 CD spectrometer and the Spectra Manager software version 1.08.01.

4.5.2 N-Fmoc-azidohomoalanine Synthesis

Fmoc-azidohomoalanine was synthesized as previously described [176]. To a 100 mL round bottom flask containing a magnetic stir rod, sodium azide (2.340 mg, 36 mmol, 6 equiv) was added and dissolved in water (15 mL). The flask was fitted with a septum and purged with argon. The solution was allowed to cool to 0°C, after which a 1 M solution of triflic anhydride in DCM (18 mL, 18 mmol, 3 equiv) was added dropwise to

the solution. The solution was stirred on ice under argon for 2 hr. Saturated sodium bicarbonate was added until carbon dioxide no longer evolved. The organic layer was then collected by separatory funnel, and the aqueous layer was washed twice with 10.6 mL DCM. The combined organics were then returned to a separatory funnel and saturated sodium bicarbonate was added to the funnel.

In a 500 mL round bottom flask containing a magnetic stir rod, zinc chloride (57 mg, 0.42 mmol, 0.07 equiv), Fmoc-diaminobutyric acid (2.042 g, 6 mmol, 1 equiv) were dissolved in water (36 mL). Triethylamine (2.509 mL, 18 mmol, 3 equiv) was added dropwise followed by methanol (120 mL). The solution of triflic anhydride was added dropwise to the amino acid mixture. The reaction was allowed to proceed at room temperature while the reaction progress was monitored by TLC. After the starting material was consumed, approximately 2.5 hr, the organics were removed by rotary evaporation. A solution of 1% citric acid (60 mL) was added and the organics were extracted with three 60 mL portions of DCM. The combined organics were dried over magnesium sulfate, and solvent was removed by rotary evaporation. Fmoc-Azidohomoalanine was purified by silica gel chromatography using 0.5-7% methanol in DCM. The product was confirmed by LC-MS: molecular weight = 389.1 (expected 366.4; sodium adduct 389.4)

4.5.3 General Peptide Synthesis

Peptides were synthesized manually using Fmoc chemistry on solid support. Amino acids were coupled using a solution of 0.5 M amino acid in NMP (1 mL, 10 equiv.), 0.5 M HCTU in NMP (990 µL, 9.9 equiv.), and 174 µL of DIPEA (20 equiv.). Fmoc-azidohomoalanine, Fmoc-propargyl glycine, and Fmoc-PEG_3 were coupled using

half of these volumes. The solution was allowed to bubble for at least 45 min, and the resin was then washed three times with NMP to remove coupling reagents. The N-terminal Fmoc group was removed with a solution of 25% piperidine in NMP for 25 min, after which the resin was washed three times with NMP. The coupling and deprotection cycle was repeated until the peptide sequence was complete. The peptide was left Fmoc-protected during cyclization reactions. After completion of the peptide sequence and/or cyclization, the peptide was deprotected to expose the N-terminal amine. Labelled peptides (25 µmol) were reacted with 5(6)-carboxyfluorescein (19 mg, 50 µmol, 2 equiv), HCTU (19 mg, 45 µmol, 1.8 equiv) and DIPEA (20 µL, 115 µmol, 4.6 equiv) in DMF overnight. The resin was washed three times with DMF and dried after washing three times each with DCM, ether, and methanol. Peptides (25 µmol) were then cleaved in 1.5 mL solution containing 95% TFA, 2.5% triisopropylsilane, and 2.5% water for 4 hr. The solution was filtered through glass wool into 3 mL ice cold *tert*-butyl-methyl ether and centrifuged at 0-4°C and 2800 rcf for 30 min. The supernatant was decanted and the pellet containing the crude peptide was dried by forced air. Peptides were then dissolved in at least 1 mL methanol and filtered through a 0.45 µm PTFE filter for characterization by LC-MS and purification by RP-HPLC. Labeled peptides were then quantified using the absorbance at 495 nm in 10 mM Tris base pH 8 and the extinction coefficient of 68000 M^{-1}. Unlabeled peptides were quantified using the absorbance at 280 nm and the extinction coefficient of for tyrosine of 1280 M^{-1} in 6 M guanidine HCl, 0.02 M sodium phosphate monobasic, pH 6.5. PEGylated parental molecular weight = 1791.0 (expected 1791.9); uncyclized control = (expected 1569.6).

4.5.4 Copper-Catalyzed Azide-Alkyne Cycloaddition

EDA2 was synthesized according to the general peptide synthesis procedure using PAL-NovaPEG resin (resin loading 0.37-0.56 μmol/g). The resin was dried prior to Fmoc removal and 25 μmol (according to initial resin loading) was loaded into a 2 mL reaction vial and equilibrated with 1.5 mL 2:1 water/*t*-butanol. Copper (II) sulfate (55 mg) and sodium ascorbate (160 mg) were added and the mixture was agitated until the color of the solution changed to a bright orange color. The vial was placed on a rotisserie overnight, after which the resin was returned to a fritted column, washed three times each with 2:1 water/*t*-butanol and methanol and dried. Resin (10-12 mg) was removed for cleavage in 0.5 mL cleavage solution using standard procedures. Cyclization was confirmed by a shift in retention time compared to the starting material. The remaining peptide was then deprotected, labeled, and cleaved using standard procedures. Unlabeled 1,4-EDA2 molecular weight = 1218.8 (expected 1219.3); 1,4-EDA2 = 1647.6 (expected = 1648.7).

4.5.5 Solvent Effects on Ruthenium-Catalyzed Azide-Alkyne Cycloaddition (RuAAC)

The EDA2 sequence was synthesized according to general peptide synthesis procedures using Rink Amide MBHA. The resin was dried and 10 μmol resin was transferred into 2 mL reaction vials. The vials were purged with argon and the resin was equilibrated in 0.25 mL dry toluene, THF or DMF. To the resin, 4 mM Cp*RuCl(PPh_3)$_2$ (0.5 mL, 2 μmol, 0.2 equiv) in either toluene, THF or DMF was added. The caps of the vials were vented with a needle, and the reaction mixture was agitated on a thermomixer at 60°C and 800 rpm for 6-24 hrs. Solvent was replaced as necessary due to evaporation. The reaction was terminated by washing three times each with methanol, 0.5% sodium

diethyldithiocarbamate in DMF, and DMF. The resin was dried and cleaved using standard procedures. LC-MS was used to detect cyclization.

4.5.6 The Effect of Catalyst on RuAAC

The EDA2 peptide sequence was prepared according to general procedures on Rink amide AM resin (loading of 0.43 mmol/g). The dried resin containing Fmoc-protected peptide (25 µmol) was transferred to a dry, 10 mL round bottom flask with a magnetic stir bar. The flask was fitted with a septum and purged with argon. Dry DMF (0.75 mL) was added and the resin was equilibrated. Cp*RuCl(PPh_3)$_2$ (11 mg, 14 µmol) or Cp*RuCl(COD) (5 mg, 13 µmol) was added to a dry teardrop flask. The flask was fitted with a septum and purged with argon. Dry DMF (2.5 mL) was added and the solution was heated to 60°C and stirred under argon. The catalyst solution (2.19 mL, 12 µmol, 0.5 equiv.) was then added to the resin, and the solution was stirred at 60°C under argon for 24 hr. After 24 hours, the resin was washed three times each with methanol, 0.5% sodium diethyldithiocarbamate in DMF, and DMF. The resin was dried and 11 mg of resin was removed for cleavage in 0.5 mL cleavage solution using standard procedures. The cleaved peptide was dissolved in methanol, and cyclization was confirmed by detecting a shift in retention time compared to the starting material using LC-MS. The remaining peptide was deprotected, labelled and cleaved using standard procedures. 1,5-EDA2 molecular weight = 1648.0 (expected 1648.7).

4.5.7 Effect of Reaction Time on RuAAC

The EDA2 sequence was prepared as described above on Rink amide AM resin (loading = 0.43 mmol/g). After completion of the sequence, the resin was dried and 25 µmol was transferred to 3 dry, 10 mL round bottom flask with a magnetic stir rod. The

flask was fitted with a septum and purged with argon. The resin was then swelled in 0.75 mL of dry DMF. A solution of Cp*RuCl(COD) (16 mg, 42 μmol) in dry DMF (7.5 mL) was prepared, and 2.2 mL of this solution was added to the resin in each flask (12 μmol, 0.5 equiv catalyst). The reaction mixture was stirred at 37°C under argon. After 6, 12 or 25 hours, the catalyst was removed by washing three times each with methanol, 0.5% diethyldithiocarbamate in DMF, and DMF. The resin was equilibrated in NMP and the peptide was deprotected in 25% piperidine in NMP for 25 min. The resin was dried and the peptide was cleaved using standard procedures, and cyclization was confirmed by a shift in retention time compared to the starting material using LC-MS. Peptides were eluted using a gradient of 10%-100% acetonitrile in water with 0.1% TFA over 18 minutes, a flow rate of 0.75 mL/min, and a column temperature of 35°C. Purity was calculated as percent peptide absorbance at 280 nm relative to the total absorbance of peaks eluting after 5 minutes using the auto integration function in ChemStation. Uncyclized EDA2 molecular weight = 1219.2 (expected 1219.3); unlabeled 1,5-EDA2 = 1219.0 (expected 1219.3).

4.5.8 Circular Dichroism Spectra

Circular Dichroism Spectra were obtained for the non-modified peptide, 1,4-EDA2, and 1,5-EDA2. The peptides were dissolved in 10 mM sodium phosphate buffer pH 7.0 and filtered through a 0.45 μm PTFE filter. Spectra were collected from 190-260 nm at 25 °C using a Jasco circular dichroism spectrometer. Response time = 4 sec, bandwidth = 2 nm, and scan rate = 50 nm/min. A smoothing filter was applied in to the spectra using the Prism's Savitzky-Golay algorithm with a smoothing factor of 11.

4.5.9 Serum Stability Assay

Solutions containing 0.2 mM peptide, 2.5% DMSO, 0.2% benzyl alcohol and 75% mouse serum (previously frozen) in PBS were prepared in triplicate. A 10 µL aliquot from each was immediately removed and quenched with 10 µL acetonitrile. The precipitates were pelleted by centrifugation for 5 min at 14,000 rpm. The supernatant was collected and analyzed by LC-MS. The remaining samples were incubated at 37°C on a thermomixer at 300 rpm. Aliquots were removed and quenched as described after 3, 6, 12, and 24 hr. Peaks were integrated manually at 280 nm, and the average of three manual integrations were recorded for each sample. The integrations of the parent peptide peak were normalized to those of the internal standard. Percent parent peptide is plotted as the average of three replicates, where error bars represent SD.

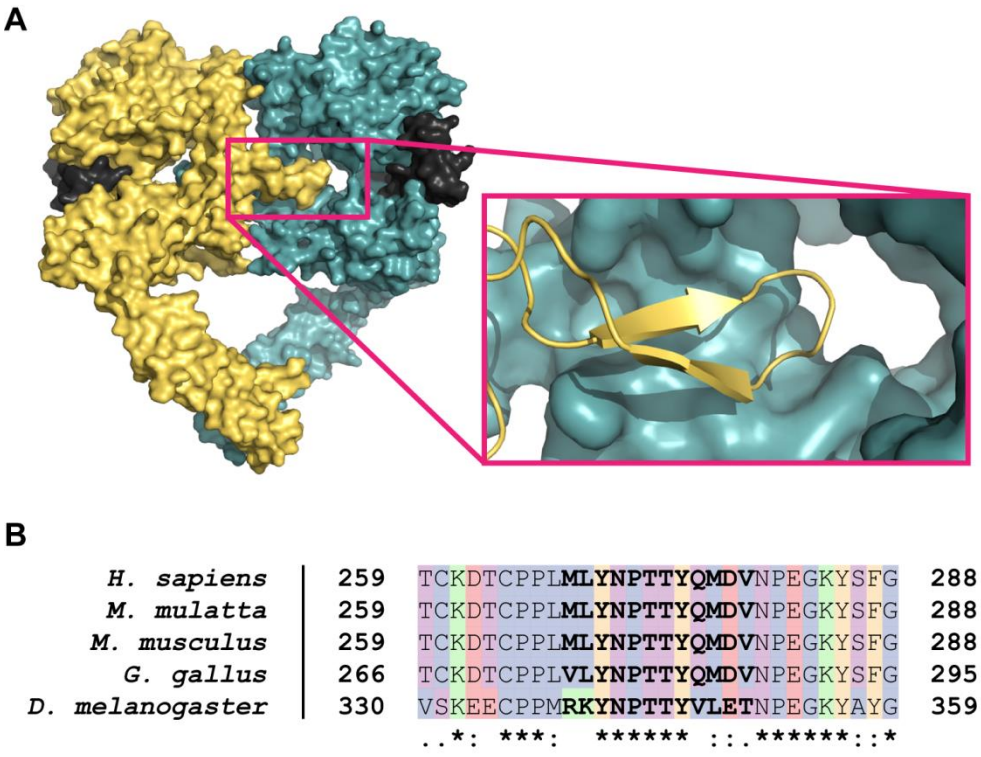

FIGURE 4.1 Sequence and Structure of the EGFR Dimerization Arm
(a) EGFR dimerizes upon ligand binding, allowing for activation of the kinases. The receptor dimer is shown in yellow and teal. EGF is shown in dark grey. A magnification of the dimerization arm (yellow cartoon) is shown bound to domain II of the activated receptor (inset). Structures were generated in Pymol using the PDB file 3NJP. (b) Sequence alignment of the dimerization arm and surrounding residues in human (P00533), rhesus macaque (P55255), mouse (Q01279), chicken (P13387) and fruit fly (P04412). The dimerization arm beta-loop residues are shown in bold. The turn residues of the dimerization arm are conserved between the selected species. Residues are highlighted as polar uncharged (purple), basic (green), acidic (red), hydrophobic (blue), and aromatic (yellow).

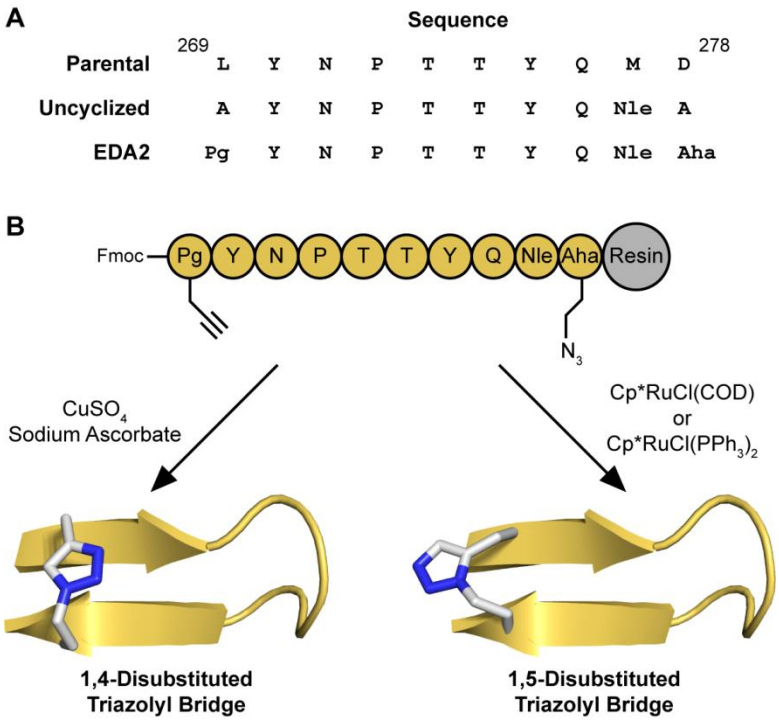

FIGURE 4.2 Design of Triazolyl-Bridged Dimerization Arm Mimics
(a) Sequences of the EGFR dimerization arm peptides. Triazolyl-bridged peptides were based on the native dimerization arm sequence with the azide and alkyne functionalities incorporated at the termini. (b) Synthesis of 1,4- and 1,5-disubstituted triazolyl-bridged dimerization arm mimics using copper- and ruthenium-catalyzed azide-alkyne cycloaddition. Avogadro was used to generate and energy minimize the triazolyl bridge structure. The bridge is shown relative to the native dimerization arm structure to emphasize differences in the bridge structure.

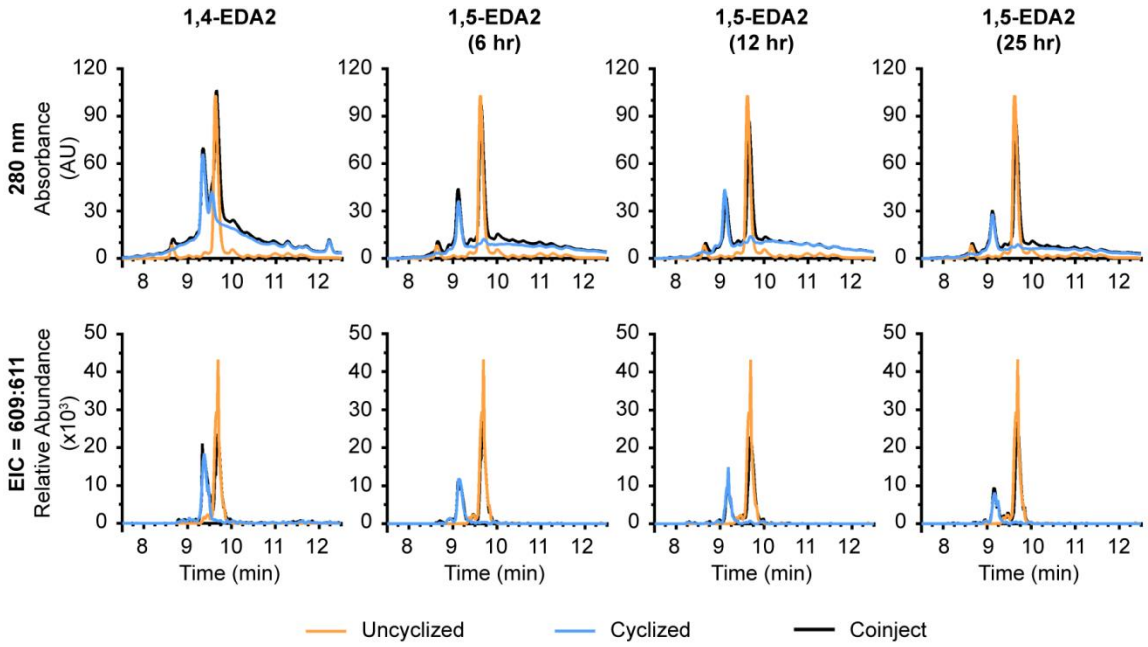

FIGURE 4.3 Confirmation of Cyclization in Crude Peptide Products
Cyclization was confirmed by a shift in the retention time of cyclized peptide relative to the uncyclized peptide using LC-MS. The absorbance at 280 nm is plotted over time (top). The relative abundance of ions of m/z = 610 is plotted over time (bottom). Uncyclized peptide had a retention time of approximately 9.6 min, while cyclized 1,4-EDA2 had a retention time of 9.3 min. Cyclized 1,5-EDA2 had a greater shift in retention to 9.1 min. Cyclized and uncyclized peptide were coinjected to confirm the presence of two separate products. The duration of the ruthenium catalyzed cyclization did not appear to have a significant effect on the purity of the crude peptide.

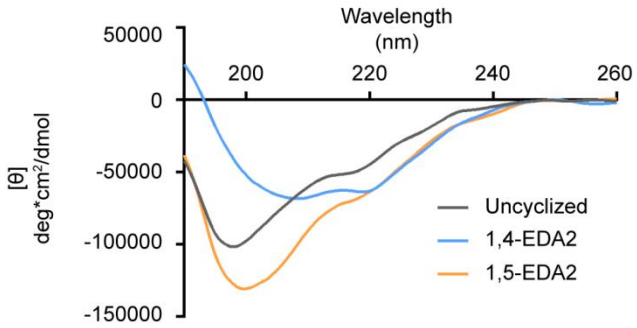

FIGURE 4.4 Circular Dichroism Spectra of Triazolyl-Bridged Peptides
Circular dichroism spectra were obtained for 1,4-EDA2, 1,5-EDA2 and the uncyclized peptide control. A minimum of 198 nm was observed for uncyclized peptide, representative of a disordered structure. Two minima were observed at approximately 209 nm and 220 nm for 1,4-EDA2. A minimum was observed at approximately 200 nm for 1,5-EDA2. Differences in the spectra of 1,4-EDA2 and 1,5-EDA2 suggest that the structure of the triazolyl-bridge may affect the overall conformation of the peptide.

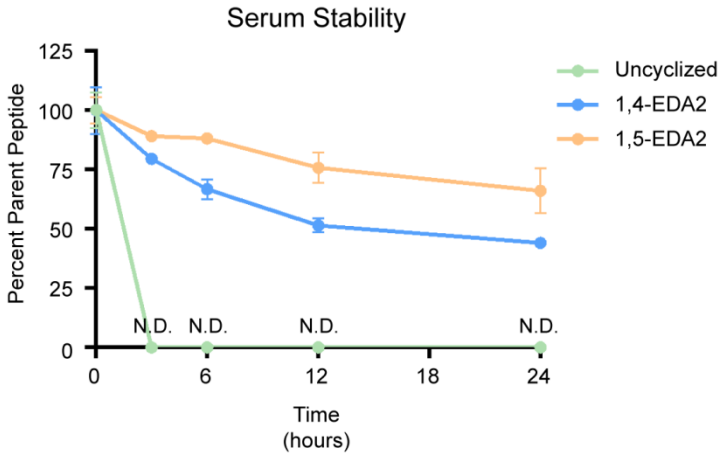

FIGURE 4.5 Serum Stability of Triazolyl-Bridged Peptides
The stability of the peptides towards serum proteases was determined. Peptides were incubated with 75% mouse serum over a time course of 24 hours. The absorbance of the peptide and internal standard were measured at 280 nm using LC-MS. The absorbance was normalized to the internal standard. Data is plotted as the average percent parent peptide relative to T0, where error bars represent SD. The mass of the uncyclized peptide could not be detected after 3 hours (N.D.), indicating complete degradation. After 24 hours, 1,4-EDA2 and 1,5-EDA2 were degraded by approximately 56% and 34%, respectively.

CHAPTER 5

CONCLUSIONS

5.1 Summary of Results

In summary, three chemistries were tested as cyclization strategies for the development of stable peptides mimicking the β-loop fold of the EGFR dimerization arm. The 1,4-disubstituted triazolyl bridge and the 1,5-disubstituted triazolyl bridge were selected as irreversible constraints with easily modified structures. The selenylsulfide was selected as a redox stable constraint that that could closely mimic the structure and chemical nature of a previously used disulfide bond [57,60]. The constrained peptides were synthesized on solid support using Fmoc chemistry, and the effect of the constraints on peptide conformation and stability were evaluated. Comparison of the three constraints revealed variations in peptide conformation, stability and ease of synthesis (Table 5.1).

Each of the constrained peptides differed in overall conformation as indicated by variations in the circular dichroism spectra. While 1,4-EDA2 showed the greatest difference compared to the unconstrained peptide, 1,5-EDA2 and the selenylsulfide-bridged peptide showed similarities, with minima of 200 nm and 201 nm, respectively. All minima were shifted compared to the unconstrained minima of 198 nm, indicating an increase in secondary structure content. Thus, these results demonstrate that the chemical constraints alter the overall conformation of the cyclic peptides. Although, circular dichroism provides information on the overall conformation of the peptides, it does not

provide complete structural information. Future studies using nuclear magnetic resonance spectroscopy or x-ray crystallography may provide detailed information on the geometry of the peptide bonds, helping to elucidate the structure of the peptides.

Although the chemical constraints differed in effect on the overall conformation of the peptides, all cyclic peptides exhibited increased resistance to proteolytic degradation. It is also interesting to note that despite similarities in the circular dichroism spectra, the unconstrained peptide was significantly less stable to proteolysis than 1,5-EDA2 and the selenylsulfide-bridged peptide. However, in contrast to the triazolyl bridge, the selenylsulfide bridge was susceptible to degradation by elimination of the selenol. Thus, the triazolyl bridge provides a more stable chemical constraint compared to the selenylsulfide bridge.

In addition to variations in the effect of the constraints on conformation and stability, differences in the ease of synthesis of the constrained peptides were noted. 1,4-EDA2 was easily synthesized on solid support using copper-catalyzed azide-alkyne cycloaddition. However, selection of a resin with suitable swelling properties in water is necessary. In contrast to 1,4-EDA2, synthesis of 1,5-EDA2 required optimization. While the formation of the 1,4-triazole was accomplished in an aqueous environment, formation of the 1,5-triazole was performed under anhydrous conditions and inert gas. Additionally, the concentration of the catalyst used in ruthenium-catalyzed azide-alkyne cycloaddition may affect the overall yield and purity of 1,5-EDA2. Furthermore, the yield and purity 1,5-EDA2 may also be affected by temperature and reaction time. Although formation of 1,5-EDA2 was accomplished on resin using 0.5 equiv. Cp*RuCl(COD) at 60°C for 6

hours, further optimization of the reaction conditions may be necessary to achieve overall yields greater than 2%.

In contrast to the triazolyl-bridged peptides, the major obstacle in the synthesis of the selenylsulfide bridged peptide was the incorporation of selenocysteine to form the bridge. The alkyne and azide that form the triazole are relatively unreactive to conditions used for Fmoc-based solid phase peptide synthesis. However, the *p*-methoxybenzyl-protected selenocysteine is susceptible to beta-elimination in the presence of base, resulting in formation of dehydroalanine. This side reaction presents limitations using Fmoc chemistry, as base is required for deprotection. Peptide synthesis using acid labile Boc chemistry is more suitable for the preparation of selenopeptides, yet this approach requires specialized equipment and harsh hydrofluoric acid for cleavage. Here, we show that synthesis of selenopeptides using Fmoc chemistry can be accomplished by incorporating the selenocysteine at the N-terminus, minimizing repeated exposure to basic deprotection conditions. This strategy presents limitations for peptide labeling, as incorporation of the label at the N-terminus results in exposure of the selenocysteine to base during deprotection. However, the C-terminal labeling procedure used for the synthesis of the selenylsulfide-bridged dimerization arm mimics circumvents this issue by enabling incorporation of the label prior to selenocysteine coupling.

Based upon these observations, the selenylsulfide bridge appears to be more limited in its applications due to potential side reactions of the selenol, yet the triazolyl bridge appears to be more versatile. Using Fmoc-based methods, the amino acids forming the triazolyl bridge can be incorporated at either terminus of the peptide, while the selenocysteine forming the selenylsulfide bridge may be more suited for the N-terminus

to minimize potential side reactions during synthesis. Additionally, the triazolyl bridges appeared to be fairly stable during serum stability assays, while elimination of the selenol was observed for the selenylsulfide-bridged peptide. However, all peptide backbones exhibited increased resistance to proteolysis. Although the overall yield of 1,5-EDA2 was relatively low, the circular dichroism spectrum was comparable to that of the selenylsulfide-bridged peptide, suggesting that the 1,5-triazole may provide a more stable alternative to the selenylsulfide while maintaining similar effects on peptide conformation. As an additional observation, the selenylsulfide-bridged peptides were less soluble than the triazolyl-bridged peptides, requiring incorporation of a short polyethylene glycol linker to improve solubility. Thus, using the two triazole constraints, enhanced stability, aqueous solubility, and multiple peptide conformations can be achieved.

Although it was not within the scope of this research to compare the binding affinities or inhibitory activities of each constrained peptide, 1,4-EDA2 was tested to evaluate the potential of the constrained β-loop mimics as PPI disruptors. Cell-based assays demonstrated that 1,4-EDA2 disrupts EGFR dimerization and phosphorylation in cells. Furthermore, 1,4-EDA2 reduced cell viability in a panel of EGFR overexpressing cell-lines. Treatment of cells with the selenylsulfide-bridged peptide also resulted in a modest reduction in viability. Notably, this activity was observed without optimization of the peptide sequence, demonstrating significant potential for this strategy in the development of optimized peptides targeting EGFR dimerization. Thus, these results suggest that constrained peptides mimicking β-loop features of the protein interface may be effective PPI disruptors with therapeutic potential.

5.2 Future Directions

The development of constrained peptides mimicking the EGFR dimerization arm and the demonstration of their potential as PPI disruptors serves as a foundation for future studies. Results indicate that the constraints alter the overall conformation of the peptides, yet the specific effects that the constraints have on the peptide structure are not well defined by circular dichroism. Additional structural information can be obtained using techniques such as nuclear magnetic resonance (NMR) spectroscopy or X-ray crystallography. Two dimensional homonuclear NMR spectroscopy techniques such as nuclear Overhauser effect spectroscopy (NOESY) or rotating frame Overhauser effect spectroscopy (ROESY) can be used to study the distances between backbone hydrogens. These techniques have previously been used to evaluate the structure of β-hairpins and may help to reveal the effects that the constraints may have on the backbone conformation of the dimerization arm peptides [212,213]. As variations in the constraints used to cyclize the peptides may affect the overall conformation of the peptide, the alterations in the constraints could ultimately affect binding affinity. Thus, in combination with structure elucidation, the results of binding studies such as co-immunoprecipitation, fluorescence anisotropy or surface plasmon resonance may help to reveal the effect of each constraint and conformation on affinity. This information can then be applied to predict the optimal conformation for binding and aid in optimization of the crosslink. Additional chemistries are available for peptide cyclization, including the all-hydrocarbon staple. Like the triazolyl-bridge, the length of the all-hydrocarbon staple can be varied by incorporating alkenyl amino acids that differ in the number of methylene units within the side chain. In contrast to the triazolyl-bridge, the all-hydrocarbon staple

introduces a large hydrophobic patch within the peptide, which may expand hydrophobic interactions with the dimerization arm binding surface.

Additional sequence optimization may also enhance the binding affinity of the peptide for EGFR. For example, substitution of Met277 with a branched aliphatic amino acid such as leucine may increase binding interactions with a nearby hydrophobic patch (Figure 5.1a). Alternatively, Met277 could be substituted with glutamic acid or glutamine to take advantage of potential hydrogen bonding interactions with His304 or Ser306 (Figure 5.1b). Since Met268 appears to have interactions with the binding interface, methionine could be added at the N-terminus of the peptide to mimic these interactions, or a glutamic acid or glutamine could be added to the N-terminus for interactions with His304 (Figure 5.1c). Computational methods would greatly aid in the prediction of favorable mutations in the peptide sequence for optimization of binding.

As the EGFR dimerization arm contributes interactions with other members of the ErbB family in the heterodimer, binding studies may also reveal the selectivity of the peptides for individual ErbB members. Since overexpression of members of the ErbB family contributes to resistance against EGFR targeted therapies, the ability of the dimerization arm mimics to bind to multiple ErbB receptors may be advantageous in therapeutic development. Alternatively, increasing the selectivity of the peptides for specific ErbB members could provide useful molecular probes in chemical biology. Since 1,4-EDA2 demonstrated the ability to disrupt EGFR dimerization, phosphorylation and cell viability, additional optimization of the peptide sequence may be performed to potentially increase selectivity for specific ErbB members. By targeting specific ErbB members, the role of the homo- or heterodimer can be studied without alteration of gene

expression. This strategy could be useful in cell lines expressing multiple members of the ErbB family, including those with ErbB2 and ErbB3 overexpression as a resistance mechanism to EGFR inhibitors. Disrupting the dimer interactions of a particular member could reveal the contributions of a particular member to downstream signaling. Thus, upon optimization, the dimerization arm mimics may serve as molecular probes of ErbB dimerization mechanisms to assess their role in signaling pathways.

The synthetic approaches used to develop the cyclic EGFR dimerization arm mimics have broader applications in the disruption of additional β-loop mediated PPIs. While many studies have focused on the development of helix mimics, relatively fewer have examined constrained peptides as disruptors of β-loop mediated interactions. The constraints used here to stabilize the EGFR dimerization arm mimics may be applied to novel β-loops targeting specific PPIs that contribute to cell signaling and disease. For example, the CD4-gp120 interaction of HIV-1 is mediated by a β-loop interaction and is considered a potential target for anti-HIV therapies (Figure 5.2) [132,183]. The CD4-gp120 interaction is reported to be involved in viral entry into the host cell, promoting conformation changes in gp120 that enable binding to chemokine receptors [214]. Current methods targeting this interaction include the development of a scorpion toxin miniprotein mimicking the CD4 loop, small molecule CD4 mimics, and a short peptide segment mimicking the turn of the CD4 loop [215-219]. Generating a constrained peptide mimicking the entire CD4 loop enables the peptide to target a larger surface area than small molecules, while reducing the size compared to the miniprotein, and maintaining stability through cyclization. Triazolyl-bridged peptides mimicking the CD4 loop may be able to disrupt this interaction and prevent viral entry. In addition to proteins involved in

viral infections, growth factor receptors are promising targets in chemical biology and drug discovery. Although many growth factor receptor dimers are stabilized through interactions of their ligands, crystal structures reveal that many have β-strand or loop interactions at the dimer interface, including fibroblast growth factor receptor (FGFR) [220], vascular endothelial growth factor receptor (VEGFR) [75], stem cell growth factor receptor kit (Kit) [68], and tyrosine kinase receptor A (TrkA) [74] (Figure 5.3). Allosteric modulators binding the extracellular domains of receptor tyrosine kinases have been reported to disrupt signaling without targeting ligand binding [221]. Thus, it may be possible for peptides that target the interface of these receptors to perturb the dimeric structure and alter kinase activity without complete ligand-receptor or dimer disruption.

Overall, the three chemistries tested here are promising cyclization strategies for the stabilization of peptides mimicking the EGFR dimerization arm. They demonstrated promise as disruptors of EGFR dimerization, and with further optimization they may have therapeutic potential. This is a significant step in the development of peptides targeting β-loop interactions as this approach may be applied to numerous PPIs mediated by β-loops, providing novel molecular probes and potential therapeutic peptides for a variety of cellular processes and disease states.

TABLE 5.1 Summary of Constraint Synthesis, Stability and Conformation

	Unconstrained	1,4-Triazole	1,5-Triazole	Selenylsulfide
Synthesis	• Facile synthesis • High yield	• **Facile synthesis** • Requires water compatible resin	• Potential sensitivity to moisture and air • Low yield	• Selenocysteine is sensitive to base • Position of selenocysteine is limited to the N-terminus
Constraint Stability	• N/A	• **Stable**	• **Stable**	• Susceptible to elimination of the selenol
Proteolytic Stability	• Rapidly degraded	• **Resistant**	• **Resistant**	• **Resistant**
Conformation	• Representative random coil spectrum with a minimum of 198 nm	• Unique spectrum with a broad minimum of at 209 nm and a second minimum at 220 nm	• Spectrum similar to unconstrained peptide with a minimum of 200 nm	• Spectrum similar to unconstrained peptide with a minimum of 201 nm

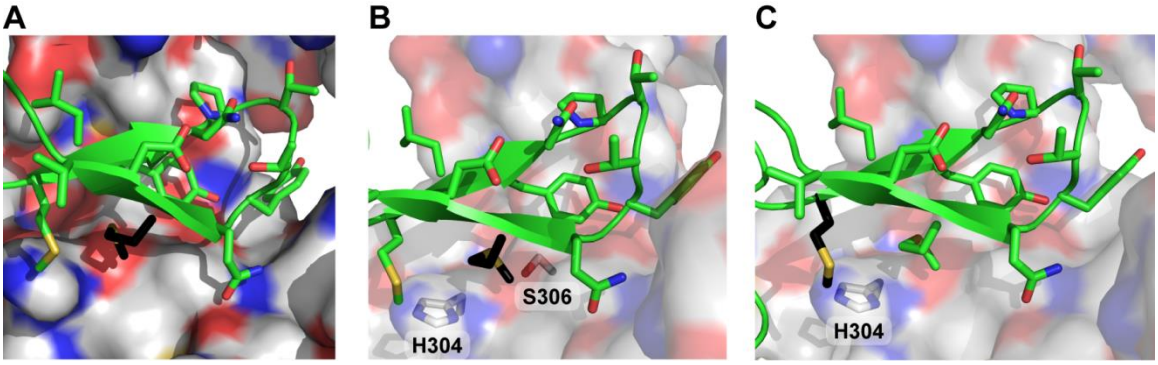

FIGURE 5.1 Selected Dimerization Arm Interactions for Optimization
Structures of the EGFR dimerization arm (green) are shown bound to EGFR. (a) Met277 (black) could be mutated to take advantage of the hydrophobic patch. (b) His304 and Ser306 are available for hydrogen bonding interactions. Mutation of Met277 (black) to a glutamic acid may take advantage of these interactions. (c) Met268 (black) could be mutated to glutamic acid for potential interactions with His204. Structures were generated in Pymol (PDB: 3NJP).

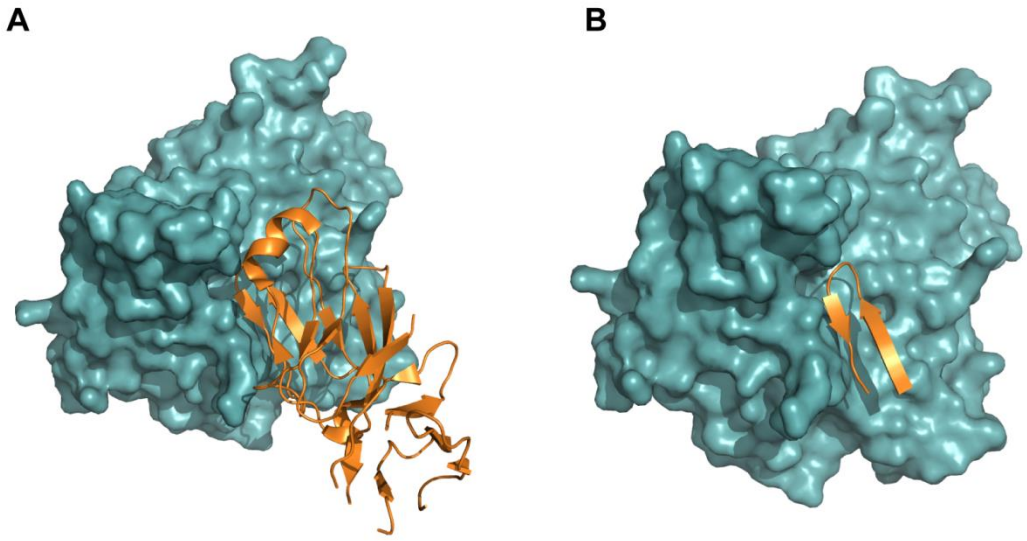

FIGURE 5.2 Structure of the CD4-gp120 Interaction
Binding of human CD4 (orange) to HIV gp120 (teal). (a) The first two domains of CD4 are shown bound to gp120. (b) The loop region of CD4 contributing a majority of the binding interactions is shown bound to gp120. A constrained peptide mimicking the β-loop fold of this structure may have potential as a disruptor of the CD4-gp120 interaction that contributes to HIV entry into host cells. Structures were generated in Pymol (PDB: 5CAY).

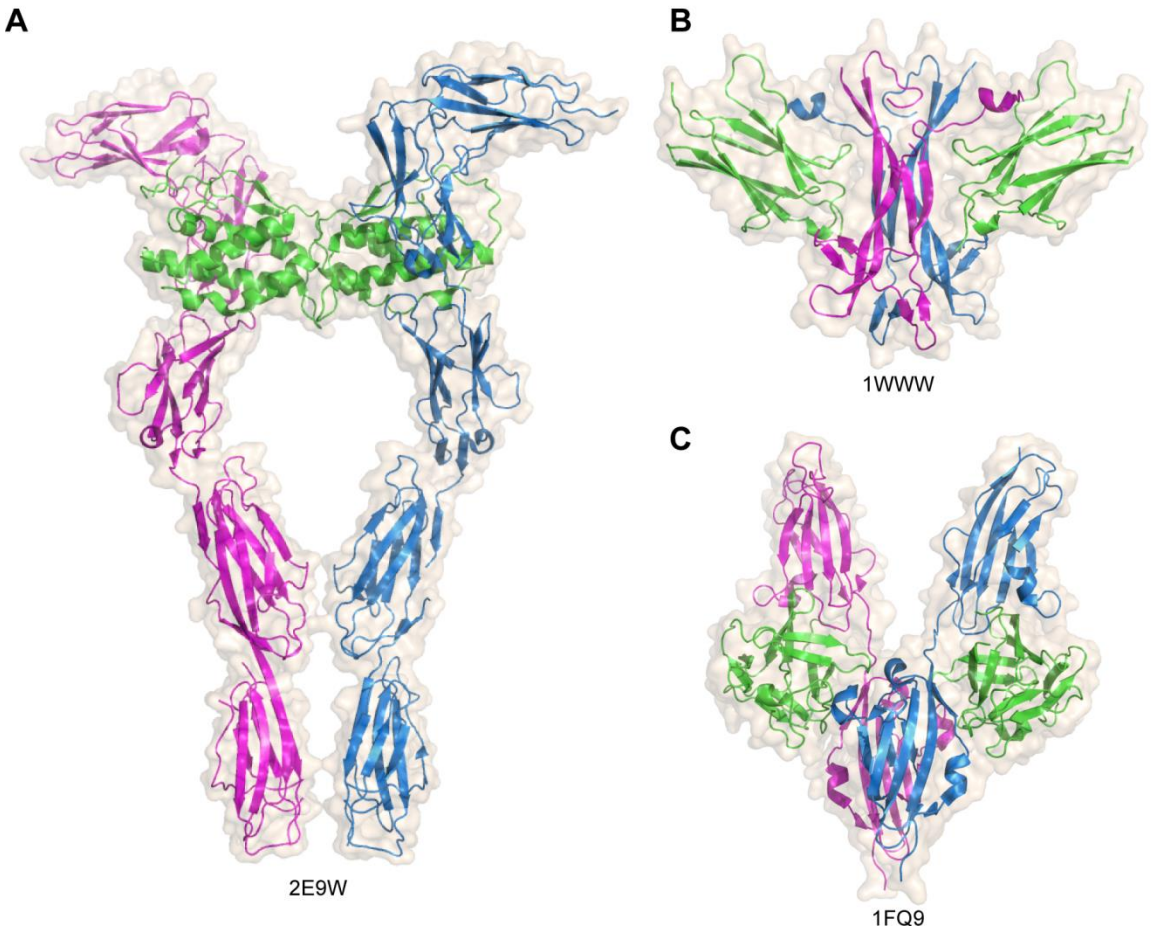

FIGURE 5.3 Oligomeric Protein Structures Showing High β-Strand Content
Structures of dimeric receptors (blue and magenta) with high β-strand content are shown in complex with growth factors (green). (a) SCF bound to the c-Kit dimer (PDB: 2E9W). (b) NGF bound to domain V of the TrkA dimer (PDB: 1WWW). (c) FGF bound to domains II and III of the FGFR1 dimer (PDB: 1FQ9).

REFERENCES

1. Braun P, Gingras A-C (2012) History of Protein–Protein Interactions: From Egg-White to Complex Networks. *Proteomics* 12: 1478-1498.

2. Sammak S, Zinzalla G (2015) Targeting Protein–Protein Interactions (Ppis) of Transcription Factors: Challenges of Intrinsically Disordered Proteins (Idps) and Regions (Idrs). *Prog Biophys Mol Biol* 119: 41-46.

3. Langeberg LK, Scott JD (2015) Signalling Scaffolds and Local Organization of Cellular Behaviour. *Nat Rev Mol Cell Biol* 16: 232-244.

4. Guarracino DA, Bullock BN, Arora PS (2011) Protein–Protein Interactions in Transcription: A Fertile Ground for Helix Mimetics. *Biopolymers* 95: 1-7.

5. Arkin MR, Wells JA (2004) Small-Molecule Inhibitors of Protein-Protein Interactions: Progressing Towards the Dream. *Nat Rev Drug Discov* 3: 301-317.

6. Fry DC, Vassilev LT (2005) Targeting Protein-Protein Interactions for Cancer Therapy. *J Mol Med (Berl)* 83: 955-963.

7. Loregian A, Palù G (2005) Disruption of Protein–Protein Interactions: Towards New Targets for Chemotherapy. *J Cell Physiol* 204: 750-762.

8. White AW, Westwell AD, Brahemi G (2008) Protein-Protein Interactions as Targets for Small-Molecule Therapeutics in Cancer. *Expert Rev Mol Med* 10: e8-e8.

9. Nero TL, Morton CJ, Holien JK, Wielens J, Parker MW (2014) Oncogenic Protein Interfaces: Small Molecules, Big Challenges. *Nat Rev Cancer* 14: 248-262.

10. Petta I, Lievens S, Libert C, Tavernier J, De Bosscher K (2015) Modulation of Protein-Protein Interactions for the Development of Novel Therapeutics. *Mol Ther*.

11. Tsomaia N (2015) Peptide Therapeutics: Targeting the Undruggable Space. *Euro J Med Chem* 94: 459-470.

12. Valkov E, Sharpe T, Marsh M, Greive S, Hyvonen M (2012) Targeting Protein-Protein Interactions and Fragment-Based Drug Discovery. *Top Curr Chem* 317: 145-179.

13. Wells JA, McClendon CL (2007) Reaching for High-Hanging Fruit in Drug Discovery at Protein–Protein Interfaces. *Nature* 450: 1001-1009.

14. Yan C, Higgins PJ (2013) Drugging the Undruggable: Transcription Therapy for Cancer. *BBA-Rev Cancer* 1835: 76-85.

15. Gonda TJ, Ramsay RG (2015) Directly Targeting Transcriptional Dysregulation in Cancer. *Nat Rev Cancer* 15: 686-694.

16. Phillips C, Roberts LR, Schade M, Bazin R, Bent A, et al. (2011) Design and Structure of Stapled Peptides Binding to Estrogen Receptors. *J Am Chem Soc* 133: 9696-9699.

17. Nilsson S, Koehler KF, Gustafsson J-Å (2011) Development of Subtype-Selective Oestrogen Receptor-Based Therapeutics. *Nat Rev Drug Discov* 10: 778-792.

18. Carry J-C, Garcia-Echeverria C (2013) Inhibitors of the P53/Hdm2 Protein–Protein Interaction—Path to the Clinic. *Bioorg Med Chem Lett* 23: 2480-2485.

19. Fagard R, Metelev V, Souissi I, Baran-Marszak F (2013) Stat3 Inhibitors for Cancer Therapy: Have All Roads Been Explored? *JAKSTAT* 2: e22882.

20. Becerril J, Hamilton AD (2007) Helix Mimetics as Inhibitors of the Interaction of the Estrogen Receptor with Coactivator Peptides. *Angew Chem Int Ed* 46: 4471-4473.

21. Galande AK, Bramlett KS, Burris TP, Wittliff JL, Spatola AF (2004) Thioether Side Chain Cyclization for Helical Peptide Formation: Inhibitors of Estrogen Receptor–Coactivator Interactions. *J Pept Res* 63: 297-302.

22. Leduc A-M, Trent JO, Wittliff JL, Bramlett KS, Briggs SL, et al. (2003) Helix-Stabilized Cyclic Peptides as Selective Inhibitors of Steroid Receptor–Coactivator Interactions. *Proc Natl Acad Sci* 100: 11273-11278.

23. Phan T, Nguyen HD, Goksel H, Mocklinghoff S, Brunsveld L (2010) Phage Display Selection of Miniprotein Binders of the Estrogen Receptor. *Chem Commun* 46: 8207-8209.

24. Rodriguez AL, Tamrazi A, Collins ML, Katzenellenbogen JA (2004) Design, Synthesis, and in Vitro Biological Evaluation of Small Molecule Inhibitors of Estrogen Receptor A Coactivator Binding. *J Med Chem* 47: 600-611.

25. Shiau AK, Barstad D, Loria PM, Cheng L, Kushner PJ, et al. (1998) The Structural Basis of Estrogen Receptor/Coactivator Recognition and the Antagonism of This Interaction by Tamoxifen. *Cell* 95: 927-937.

26. Kussie PH, Gorina S, Marechal V, Elenbaas B, Moreau J, et al. (1996) Structure of the Mdm2 Oncoprotein Bound to the P53 Tumor Suppressor Transactivation Domain. *Science* 274: 948-953.

27. Hoe KK, Verma CS, Lane DP (2014) Drugging the P53 Pathway: Understanding the Route to Clinical Efficacy. *Nat Rev Drug Discov* 13: 217-236.

28. Duffy MJ, Synnott NC, McGowan PM, Crown J, O'Connor D, et al. (2014) P53 as a Target for the Treatment of Cancer. *Cancer Treat Rev* 40: 1153-1160.

29. Fasan R, Dias RLA, Moehle K, Zerbe O, Vrijbloed JW, et al. (2004) Using a B-Hairpin to Mimic an A-Helix: Cyclic Peptidomimetic Inhibitors of the P53–Hdm2 Protein–Protein Interaction. *Angew Chem Int Ed* 43: 2109-2112.

30. Kritzer JA, Lear JD, Hodsdon ME, Schepartz A (2004) Helical B-Peptide Inhibitors of the P53-Hdm2 Interaction. *J Am Chem Soc* 126: 9468-9469.

31. Grasberger BL, Lu T, Schubert C, Parks DJ, Carver TE, et al. (2005) Discovery and Cocrystal Structure of Benzodiazepinedione Hdm2 Antagonists That Activate P53 in Cells. *J Med Chem* 48: 909-912.

32. Parks DJ, LaFrance LV, Calvo RR, Milkiewicz KL, Gupta V, et al. (2005) 1,4-Benzodiazepine-2,5-Diones as Small Molecule Antagonists of the Hdm2–P53 Interaction: Discovery and Sar. *Bioorg Med Chem Lett* 15: 765-770.

33. Yin H, Lee G-i, Park HS, Payne GA, Rodriguez JM, et al. (2005) Terphenyl-Based Helical Mimetics That Disrupt the P53/Hdm2 Interaction. *Angew Chem Int Ed* 44: 2704-2707.

34. Bernal F, Tyler AF, Korsmeyer SJ, Walensky LD, Verdine GL (2007) Reactivation of the P53 Tumor Suppressor Pathway by a Stapled P53 Peptide. *J Am Chem Soc* 129: 2456-2457.

35. Bernal F, Wade M, Godes M, Davis TN, Whitehead DG, et al. (2010) A Stapled P53 Helix Overcomes Hdmx-Mediated Suppression of P53. *Cancer Cell* 18: 411-422.

36. Baek S, Kutchukian PS, Verdine GL, Huber R, Holak TA, et al. (2012) Structure of the Stapled P53 Peptide Bound to Mdm2. *J Am Chem Soc* 134: 103-106.

37. Wade M, Li Y-C, Wahl GM (2013) Mdm2, Mdmx and P53 in Oncogenesis and Cancer Therapy. *Nat Rev Cancer* 13: 83-96.

38. Holzer P, Masuya K, Furet P, Kallen J, Valat-Stachyra T, et al. (2015) Discovery of a Dihydroisoquinolinone Derivative (Nvp-Cgm097): A Highly Potent and Selective Mdm2 Inhibitor Undergoing Phase 1 Clinical Trials in P53wt Tumors. *J Med Chem* 58: 6348-6358.

39. Delbridge ARD, Grabow S, Strasser A, Vaux DL (2016) Thirty Years of Bcl-2: Translating Cell Death Discoveries into Novel Cancer Therapies. *Nat Rev Cancer* 16: 99-109.

40. Cromm PM, Spiegel J, Grossmann TN (2015) Hydrocarbon Stapled Peptides as Modulators of Biological Function. *ACS Chem Biol* 10: 1362-1375.

41. Kawamoto SA, Coleska A, Ran X, Yi H, Yang C-Y, et al. (2012) Design of Triazole-Stapled Bcl9 A-Helical Peptides to Target the B-Catenin/B-Cell Cll/Lymphoma 9 (Bcl9) Protein–Protein Interaction. *J Med Chem* 55: 1137-1146.

42. Pelay-Gimeno M, Glas A, Koch O, Grossmann TN (2015) Structure-Based Design of Inhibitors of Protein–Protein Interactions: Mimicking Peptide Binding Epitopes. *Angew Chem Int Ed* 54: 8896-8927.

43. Walensky LD, Kung AL, Escher I, Malia TJ, Barbuto S, et al. (2004) Activation of Apoptosis in Vivo by a Hydrocarbon-Stapled Bh3 Helix. *Science* 305: 1466-1470.

44. Walensky LD, Pitter K, Morash J, Oh KJ, Barbuto S, et al. (2006) A Stapled Bid Bh3 Helix Directly Binds and Activates Bax. *Mol Cell* 24: 199-210.

45. Fulda S, Vucic D (2012) Targeting Iap Proteins for Therapeutic Intervention in Cancer. *Nat Rev Drug Discov* 11: 109-124.

46. Flygare JA, Beresini M, Budha N, Chan H, Chan IT, et al. (2012) Discovery of a Potent Small-Molecule Antagonist of Inhibitor of Apoptosis (Iap) Proteins and Clinical Candidate for the Treatment of Cancer (Gdc-0152). *J Med Chem* 55: 4101-4113.

47. Heldin C-H (1995) Dimerization of Cell Surface Receptors in Signal Transduction. *Cell* 80: 213-223.

48. Lemmon MA, Bu Z, Ladbury JE, Zhou M, Pinchasi D, et al. (1997) Two Egf Molecules Contribute Additively to Stabilization of the Egfr Dimer. *EMBO J* 16: 281-294.

49. Schlessinger J (2002) Ligand-Induced, Receptor-Mediated Dimerization and Activation of Receptor. *Cell* 110: 669-672.

50. Hynes NE, Lane HA (2005) Erbb Receptors and Cancer: The Complexity of Targeted Inhibitors. *Nat Rev Cancer* 5: 341-354.

51. Pines G, Köstler WJ, Yarden Y (2010) Oncogenic Mutant Forms Fo Egfr: Lessons in Signal Transduction and Targets for Cancer Therapy. *FEBS Lett* 584: 2699-2706.

52. Ogiso H, Ishitani R, Nureki O, Fukai S, Yamanaka M, et al. (2002) Crystal Structure of the Complex of Human Epidermal Growth Factor and Receptor Extracellular Domains. *Cell* 110: 775-787.

53. Burgess AT, Cho H-S, Eigenbrot C, Ferguson KM, Garret TPJ, et al. (2003) An Open-and-Shut Case? Recent Insights into the Activation of Egf/Erbb Receptors. *Mol Cell Biol* 12: 541-552.

54. Dawson JP, Berger MB, Lin CC, Schlessinger J, Lemmon MA, et al. (2005) Epidermal Growth Factor Receptor Dimerization and Activation Require Ligand-

Induced Conformational Changes in the Dimer Interface. *Mol Cell Biol* 25: 7734-7742.

55. Lu C, Mi L-Z, Grey MJ, Zhu J, Graef E, et al. (2010) Structural Evidence for Loose Linkage between Ligand Binding and Kinase Activation in the Epidermal Growth Factor Receptor. *Mol Cell Biol* 30: 5432-5443.

56. Berezov A, Chen J, Liu Q, Zhang H-T, Greene MI, et al. (2002) Disabling Receptor Ensembles with Rationally Designed Interface Peptidomimetics. *J Biol Chem* 277: 28330-28339.

57. Mizuguchi T, Uchimura H, Kakizawa T, Kimura T, Yokoyama S, et al. (2009) Inhibitory Effect of a Dimerization-Arm-Mimetic Peptide on Egf Receptor Activation. *Bioorg Med Chem Lett* 19: 3279-3282.

58. Xu R, Povlsen GK, Soroka V, Bock E, Berezin V (2010) A Peptide Antagonist of the Erbb1 Receptor Inhibits Receptor Activation, Tumor Cell Growth and Migration *in Vitro* and Xenograft Tumor Growth *in Vivo*. *Cell Oncol* 32: 259-274.

59. Boran ADW, Seco J, Jayaraman V, Jayaraman G, Zhao S, et al. (2012) A Potential Peptide Therapeutic Derived from the Juxtamembrane Domain of the Epidermal Growth Factor Receptor. *PLoS One* 7: e49702.

60. Mizuguchi T, Ohara N, Iida M, Ninomiya R, Wada S, et al. (2012) Evaluation of Dimerization-Inhibitory Activities of Cyclic Peptides Containing a B-Hairpin Loop Sequence of the Egf Receptor. *Bioorg Med Chem* 20: 5730-5737.

61. Staberg M, Riemer C, Xu R, Dmytriyeva O, Bock E, et al. (2013) Identification of a Novel Antagonist of the Erbb1 Receptor Capable of Inhibiting Migration of Human Glioblastoma Cells. *Cell Oncol* 36: 201-211.

62. Yin H, Hamilton AD (2005) Strategies for Targeting Protein–Protein Interactions with Synthetic Agents. *Angew Chem Int Ed* 44: 4130-4163.

63. Wójcik P, Berlicki Ł (2016) Peptide-Based Inhibitors of Protein–Protein Interactions. *Bioorg Med Chem Lett* 26: 707-713.

64. Ye C, Brooks B, Marshall G (2006) Development of Small Molecules Designed to Modulate Protein–Protein Interactions. *J Comput Aided Mol Des* 20: 109-130.

65. Azzarito V, Long K, Murphy NS, Wilson AJ (2013) Inhibition of [Alpha]-Helix-Mediated Protein-Protein Interactions Using Designed Molecules. *Nat Chem* 5: 161-173.

66. Gavenonis J, Sheneman BA, Siegert TR, Eshelman MR, Kritzer JA (2014) Comprehensive Analysis of Loops at Protein-Protein Interfaces for Macrocycle Design. *Nat Chem Biol* 10: 716-722.

67. Watkins AM, Arora PS (2014) Anatomy of B-Strands at Protein–Protein Interfaces. *ACS Chem Biol* 9: 1747-1754.

68. Yuzawa S, Opatowsky Y, Zhang Z, Mandiyan V, Lax I, et al. (2007) Structural Basis for Activation of the Receptor Tyrosine Kinase Kit by Stem Cell Factor. *Cell* 130: 323-334.

69. Remaut H, Waksman G (2006) Protein–Protein Interaction through B-Strand Addition. *Trends Biochem Sci* 31: 436-444.

70. Robinson JA (2008) B-Hairpin Peptidomimetics: Design, Structures and Biological Activities. *Acc Chem Res* 41: 1278-1288.

71. Bernard E, Buckley V, Moman E, Coleman L, Meade G, et al. (2012) Inhibition of Platelet Adhesion by Peptidomimetics Mimicking the Interactive B-Hairpin of Glycoprotein Ibα. *Bioorg Med Chem Lett* 22: 3323-3326.

72. Gokhale A, Weldeghiorghis TK, Taneja V, Satyanarayanajois SD (2011) Conformationally Constrained Peptides from Cd2 to Modulate Protein–Protein Interactions between Cd2 and Cd58. *J Med Chem* 54: 5307-5319.

73. Tyndall JDA, Nall T, Fairlie DP (2005) Proteases Universally Recognize Beta Strands in Their Active Sites. *Chem Rev* 105: 973-1000.

74. Wiesmann C, Ultsch MH, Bass SH, de Vos AM (1999) Crystal Structure of Nerve Growth Factor in Complex with the Ligand-Binding Domain of the Trka Receptor. *Nature* 401: 184-188.

75. Leppänen V-M, Tvorogov D, Kisko K, Prota AE, Jeltsch M, et al. (2013) Structural and Mechanistic Insights into Vegf Receptor 3 Ligand Binding and Activation. *Proc Natl Acad Sci* 110: 12960-12965.

76. Franklin MC, Carey KD, Vajdos FF, Leahy DJ, Vos AMd, et al. (2004) Insights into Erbb Signaling from the Structure of the Erbb2-Pertuzumab Complex. *Cancer Cell* 5: 317-328.

77. Robinson JA (2009) Design of Protein–Protein Interaction Inhibitors Based on Protein Epitope Mimetics. *ChemBioChem* 10: 971-973.

78. Kovacs E, Zorn JA, Huang Y, Barros T, Kuriyan J (2015) A Structural Perspective on the Regulation of the Epidermal Growth Factor Receptor. *Annu Rev Biochem* 84: 739-764.

79. Wilson KJ, Gilmore JL, Foley J, Lemmon MA, Riese DJ (2009) Functional Selectivity of Egf Family Peptide Growth Factors: Implications for Cancer. *Pharmacol Ther* 122: 1-8.

80. Dawson JP, Bu Z, Lemmon MA (2007) Ligand-Induced Structural Transitions in Erbb Receptor Extracellular Domains. *Structure* 15: 942-954.

81. Ferguson KM, Berger MB, Mendrola JM, Cho H-S, Leahy DJ, et al. (2003) Egf Activates Its Receptor by Removing Interactions That Autoinhibit Ectodomain Dimerization. *Mol Cell* 11: 507-517.

82. Zhang X, Gureasko J, Shen K, Cole PA, Kuriyan J (2006) An Allosteric Mechanism for Activation of the Kinase Domain of Epidermal Growth Factor Receptor. *Cell* 125: 1137-1149.

83. Jura N, Endres NF, Engel K, Deindl S, Das R, et al. (2009) Mechanism for Activation of the Egf Receptor Catalytic Domain by the Juxtamembrane Segment. *Cell* 137: 1293.

84. Brewer MR, Choi SH, Alvarado D, Moravcevic K, Pozzi A, et al. (2009) The Juxtamembrane Region of the Egf Receptor Functions as an Activation Domain. *Mol Cell* 34: 641-651.

85. Ward MD, Leahy DJ (2014) Kinase Receiver-Activator Preference in Erbb Heterodimers Determined by Intracellular Regions and Not Coupled to Extracellular Asymmetry. *J Biol Chem*.

86. Kovacs E, Das R, Wang Q, Collier TS, Cantor A, et al. (2015) Analysis of the Role of the C-Terminal Tail in the Regulation of the Epidermal Growth Factor Receptor. *Mol Cell Biol* 35: 3083-3102.

87. Batzer AG, Rotin D, Ureña JM, Skolnik EY, Schlessinger J (1994) Hierarchy of Binding Sites for Grb2 and Shc on the Epidermal Growth Factor Receptor. *Mol Cell Biol* 14: 5192-5201.

88. Kolch W, Pitt A (2010) Functional Proteomics to Dissect Tyrosine Kinase Signalling Pathways in Cancer. *Nat Rev Cancer* 10: 618-629.

89. Tebbutt N, Pedersen MW, Johns TG (2013) Targeting the Erbb Family in Cancer: Couples Therapy. *Nat Rev Cancer* 13: 663-673.

90. Lemmon MA, Schlessinger J, Ferguson KM (2014) The Egfr Family: Not So Prototypical Receptor Tyrosine Kinases. *Cold Spring Harb Perspect Biol* 6.

91. Endres NF, Engel K, Das R, Kovacs E, Kuriyan J (2011) Regulation of the Catalytic Activity of the Egf Receptor. *Curr Opin Struct Biol* 21: 777-784.

92. Arkhipov A, Shan Y, Das R, Endres NF, Eastwood MP, et al. (2013) Architecture and Membrane Interactions of the Egf Receptor. *Cell* 152: 557-569.

93. Ferguson KM, Darling PJ, Mohan MJ, Macatee TL, Lemmon MA (2000) Extracellular Domains Drive Homo- but Not Hetero-Dimerization of Erbb Receptors. *EMBO J* 19: 4632-4643.

94. Bessman Nicholas J, Bagchi A, Ferguson Kathryn M, Lemmon Mark A (2014) Complex Relationship between Ligand Binding and Dimerization in the Epidermal Growth Factor Receptor. *Cell Rep* 9: 1306-1317.

95. Sako Y, Minoghchi S, Yanagida T (2000) Single-Molecule Imaging of Egfr Signalling on the Surface of Living Cells. *Nat Cell Biol* 2: 168-172.

96. Clayton AHA, Walker F, Orchard SG, Henderson C, Fuchs D, et al. (2005) Ligand-Induced Dimer-Tetramer Transition During the Activation of the Cell Surface

Epidermal Growth Factor Receptor-a Multidimensional Microscopy Analysis. *J Biol Chem* 280: 30392-30399.

97. Olayioye MA, Neve RM, Lane HA, Hynes NE (2000) The Erbb Signaling Network: Receptor Heterodimerization in Development and Cancer. *EMBO J* 19: 3159-3167.

98. Chung I, Akita R, Vandlen R, Toomre D, Schlessinger J, et al. (2010) Spacial Control of Egf Receptor Activation by Reversible Dimerization on Living Cells. *Nature* 464: 783-787.

99. Wang Q, Villeneuve G, Wang Z (2005) Control of Epidermal Growth Factor Receptor Endocytosis by Receptor Dimerization, Rather Than Receptor Kinase Activation. *EMBO Rep* 6: 942-948.

100. Endres NF, Das R, Smith AW, Arkhipov A, Kovacs E, et al. (2013) Conformational Coupling across the Plasma Membrane in Activation of the Egf Receptor. *Cell* 152: 543-556.

101. Liu P, Cleveland TE, Bouyain S, Byrne PO, Longo PA, et al. (2012) A Single Ligand Is Sufficient to Activate Egfr Dimers. *Proc Natl Acad Sci* 109: 10861-10866.

102. Özcan F, Klein P, Lemmon MA, Lax I, Schlessinger J (2006) On the Nature of Low- and High-Affinity Egf Receptors on Living Cells. *Proc Natl Acad Sci* 103: 5735-5740.

103. Ganetzky R, Finn E, Bagchi A, Zollo O, Conlin L, et al. (2015) Egfr Mutations Cause a Lethal Syndrome of Epithelial Dysfunction with Progeroid Features. *Mol Genet Genomic Med* 3: 452-458.

104. Makki N, Thiel KW, Francis J. Miller J (2013) The Epidermal Growth Factor Receptor and Its Ligans in Cardiovascular Disease. *Int J Mol Sci* 14: 20597-20613.

105. Yarden Y, Pines G (2012) The Erbb Network: At Last, Cancer Therapy Meets Systems Biology. *Nat Rev Cancer* 12: 553-563.

106. Fry DW, Kraker AJ, McMichael A, Ambrosso LA, Nelson JM, et al. (1994) A Specific Inhibitor of the Epidermal Growth Factor Receptor Tyrosine Kinase. *Science* 265: 1093-1095.

107. Schmidt E, Wong R (2003) 'New' Fda Delivers in 2003. *Nat Rev Drug Discov* 2: 941-942.

108. Muhsin M, Graham J, Kirkpatrick P (2003) Gefitinib. *Nat Rev Drug Discov* 2: 515-516.

109. U.S. Food and Drug Administration. Fda Approves Targeted Therapy for First-Line Treatment of Patients with a Type of Metastatic Lung Cancer. http://www.fda.gov/NewsEvents/Newsroom/PressAnnouncements/ucm454678.htm (Accessed March 7, 2016).

110. U.S. Food and Drug Administration. Fda Approves Erlotinib. http://www.fda.gov/Drugs/InformationOnDrugs/ApprovedDrugs/ucm352317.htm (Accessed March 7, 2016).

111. Dowell J, Minna JD, Kirkpatrick P (2005) Erlotinib Hydrochloride. *Nat Rev Drug Discov* 4: 13-14.

112. Moy B, Kirkpatrick P, Kar S, Goss P (2007) Lapatinib. *Nat Rev Drug Discov* 6: 431-432.

113. U.S. Food and Drug Administration. Fda Approves Tykerb for Advanced Breast Cancer Patients. http://www.fda.gov/NewsEvents/Newsroom/PressAnnouncements/2007/ucm108866.htm (Accessed March 7, 2016).

114. Mullard A (2014) 2013 Fda Drug Approvals. *Nat Rev Drug Discov* 13: 85-89.

115. U.S. Food and Drug Administration. Fda Approves Afatinib. http://www.fda.gov/Drugs/InformationOnDrugs/ApprovedDrugs/ucm360574.htm (Accessed March 7, 2016).

116. Gazdar AF (2009) Activating and Resistance Mutations of Egfr in Non-Small-Cell Lung Cancer: Role in Clinical Response to Egfr Tyrosine Kinase Inhibitors. *Oncogene* 28: S24-S31.

117. Nguyen K-SH, Kobayashi S, Costa DB (2009) Acquired Resistance to Epidermal Growth Factor Receptor Tyrosine Kinase Inhibitors in Non-Small-Cell Lung Cancers Dependent on the Epidermal Growth Factor Receptor Pathway. *Clin Lung Cancer* 10: 281-289.

118. Mullard A (2016) 2015 Fda Drug Approvals. *Nat Rev Drug Discov* 15: 73-76.

119. U.S. Food and Drug Administration. Fda Approves New Pill to Treat Certain Patients with Non-Small Cell Lung Cancer. http://www.fda.gov/NewsEvents/Newsroom/PressAnnouncements/ucm472525.htm (Accessed March 7, 2016).

120. Reichert J, Pavlou A (2004) Monoclonal Antibodies Market. *Nat Rev Drug Discov* 3: 383-384.

121. Cho H-S, Mason K, Ramyar KX, Stanley AM, Gabelli SB, et al. (2003) Structure of the Extracellular Region of Her2 Alone and in Complex with the Herceptin Fab. *Nature* 421: 756-760.

122. U.S. Food and Drug Administration. Fda Approval for Trastuzumab. http://www.cancer.gov/about-cancer/treatment/drugs/fda-trastuzumab (Accessed March 8, 2016).

123. Li S, Schmitz KR, Jeffrey PD, Wiltzius JJW, Kussie P, et al. (2005) Structural Basis for Inhibition of the Epidermal Growth Factor Receptor by Cetuximab. *Cancer Cell* 7: 301-311.

124. U.S. Food and Drug Administration. Fda Approves First Head & Neck Cancer Treatment in 45 Years Data Shows Treatment with Erbitux Extends Survival. http://www.fda.gov/NewsEvents/Newsroom/PressAnnouncements/2006/ucm108609.htm (Accessed March 8, 2016).

125. Saltz L, Easley C, Kirkpatrick P (2006) Panitumumab. *Nat Rev Drug Discov* 5: 987-988.

126. U.S. Food and Drug Administration. Novel Drug Approvals for 2012. http://www.fda.gov/drugs/developmentapprovalprocess/druginnovation/ucm336115.htm (Accessed March 8, 2016).

127. da Cunha Santos G, Shepherd FA, Tsao MS (2011) Egfr Mutations and Lung Cancer. *Annu Rev Pathol-Mech* 6: 49-69.

128. Zhang X, Pickin KA, Bose R, Jura N, Cole PA, et al. (2007) Inhibition of the Egf Receptor by Binding of Mig6 to an Activating Kinase Domain Interface. *Nature* 450: 741-744.

129. Sinclair JKL, Schepartz A (2014) Influence of Macrocyclization on Allosteric, Juxtamembrane-Derived, Stapled Peptide Inhibitors of the Epidermal Growth Factor Receptor (Egfr). *Org Lett* 16: 4916-4919.

130. Hill TA, Shepherd NE, Diness F, Fairlie DP (2014) Constraining Cyclic Peptides to Mimic Protein Structure Motifs. *Angew Chem Int Ed* 53: 13020-13041.

131. Chu Q, Moellering RE, Hilinski GJ, Kim Y-W, Grossmann TN, et al. (2015) Towards Understanding Cell Penetration by Stapled Peptides. *MedChemComm* 6: 111-119.

132. Góngora-Benítez M, Tulla-Puche J, Albericio F (2014) Multifaceted Roles of Disulfide Bonds. Peptides as Therapeutics. *Chem Rev* 114: 901-926.

133. Lau YH, de Andrade P, Wu Y, Spring DR (2015) Peptide Stapling Techniques Based on Different Macrocyclisation Chemistries. *Chem Soc Rev* 44: 91-102.

134. Venkatraman J, Shankaramma SC, Balaram P (2001) Design of Folded Peptides. *Chem Rev* 101: 3131-3152.

135. Kritzer JA, Stephens OM, Guarracino DA, Reznik SK, Schepartz A (2005) B-Peptides as Inhibitors of Protein–Protein Interactions. *Bioorg Med Chem* 13: 11-16.

136. Verdine GL, Hilinski GJ (2012) Stapled Peptides for Intracellular Drug Targets. *Method Enzymol* 503: 3-33.

137. Moellering RE, Cornejo M, Davis TN, Bianco CD, Aster JC, et al. (2009) Direct Inhibition of the Notch Transcription Factor Complex. *Nature* 462: 182-188.

138. Glas A, Bier D, Hahne G, Rademacher C, Ottmann C, et al. (2014) Constrained Peptides with Target-Adapted Cross-Links as Inhibitors of a Pathogenic Protein–Protein Interaction. *Angew Chem Int Ed* 53: 2489-2493.

139. Wang Y, Ho TG, Bertinetti D, Neddermann M, Franz E, et al. (2014) Isoform-Selective Disruption of Akap-Localized Pka Using Hydrocarbon Stapled Peptides. *ACS Chem Biol* 9: 635-642.

140. Teng Y, Bahassan A, Dong D, Hanold LE, Ren X, et al. (2015) Targeting the Wasf3-Cyfip1 Complex Using Stapled Peptides Suppresses Cancer Cell Invasion. *Cancer Res*.

141. Loughlin WA, Tyndall JDA, Glenn MP, Hill TA, Fairlie DP (2010) Update 1 Of: Beta-Strand Mimetics. *Chem Rev* 110: PR32-PR69.

142. Kang CW, Sarnowski MP, Ranatunga S, Wojtas L, Metcalf RS, et al. (2015) B-Strand Mimics Based on Tetrahydropyridazinedione (Tpd) Peptide Stitching. *Chem Commun* 51: 16259-16262.

143. Walewska A, Zhang M-M, Skalicky JJ, Yoshikami D, Olivera BM, et al. (2009) Integrated Oxidative Folding of Cysteine/Selenocysteine Containing Peptides: Improving Chemical Synthesis of Conotoxins. *Angew Chem Int Ed* 48: 2221.

144. Muttenhaler M (2008) Selenopeptide Chemistry. *J Pepti Sci* 14: 1223-1239.

145. Gowd KH, Yarotskyy V, Elmslie KS, Skalicky JJ, Olivera BM, et al. (2010) Site-Specific Effects of Diselenide Bridges on the Oxidative Folding of a Cystine Knot Peptide, Ω-Selenoconotoxin Gvia. *Biochemistry* 49: 2741.

146. Davies JS (2003) The Cyclization of Peptides and Depsipeptides. *J Pept Sci* 9: 471-501.

147. Pedersen DS, Abell A (2011) 1,2,3-Triazoles in Peptidomimetic Chemistry. *Euro J Org Chem* 2011: 2399-2411.

148. Li H, Aneja R, Chaiken I (2013) Click Chemistry in Peptide-Based Drug Design. *Molecules* 18: 9797.

149. Liang L, Astruc D (2011) The Copper(I)-Catalyzed Alkyne-Azide Cycloaddition (Cuaac) "Click" Reaction and Its Applications. An Overview. *Coord Chem Rev* 255: 2933-2945.

150. Zhang L, Chen X, Xue P, Sun HHY, Williams ID, et al. (2005) Ruthenium-Catalyzed Cycloaddition of Alkynes and Organic Azides. *J Am Chem Soc* 127: 15998-15999.

151. Ahsanullah, Schmieder P, Kühne R, Rademann J (2009) Metal-Free, Regioselective Triazole Ligations That Deliver Locked Cis Peptide Mimetics. *Angew Chem Int Ed* 48: 5042-5045.

152. Ahsanullah, Rademann J (2010) Cyclative Cleavage through Dipolar Cycloaddition: Polymer-Bound Azidopeptidylphosphoranes Deliver Locked Cis-Triazolylcyclopeptides as Privileged Protein Binders. *Angew Chem Int Ed* 49: 5378-5382.

153. White CJ, Yudin AK (2011) Contemporary Strategies for Peptide Macrocyclization. *Nature Chem* 3: 509-524.

154. Empting M, Avrutina O, Meusinger R, Fabritz S, Reinwarth M, et al. (2011) "Triazole Bridge": Disulfide-Bond Replacement by Ruthenium-Catalyzed Formation of 1,5-Disubstituted 1,2,3-Triazoles. *Angew Chem Int Ed* 50: 5207-5211.

155. Holland-Nell K, Meldal M (2011) Maintaining Biological Activity by Using Triazoles as Disulfide Bond Mimetics. *Angew Chem Int Ed* 50: 5204-5206.

156. Wels B, Kruijtzer JAW, Garner K, Nijenhuis WAJ, Gispen WH, et al. (2005) Synthesis of a Novel Potent Cyclic Peptide Mc4-Ligand by Ring-Closing Metathesis. *Bioorg Med Chem* 13: 4221-4227.

157. Oishi S, Shi Z-D, Worthy KM, Bindu LK, Fisher RJ, et al. (2005) Ring-Closing Metathesis of C-Terminal Allylglycine Residues with an N-Terminal B-Vinyl-Substituted Phosphotyrosyl Mimetic as an Approach to Novel Grb2 Sh2 Domain-Binding Macrocycles. *ChemBioChem* 6: 668-674.

158. Deshmukh PH, Schulz-Fademrecht C, Procopiou PA, Vigushin DA, Coombes RC, et al. (2007) Ring-Closing Metathesis in the Synthesis of Biologically Active Peptidomimetics of Apicidin A. *Adv Synth Catal* 349: 175-183.

159. Reichwein JF, Versluis C, Liskamp RMJ (2000) Synthesis of Cyclic Peptides by Ring-Closing Metathesis. *J Org Chem* 65: 6187-6195.

160. Stymiest JL, Mitchell BF, Wong S, Vederas JC (2003) Synthesis of Biologically Active Dicarba Analogues of the Peptide Hormone Oxytocin Using Ring-Closing Metathesis. *Org Lett* 5: 47-49.

161. Yarden Y, Sliwkowski MX (2001) Untangling the Erbb Signalling Network. *Nat Rev Mol Cell Biol* 2: 127-137.

162. Sorkin A, von Zastrow M (2002) Signal Transduction and Endocytosis: Close Encouters of Many Kinds. *Nat Rev Mol Cell Biol* 3: 600-614.

163. Sliwkowski MX, Mellman I (2013) Antibody Therapeutics in Cancer. *Science* 341: 1192-1198.

164. Wojtkowiak JW, Verduzco D, Schramm KJ, Gillies RJ (2011) Drug Resistance and Cellular Adaptation to Tumor Acidic Ph Microenvironment. *Mol Pharm* 8: 2032-2038.

165. Ceresa BP (2013) Spacial Regulation of Epidermal Growth Factor Receptor Signaling by Endocytosis. *Int J Mol Sci* 14: 72-87.

166. Tornoe CW, Christensen C, Meldal M (2002) Peptidotriazoles on Solid Phase: [1,2,3]-Triazoles by Regiospecific Copper(I)-Catalyzed 1,3-Dipolar Cycloadditions of Terminal Alkynes to Azides. *J Org Chem* 67: 3057-3064.

167. Bock VD, Perciaccante R, Jansen TP, Hiemstra H, van Maarseveen JH (2006) Click Chemistry as a Route to Cyclic Tetrapeptide Analogues: Synthesis of Cyclo-[Pro-Val-Psi(Triazole)-Pro-Tyr]. *Org Lett* 8: 919-922.

168. Goncalves V, Gautier B, Regazzetti A, Coric P, Bouaziz S, et al. (2007) On-Resin Cyclization of Peptide Ligands of the Vascular Endothelial Growth Factor Receptor 1 by Copper(I)-Catalyzed 1,3-Dipolar Azide-Alkyne Cycloaddition. *Bioorg Med Chem Lett* 17: 5590-5594.

169. Jagasia R, Holub JM, Bollinger M, Kirshenbaum K, Finn MG (2009) Peptide Cyclization and Cyclodimerization by Cu(I)-Mediated Azide-Alkyne Cycloaddition. *J Org Chem* 74: 2964-2974.

170. Oh K, Guan Z (2006) A Convergent Synthesis of New Beta-Turn Mimics by Click Chemistry. *Chem Comm*: 3069-3071.

171. Angell Y, Chen D, Brahimi F, Saragovi HU, Burgess K (2008) A Combinatorial Method for Solution-Phase Synthesis of Labeled Bivalent Beta-Turn Mimics. *J Am Chem Soc* 130: 556-565.

172. Angelo NG, Arora PS (2005) Nonpeptidic Foldamers from Amino Acids: Synthesis and Characterization of 1,3-Substituted Triazole Oligomers. *J Am Chem Soc* 127: 17134-17135.

173. Li H, Anja R, Chaiken I (2013) Click Chemistry in Peptide-Based Drug Design. *Molecules* 18: 9797-9817.

174. Rostovtsev VV, Green LG, Fokin VV, Sharpless KB (2002) A Stepwise Huisgen Cycloaddition Process: Copper(I)-Catalyzed Regioselective "Ligation" of Azides and Terminal Alkynes. *Angew Chem Int Ed* 41: 2596-2599.

175. Kolb HC, Finn MG, Sharpless KB (2001) Click Chemistry: Diverse Chemical Function from a Few Good Reactions. *Angew Chem Int Ed* 40: 2004-2021.

176. Nyffeler PT, Liang CH, Koeller KM, Wong CH (2002) The Chemistry of Amine-Azide Interconversion: Catalytic Diazotransfer and Regioselective Azide Reduction. *J Am Chem Soc* 124: 10773-10778.

177. Izetti P, Hautefeuille A, Abujamra A, de Farias C, Giacomazzi J, et al. (2014) Prima-1, a Mutant P53 Reactivator, Induces Apoptosis and Enhances Chemotherapeutic Cytotoxicity in Pancreatic Cancer Cell Lines. *Invest New Drugs* 32: 783-794.

178. Kulczar C, Roth W, Carl S, Gundmundsson O, Knipp G (2015) Peptide and Protein Drug Delivery. In: Mitra AK, Kwatra D, Vadlapudi AD, editors. *Drug Delivery*. 1 ed. Burlington, MA: Jones & Bartlett Learning. pp. 405-428.

179. Wolfson W (2009) Aileron Staples Peptides. *Chem Biol* 16: 910-912.

180. Sawyer TK (2009) Aileron Therapeutics. *Chem Biol Drug Des* 73: 3-6.

181. Safety Study of Alrn-6924 in Patients with Advanced Solid Tumors. In:ClinicalTrialsgov [Internet]. Bethesda (MD): National Library of Medicine (US). 2000- [cited 2015 Jan 29]. Available from: https://clinicaltrials.gov/show/NCT02264613 NLM Identifier: NCT02264613.

182. Laketa V, Zarbakhsh S, Traynor-Kaplan A, MacNamara A, Subramanian D, et al. (2014) Pip3 Induces the Recycling of Receptor Tyrosine Kinases. *Sci Signal* 7: ra5.

183. Liskamp RMJ, Rijkers DTS, Kruijtzer JAW, Kemmink J (2011) Peptides and Proteins as a Continuing Exciting Source of Inspiration for Peptidomimetics. *ChemBioChem* 12: 1626-1653.

184. Perez de Vega MJ, Garcia-Aranda MI, Gonzalez-Muniz R (2011) A Role for Ring-Closing Metathesis in Medicinal Chemistry: Mimicking Secondary Architectures in Bioactive Peptides. *Med Res Rev* 31: 677-715.

185. Ganesh Kumar M, Mali SM, Raja KM, Gopi HN (2015) Design of Stable Beta-Hairpin Mimetics through Backbone Disulfide Bonds. *Org Lett* 17: 230-233.

186. Angell Y, Burgess K (2005) Ring Closure to Beta-Turn Mimics Via Copper-Catalyzed Azide/Alkyne Cycloadditions. *J Org Chem* 70: 9595-9598.

187. Hanold LE, Oruganty K, Ton NT, Beedle AM, Kannan N, et al. (2015) Inhibiting Egfr Dimerization Using Triazolyl-Bridged Dimerization Arm Mimics. *PLoS One* In Press.

188. Miller SJ, Blackwell HE, Grubbs RH (1996) Application of Ring-Closing Metathesis to the Synthesis of Rigidified Amino Acids and Peptides. *Journal of the American Chemical Society* 118: 9606-9614.

189. Sievers F, Wilm A, Dineen D, Gibson TJ, Karplus K, et al. (2011) Fast, Scalable Generation of High-Quality Protein Multiple Sequence Alignments Using Clustal Omega. *Mol Syst Biol* 7.

190. Goujon M, McWilliam H, Li W, Valentin F, Squizzato S, et al. (2010) A New Bioinformatics Analysis Tools Framework at Embl–Ebi. *Nucleic Acids Res* 38: W695-W699.

191. Aoki K, Maeda M, Nakae T, Okada Y, Ohya K, et al. (2014) A Disulfide Bond Replacement Strategy Enables the Efficient Design of Artificial Therapeutic Peptides. *Tetrahedron* 70: 7774-7779.

192. Northfield SE, Wang CK, Schroeder CI, Durek T, Kan M-W, et al. (2014) Disulfide-Rich Macrocyclic Peptides as Templates in Drug Design. *Euro J Med Chem* 77: 248-257.

193. Besse D, Siedler F, Diercks T, Kessler H, Moroder L (1997) The Redox Potential of Selenocystine in Unconstrained Cyclic Peptides. *Angew Chem Int Ed* 36: 883-885.

194. Wessjohann LA, Schneider A, Abbas M, Brandt W (2007) Selenium in Chemistry and Biochemistry in Comparison to Sulfur. *Biol Chem* 388: 997-1006.

195. Koide T, Itoh H, Otaka A, Yasui H, Kuroda M, et al. (1993) Synthetic Study on Selenocystine-Containing Peptides. *Chem Pharm Bull* 41: 502-506.

196. Quaderer R, Sewing A, Hilvert D (2001) Selenocystein-Mediated Native Chemical Ligation. *Helv Chim Acta* 84: 1197-1206.

197. Hondal RJ, Nilsson BL, Raines RT (2001) Selenocysteine in Native Chemical Ligation and Expressed Protein Ligation. *J Am Chem Soc* 123: 5140-5141.

198. Han TS, Zhang M-M, Gowd KH, Walewska A, Yoshikami D, et al. (2010) Disulfide-Depleted Selenoconopeptides: Simplified Oxidative Folding of Cysteine-Rich Peptides. *ACS Med Chem Lett* 1: 140-144.

199. Araujo ADd, Callaghan B, Nevin ST, Daly NL, Craik DJ, et al. (2011) Total Synthesis of the Analgesic Conotoxin Mrvib through Selenocysteine-Assisted Folding. *Angew Chem Int Ed* 2011: 6527-6529.

200. Muttenhaler M, Nevin ST, Grishin AA, Ngo ST, Choy PT, et al. (2010) Solving the α-Conotoxin Folding Problem: Efficient Selenium-Directed on-Resin Generation of More Potent and Stable Nicotinic Acetylcholine Receptor Antagonsists. *J Am Chem Soc* 132: 3514-3522.

201. Harris KM, Jr SF, Hondal RJ (2007) Studies on Deprotection of Cysteine and Selenocystein Side-Chain Protecting Groups. *J Pept Sci* 13: 81-93.

202. Schroll AL, Hondal RJ, Jr. SF (2012) The Use of 2,2'-Dithiobis(5-Nitropyridine) (Dtnp) for Deprotection and Diselenide Formation in Protected Selenocysteine-Containing Peptides. *J Pept Sci* 18: 155-162.

203. Suirós-Funosas R, Prohens R, Barbas R, El-Faham A, Albericio F (2009) Oxyma: An Efficient Additive for Peptide Synthesis to Replace the Triazole-Based Hobt and Hoat with a Lower Risk of Explosion. *Chem Euro J* 15: 9394-9403.

204. Fischer R, Mader O, Jung G, Brock R (2003) Extending the Applicability of Carboxyfluorescein in Solid-Phase Synthesis. *Bioconjugate Chem* 14: 653-660.

205. Goldhaber SB (2003) Trace Element Risk Assessment: Essentiality Vs. Toxicity. *Regul Toxicol Pharmacol* 38: 232-242.

206. Gill SC, von Hippel PH (1989) Calculation of Protein Extinction Coefficients from Amino Acid Sequence Data. *Anal Biochem* 182: 319-326.

207. Whitmore L, Wallace BA (2008) Protein Secondary Structure Analyses from Circular Dichroism Spectroscopy: Methods and Reference Databases. *Biopolymers* 89: 392-400.

208. Dichroweb User Guide: Input Units. http://dichroweb.cryst.bbk.ac.uk/html/userguide.shtml (Accessed January 26, 2015).

209. Tam A, Arnold U, Soellner MB, Raines RT (2007) Protein Prosthesis: 1,5-Disubstituted[1,2,3]Triazoles as Cis-Peptide Bond Surrogates. *J Am Chem Soc* 129: 12670-12671.

210. Zhang J, Kemmink J, Rijkers DTS, Liskamp RMJ (2011) Cu(I)- and Ru(Ii)-Mediated "Click" Cyclization of Tripeptides toward Vancomycin-Inspired Mimics. *Org Lett* 13: 3438-3441.

211. Boren BC, Narayan S, Rasmussen LK, Zhang L, Zhao H, et al. (2008) Ruthenium-Catalyzed Azide−Alkyne Cycloaddition: Scope and Mechanism. *J Am Chem Soc* 130: 8923-8930.

212. Rai R, Raghothama S, Sridharan R, Balaram P (2007) Tuning the B-Turn Segment in Designed Peptide B-Hairpins: Construction of a Stable Type Iprime B-Turn Nucleus and Hairpin-Helix Transition Promoting Segments. *Biopolymers* 88: 350-361.

213. Wüthrich K, Spitzfaden C, Memmert K, Widmer H, Wider G (1991) Protein Secondary Structure Determination by Nmr. Application with Recombinant Human Cyclophilin. *FEBS Lett* 285: 237-247.

214. Kwong PD, Wyatt R, Robinson J, Sweet RW, Sodroski J, et al. (1998) Structure of an Hiv Gp120 Envelope Glycoprotein in Complex with the Cd4 Receptor and a Neutralizing Human Antibody. *Nature* 393: 648-659.

215. Melillo B, Liang S, Park J, Schön A, Courter JR, et al. (2016) Small-Molecule Cd4-Mimics: Structure-Based Optimization of Hiv-1 Entry Inhibition. *ACS Med Chem Lett* 7: 330-334.

216. Zhang W, Canziani G, Plugariu C, Wyatt R, Sodroski J, et al. (1999) Conformational Changes of Gp120 in Epitopes near the Ccr5 Binding Site Are Induced by Cd4 and a Cd4 Miniprotein Mimetic. *Biochemistry* 38: 9405-9416.

217. Stricher F, Huang C-c, Descours A, Duquesnoy S, Combes O, et al. (2008) Combinatorial Optimization of a Cd4-Mimetic Miniprotein and Cocrystal Structures with Hiv-1 Gp120 Envelope Glycoprotein. *J Mol Biol* 382: 510-524.

218. Morellato-Castillo L, Acharya P, Combes O, Michiels J, Descours A, et al. (2013) Interfacial Cavity Filling to Optimize Cd4–Mimetic Miniprotein Interactions with Hiv-1 Surface Glycoprotein. *J Med Chem* 56: 5033-5047.

219. Chen S, Chrusciel RA, Nakanishi H, Raktabutr A, Johnson ME, et al. (1992) Design and Synthesis of a Cd4 Beta-Turn Mimetic That Inhibits Human Immunodeficiency Virus Envelope Glycoprotein Gp120 Binding and Infection of Human Lymphocytes. *Proc Natl Acad Sci* 89: 5872-5876.

220. Schlessinger J, Plotnikov AN, Ibrahimi OA, Eliseenkova AV, Yeh BK, et al. (2000) Crystal Structure of a Ternary Fgf-Fgfr-Heparin Complex Reveals a Dual Role for Heparin in Fgfr Binding and Dimerization. *Mol Cell* 6: 743-750.

221. De Smet F, Christopoulos A, Carmeliet P (2014) Allosteric Targeting of Receptor Tyrosine Kinases. *Nat Biotech* 32: 1113-1120.